Summer 2017

The Chondrocyte Channelome: A Novel Ion Channel Candidate in the Pathogenesis of Pectus Deformities

Anthony J. Asmar
Old Dominion University

THE CHONDROCYTE CHANNELOME: A NOVEL ION CHANNEL CANDIDATE IN THE PATHOGENESIS OF PECTUS DEFORMITIES

by

Anthony J. Asmar
B.S. Biology May 2010, Virginia Polytechnic Institute
M.S. Biology May 2013, Old Dominion University

A Dissertation Submitted to the Faculty of
Old Dominion University in Partial Fulfillment of the
Requirements for the Degree of

DOCTOR OF PHILOSOPHY

BIOMEDICAL SCIENCES

OLD DOMINION UNIVERSITY
August 2017

Approved by:

Christopher Osgood (Co-Director)

Michael Stacey (Co-Director)

Lesley Greene (Member)

Andrei Pakhomov (Member)

Jing He (Member)

ABSTRACT

THE CHONDROCYTE CHANNELOME: A NOVEL ION CHANNEL CANDIDATE IN THE PATHOGENESIS OF PECTUS DEFORMITIES

Anthony J. Asmar

Old Dominion University, 2017

Co-Directors: Dr. Christopher Osgood

Dr. Michael Stacey

Costal cartilage is a type of rod-like hyaline cartilage connecting the ribs to the sternum. The chest wall deformities pectus excavatum (PE) and pectus carinatum (PC) involve displacement of the sternum causing a depression or protrusion of the chest. There is little knowledge about costal cartilage and pectus deformities with much of its understanding based on assumptions from articular cartilage. Chondrocytes are subjected to a constantly changing environment with fluctuations in pH and osmolarity. Ion channels detect these changes and in turn regulate proliferation, differentiation, and extracellular matrix production. Using ion channel qPCR arrays, we produced expression profiles for normal, fetal, PE-affected, and PC-affected costal chondrocytes as well as articular chondrocytes. Costal and articular chondrocytes had many commonly expressed ion channels with certain channels specific to each cartilage type. The discrepancy in ion channel expression is likely to be a reflection of the functional differences between the two cartilage types. Additionally, fetal costal chondrocytes had several other distinct ion channels possibly due to the differentiation status of the cells. In PC and PE chondrocytes, ACCN1 (ASIC2) and KCNN2 (SK2) were consistently down-regulated compared to normal

costal chondrocytes. However, Western blot analysis found deceases only in ASIC2 protein levels. ASIC2 is a proton-gated ion channel involved in cell response to extracellular pH changes. Calcium monitoring revealed a delay in the formation calcium transients in PC cells when challenged with low pH which may be caused by aberrant signaling from ASIC channels. Immunofluorescent analysis of connexins found that Cx43 was present in chondrocytes with phosphorylated Cx43 localizing in and around the nucleus. Analysis of ATP release found that release is likely a connexin-mediated process, though external acidosis did not induce ATP release. Analysis of microRNAs found upregulation and down-regulation of several microRNAs in PC versus control cells, though further studies are needed to identify a possible microRNA signature for pectus deformities. Overall, we have generated a comprehensive ion channel profile for the costal chondrocytes, as well as identified a possible contributing factor for pectus deformities.

This thesis is dedicated to my parents, Leila and Tony, and sister, Rita, for all their encouragement, support, and patience enabling me to make it to this point.

ACKNOWLEDGMENTS

I would especially like to acknowledge Dr. Michael Stacey, for all his assistance and the opportunity to perform this research under his guidance. I would also like to acknowledge Dr. Christopher Osgood for his advice and support throughout my graduate experience. For their input and help in developing my dissertation project, I would like to acknowledge my committee members, Drs. Leslie Greene, Andrei Pakhomov, and Jing He, as well as Drs. Patrick Sachs, Loree Heller, and Robert Bruno. For their continued friendship and support, I would like to thank Drs. Robert Milletich, Peter Mollica, Wassim Obeid, Hany Salaheldeen, Charalampos Brimpas, and John Reid. I would also like to thank everyone at the Frank Reidy Research Center for Bioelectrics.

TABLE OF CONTENTS

Page

LIST OF TABLES

Table Page

LIST OF FIGURES

Figure Page

Figure Page

Figure Page

CHAPTER 1

INTRODUCTION

1.1 Cartilage

Cartilage is a specialized form of connective tissue serving many important functions throughout the body. Cartilage composes many different structures and structural components in the body as well as protecting joints by covering the articulating ends of bones. Cartilage can be subcategorized into three subtypes: hyaline cartilage, fibrocartilage, and elastic cartilage.

1.2 Hyaline Cartilage

Hyaline cartilage is a subcategory of cartilage characterized by its bluish color. It is mainly comprised of type II collagen and aggrecan with chondroitin sulfate attachments. Hyaline cartilage has many different locations including the articulating surfaces of bones in the joints (articular), in the chest connecting the ribs to the sternum (costal), the nose (nasal), the larynx (arytenoid, corniculate, and cuneiform), and the trachea and bronchi (Pascual-Font and Sanudo, 2016; Zhang and Spector, 2009). Hyaline cartilage is interesting in that is sometimes has an outer layer of stem cells surrounding the tissue known as the perichondrium contributing to the growth of cartilage. There are two mechanisms of growth in hyaline cartilage, interstitial and appositional growth. Interstitial growth occurs by chondrocytes dividing to form their isogenic groups and also producing more collagen. Appositional growth is by the perichondrium producing chondroblasts which differentiate into chondrocytes, forming a new layer of cartilage on the periphery of the tissue (Hayes et al., 2001).

1.3 Extracellular Matrix

Hyaline cartilage mostly extracellular matrix (ECM) with around two-thirds of the tissue's dry weight being collagen and about 10% of the tissue being cells. The resident cells of cartilage are known as chondrocytes which produce collagen and ground substance, which is a mixture of non-collagen ECM components that contribute the cartilage's gel-like properties. Important ground substance components include hyaluronan (also known as hyaluronic acid), aggrecan, chondroitin sulfate, keratin sulfate, as well as other glycosaminoglycans and proteoglycans (Eyre, 2002; Sophia Fox et al., 2009). The cells form clusters known as isogenic groups with the matrix directly surrounding called the territorial matrix. The area between different isogenic groups and territorial matrices is known as the interterritorial matrix (Figure 1).

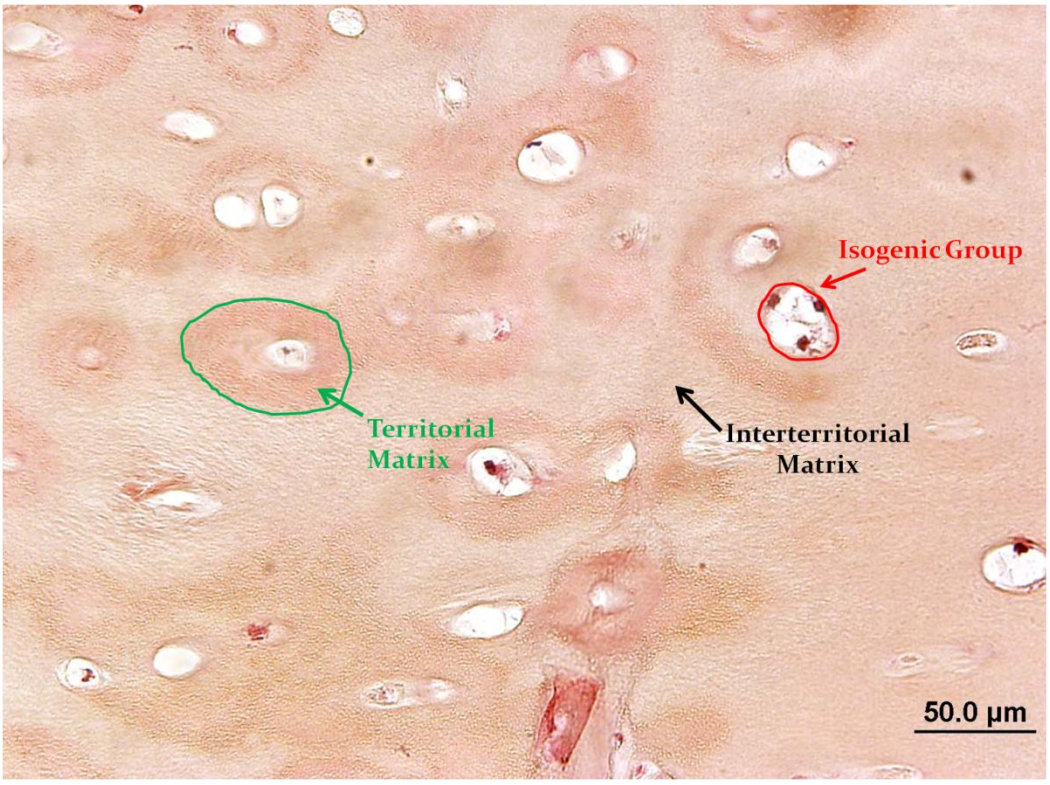

Figure 1. **Hematoxylin and Eosin staining of a transverse section of costal cartilage.** A group of isogenic chondrocytes are outlined in red (red arrow) with a territorial matrix directly surrounding an isogenic group is outlined in green (green arrow). The region between territorial matrices is known as the interterritorial matrix (black arrow). Sections imaged using an Olympus BX-51 microscope with a 20X objective.

The main structural components of hyaline cartilage are type II collagen, aggrecan, and hyaluronan. These provide a framework crucial for the functional property of cartilage. Normally, aggrecan have several sulfonated glycosaminoglycan attachments which give the proteoglycan a negative charge. The aggrecans aggregate along hyaluronic acid creating a very negative region which binds positive ion such as zinc and sodium. The positive ions, in turn,

attract water which would normally cause diffusion of the aggrecan/hyaluronic acid aggregates out of the tissue, but linker proteins anchor hyaluronic acid to the sturdy collagen framework resulting in water being drawn into the cell, giving cartilage its gel-like property (Fig. 2). This turgor pressure not only confers the tissue's function, but is important in allowing for gas exchange through the flow of water (Chandran and Horkay, 2012; Dudhia, 2005).

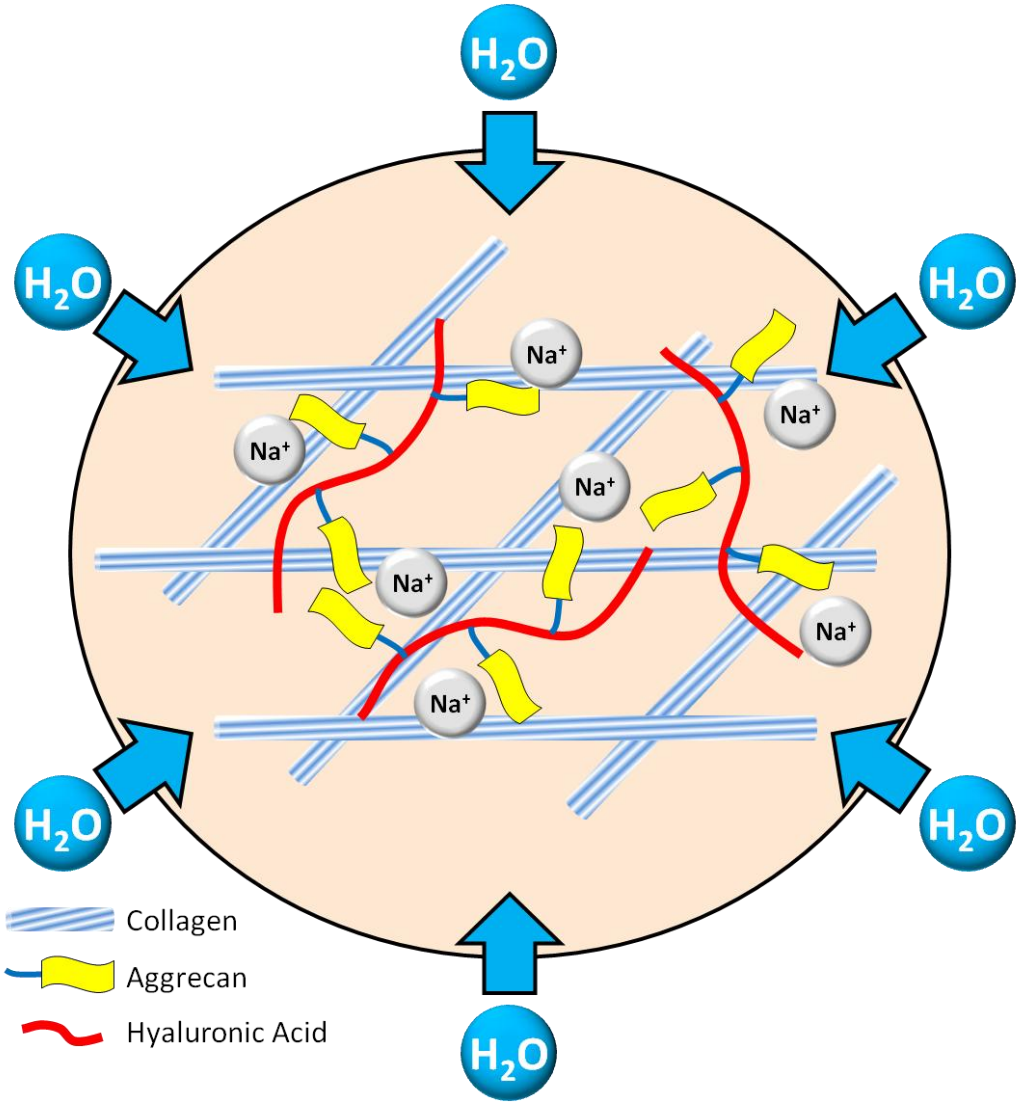

Figure 2. **Diagram of turgor pressure production in cartilage.** The sulfonated aggrecans aggregate along hyaluronic acid creating a negatively charge field. This charged field attracts positively charged ions such as sodium which in turn attracts water. The anchoring of hyaluronic acid to the collagen network prevents diffusion of the interior charged field causing the tissue to swell with water.

The charged ECM, due to the sulfonated proteoglycans, also results in an effect on cells called the Gibbs-Donnan effect. This effect, also known as the Donnan equilibrium, describes the a situation where charged particles are not evenly distributed across a semi-permeable membrane. This occurs in cartilage due to the charged nature of the ECM and has led to the proposed triphasic model of osmotic swelling by Lai et al. (1991). The triphasic model states that there are three phases: (1) the incompressible fluid phase (water), (2) the incompressible solid phase (the ECM), and (3) the fluid ionic phase. The ions tend to stay in the stationary solid phase (ECM) which not only causes the osmotic swelling of the tissue but also creates an imbalance of ions between the interstitial fluid and the cell interior. This imbalance causes a hypertonic environment which has been measured in articular cartilage to be between 310mOsm to 485mOsm depending on the depth within the tissue (Hall et al., 1996a; Lai et al., 1991). The deeper within the tissue, the higher the osmolarity is with the same occurring with the pH (7.3-6.9). The pH can be attributed to the hypoxic nature of the tissue increasing with the tissue depth. However, the Donnan equilibrium involving H^+ ions can also contribute to a difference in extracellular versus intracellular pH with deformation of the tissue causing large pH shifts as low as 6.0 while diseased intervertebral tissue showed pH levels as low as 5.5 (Wilkins and Hall, 1992; Wilkins and Hall, 1995).

1.4 ECM Maintenance

The maintenance of cartilage is a constant and continual process involving the production of enzymes which break down the surrounding ECM simultaneously with the production of new ECM proteins. Collagen is mainly produced and its fibrillogenesis is a spontaneous process which occurs after the cleavage of its propeptide. The regulation of the fibril formation, size, and

organization is determined by the small leucine-rich proteoglycans (SLRPs), decorin and biglycan. These two SLRPs have leucine repeats which form a semi-circular protein able to bind along the D-band of collagen and allow incorporation into the collagen fibrils. Multiple fibrils are then organized by the sugar attachments on the SLRP's interacting with each other (Chen and Birk, 2013; Iozzo, 1999). Another major component produced by chondrocytes is aggrecan and is produced for the purpose of drawing water into the tissue. The regulation of aggrecan production can be modulated by different cellular detection methods. Water/salt concentrations can help determine the amount of aggrecan produced or destroyed as well as hypoxia signaling (Tran et al., 2013). Cartilage is avascular and has a hypoxic interior which triggers many hypoxia-induced signaling pathways. These pathways result in up-regulation of many transcription factors leading to increased production of aggrecan and other proteins (Duval et al., 2009). As expected, the interior of the tissue is likely to have higher concentrations of aggrecan in comparison to the periphery (Fig. 3). The breakdown of collagens are performed by collagenases such as certain matrix metalloproteinases (MMPs) while in response to certain signals, the MMPs can be deactivated by TIMPs (tissue inhibitors of metalloproteinases). Aggrecans are destroyed by different aggrecanases such as the ADAMTS (a disintegrin and metalloproteinase with thrombospondin motifs) family of enzymes. The ECM is in a constant state of turnover with a balance of MMP, TIMP, and ADAMTS production based on different extracellular stimuli (Thoms et al., 2013; Vo et al., 2013).

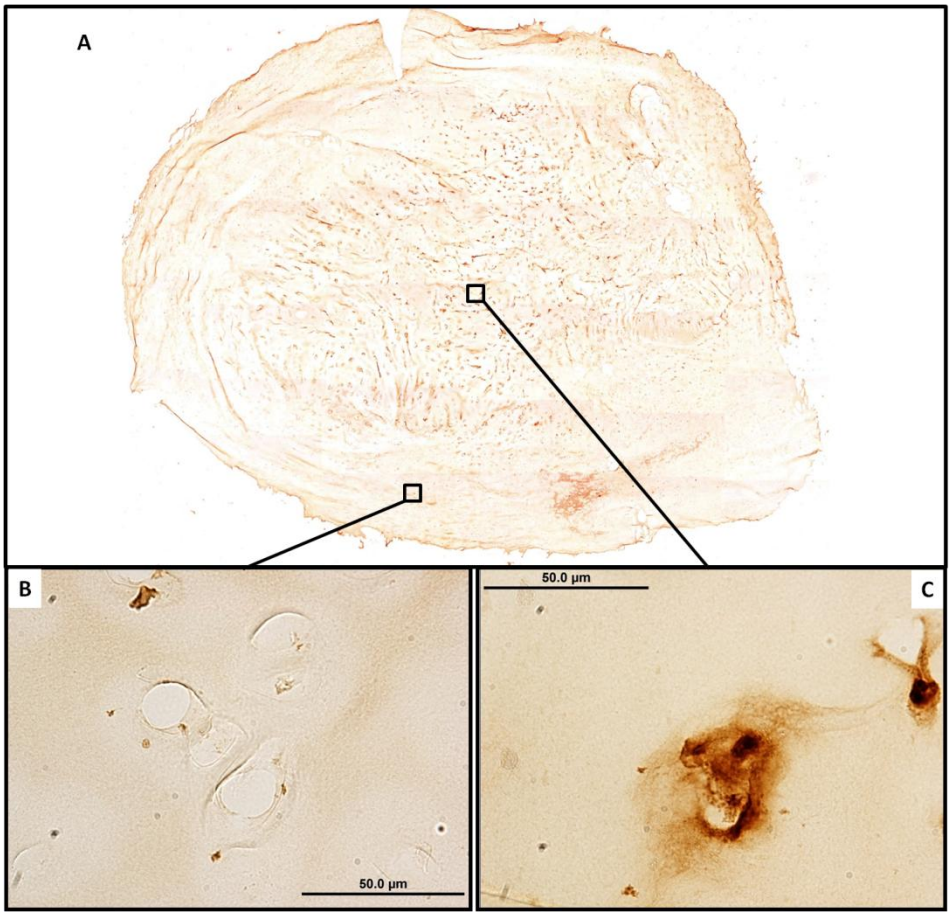

Figure 3. **Tissue distribution of aggrecan in whole costal cartilage cross-section.** (A) Immunohistochemical labeling of aggrecan in whole tissue cross-section of costal cartilage. Magnified images of aggrecan-labeled tissue from the periphery (B) and interior (C) of the tissue. Sections were imaged using an Olympus BX-51 microscope at 4X for A and 60X for B and C.

Additional environmental properties can influence the maintenance of the tissue including pH, biomechanostimulation, and temperature. When the tissue experiences external indentation or tensile forces, the cell experiences stimulation in multiple ways. The cells are normally anchored to the ECM through adhesion proteins and deformation of the tissue

translates to a mechanical force enacted on the cell. The deformation of the tissue also causes water and ions to move within the tissue resulting in changes in the pH and osmolarity. Chondrocytes are equipped with an array of detectors which induce the necessary signaling cascade to respond to these various stimuli. Many of these detectors and responders are ion channels. These stimuli and response mechanism modulate the production of ECM and its maintenance enzymes (Barrett-Jolley et al., 2010; Sun et al., 2011).

The internal pH of chondrocytes is tightly regulated using a high capacity internal buffering system. External acidosis results in stimulation through ion channels, though changes in the internal pH are less likely. External acidosis has been shown to reduce ECM synthesis rates in both bovine isolated articular chondrocytes (Wilkins and Hall, 1992) and bovine articular cartilage explants (Gray et al., 1988). Another important factor is the mechanical forces experienced by chondrocytes. In cartilage, the compressive or tensile forces from joint compression or chest expansion, during the action of breathing, result in mechanical forces to be detected by chondrocytes and converted into a cellular signal known as mechanotransduction. The dynamic mechanical loading is known to increase the production of ECM proteins, though too much force can lead to degeneration (O'Conor et al., 2014; Yokota et al., 2011). Although chondrocytes are known to express proteins capable of temperature sensing, their influence on physiology are currently unknown. However, shifts in temperature cause changes in the fluid viscosity as well as ECM properties which alters the tissue's mechanics (June and Fyhrie, 2010).

1.5 Costal Cartilage

Costal cartilage is a type of hyaline cartilage which form rod-like structures connecting the distal ends of the ribs to the sternum at the intercostal junction. It provides a flexible yet

strong support for the chest with its integrity being essential to the ability to expand and shrink during the action of breathing. The histology of the tissue has not been thoroughly investigated with assumptions made that it is similar to articular cartilage. We have previously investigated different histological aspects of costal cartilage and found some differences to articular cartilage in the structural organization of the collagen fibrils (Stacey et al., 2012). Additionally, biomechanical testing of human chests, postmortem, found that the perichondrium contributes to ~47% of the overall strength of the costal cartilage. The cartilage itself provides a structural support and resistance to compressive forces while the perichondrium contributes mainly to the tensile strength of the tissue (Forman et al., 2010). Although costal and articular cartilage are both considered hyaline, they have different functions. These two tissues experience differing forces with costal cartilage experiencing tensile and compressive forces while articular cartilage experiences significant compressive forces which is likely to lead to differences in gene expression resulting in the different phenotypes.

1.6 Pectus Deformities

Pectus deformities are diseases of the costal cartilage where the sternum becomes displaced. The two pectus deformities are pectus excavatum and pectus carinatum where pectus excavatum (PE), also known as sunken chest, is the most common deformity of the chest resulting in a depression of the sternum and costal cartilages (Fig. 4 A). Pectus carinatum (PC), also known as pigeon chest, results in a protrusion of the sternum and occurs at a lower frequency than PE (Fig. 4 C) (Iida, 2010). Pectus deformities are a congenital chest wall deformity and are known to have a familial inheritance with a 1.8- to 4-fold higher occurrence rate in males versus females. Pedigree analysis saw variations in inheritance from autosomal

dominant, autosomal recessive, X-link recessive, to complex inheritance (Creswick et al., 2006). Currently, surgical repair or braces are used to treat PE and PC. The original Ravitch method (Ravitch, 1949) involves resectioning deformed costal cartilage and sternal realignment with various modified Ravitch methods still being used to repair pectus deformities. Another method commonly used for the repair of PE is the Nuss method. The Nuss method is based on inserting a convex steel bar, formed to the desired curvature of the chest, beneath the sternum to push the depressed sternum outwards (Iida, 2010; Lopushinsky and Fecteau, 2008; Nuss, 2008; Nuss et al., 1998). The pectus deformities are normally identified by clinical manifestations with the deformity worsening throughout adolescence. In many cases, surgical intervention is mainly performed for deformities causing physical and physiological complications but mainly is sought for "cosmetic" reasons. The categorization as a cosmetic procedure denies patients from the surgical correction which can have severe psychosocial effects (Kelly et al., 2008). Kelly et al. (2008) found that perceived body image significantly increased while perceived physical difficulties significantly decreased in patients following corrective surgery. Although surgical repairs of pectus deformities have been relatively successful, the etiology of the pectus deformities still remains a mystery. There have been a variety of proposed causes with the two prominent ones being overgrowth of cartilage and weakened cartilage (Brochhausen et al., 2012). However, measurements of relative costal cartilage to rib length ratios revealed no significant differences between individuals with PE and healthy individuals (Nakaoka et al., 2010), suggesting that the deformed cartilage may not be overgrown but weakened.

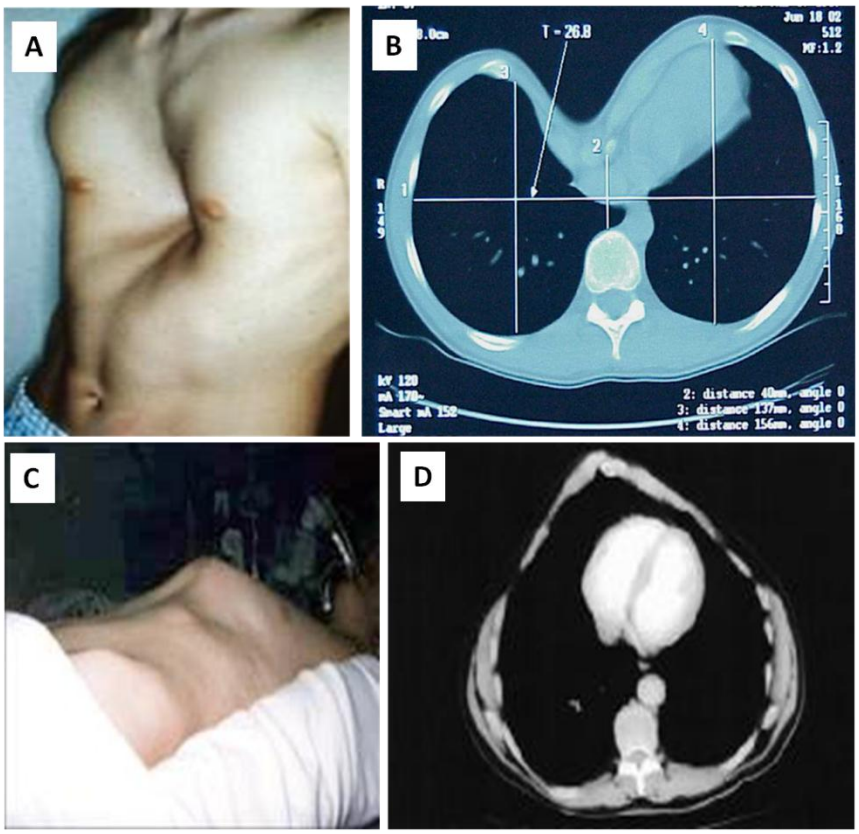

Figure 4. **Images of patients with pectus excavatum and pectus carinatum.** Images of patients preoperatively with PE and PC (A and C, respectively) as well as corresponding CT scans (B and D, respectively).

1.7 Ion Channels

Ion channels are pore-forming transmembrane proteins that regulate ion transport through the cell membrane and play an integral role in cell homeostasis by detection of and response to extracellular changes or stimuli (Barrett-Jolley et al., 2010). There are many known ion channels which are normally grouped by the ion they select for and subgrouped by their structure, gating properties, or direction of ion movement. For instance, channels involving potassium are grouped as potassium channels and can be subgrouped based on structure/function such as

voltage-gated or inwardly rectifying channels with additional types including calcium-activated and tandem pore domain potassium channels (Gopalakrishnan et al., 2006).

More recently, ion channel expression in cartilage has become a growing field in differentiation, homeostasis, and involvement in osteoarthritis. The different ion channels expressed in a cell or tissue are collectively known as the ion channelome or just channelome. Expression of a range of ion channels in hyaline cartilage have been identified using a variety of assays in different animal sources (Barrett-Jolley et al., 2010).

Potassium Channels

Potassium channels are channels that selectively transport potassium ions. They can be subgrouped into four main classes based on the structure/function of the ion channel with the structure of the channel conferring the function of the channel. These structural groupings are based on the number of transmembrane (TM) domains and P-loop (P) motifs formed (Fig. 5). The P-loop, also known as a Walker motif, spans the pore between two transmembrane domains and contributes to ion selectivity, more commonly referred to as the selectivity filter. The functional channels are typically a homo- or hetero-tetramers with associated nonpore-forming subunits which modulate the channel's biophysical properties (Choe, 2002; Gonzalez et al., 2012; Tian et al., 2014).

The first class is the 2TM/P, meaning that there are two transmembrane domains with a single pore (Fig. 5 A). The 2TM/P class is also known as the class of inwardly rectifying potassium channels (K_{ir}). The K_{ir} channels form tetrameric channels encoded by 15 different genes split into seven subgroups ($K_{ir}1.x$ - $K_{ir}7.x$) (Gonzalez et al., 2012). The channels, in excitable cells, function in long depolarization by blocking the efflux of K^+ ions in the

depolarized state which assists in tuning the depolarization of cells (Hibino et al., 2010). Additionally, some of the channels are also known as K_{ATP} channels because they are gated by intracellular ATP. The K_{ATP} is a combination of $K_{ir}6.x$ subunits combined with sulphonylurea receptor (SUR) subunits to form a functional K_{ATP} channel (Mobasheri et al., 2012).

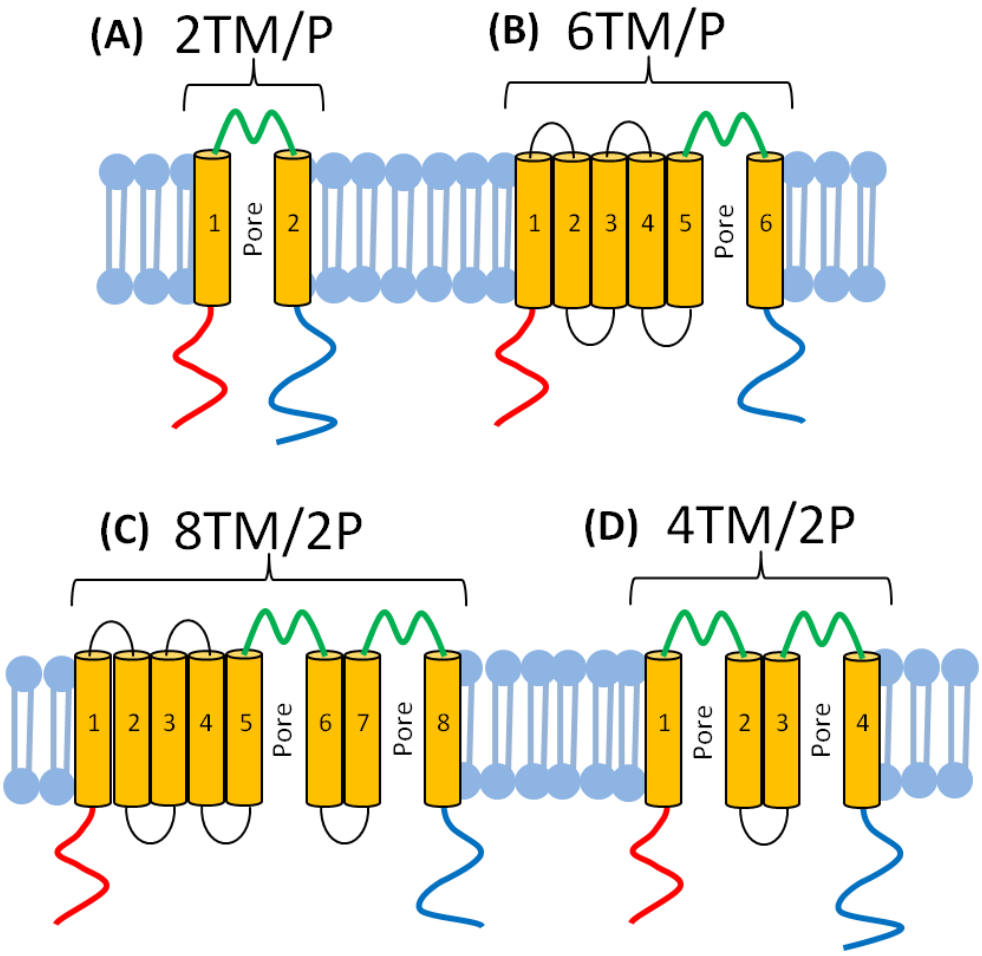

Figure 5. **Representation of the four main structural classes of potassium channels.** The channels are shown with their amino terminus (red), carboxyl terminus (blue), the transmembrane domains (TM; orange), and P-loops (P; green). (A) The 2TM/P channels are normally known as the inward rectifying potassium channels (K_{ir}). (B) The 6TM/P channels,

which comprise the bulk of potassium channels, are predominantly voltage-gated potassium channels (K_V channels) and also include calcium-gated potassium channels (KCa channels). However, the BK channel (KCa1.1) has an additional TM as well as an extracellular amino terminus. (C) The 8TM/2P is a hybrid between the 2TM/P and 6TM/P channels, but has only been observed in yeast. (D) The 4TM/2P channels are known as the tandem pore potassium channels (K2p channels). Adapted from Choe (2002), Gonzalez et al. (2012), and Tian et al. (2014).

The next class of potassium channels are the 6TM/P channels. They follow the canonical architecture of the K_{ir} channels, but have four additional transmembrane domains preceding the 2TM/P structure (Fig. 5 B). This class of potassium channels make up the voltage-gated (K_V) and other ligand-gated potassium channels such as the K_{Ca} and Slo channels. The K_V's are encoded by 40 different genes split into 12 subgroups (K_V1.x - K_V12.x) while the K_{Ca} channels are encoded by eight different genes with five subgroups (K_{Ca}1.x - K_{Ca}5.x). 6TM/P channels typically form homo- or hetero-tetramers. It is important to note the K_V5, 6, 8, and 9 alone do not form functional channels but, however, form heteromultimers with other functional K_V's and instead modulate the properties of the formed channel (Choe, 2002; Gonzalez et al., 2012; Tian et al., 2014).

The K_{Ca} channels are calcium-gated potassium channels and can be classified into three main groups based on their conductance. The three groups are BK (big conductance), IK (intermediate conductance), and SK (small conductance) channels. These channels activate based on intracellular concentrations of free calcium or through calcium bound to calmodulin. The BK

channels are slightly different in that they have an extracellular amino terminus along with an additional transmembrane domain (Fig. 6). The BK channel's carboxyl terminus is also different in that it is long with two, large calcium sensing domains known as RCK1 and RCK2 (Gonzalez et al., 2012; Gueguinou et al., 2014; Sah and Faber, 2002).

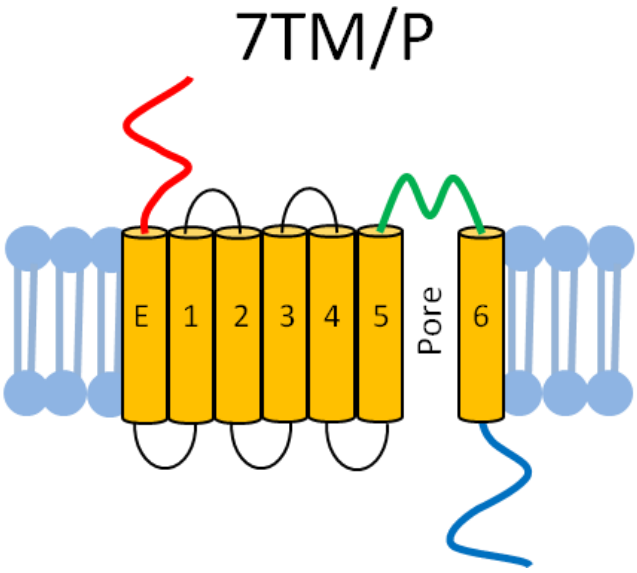

Figure 6. **Structure of the BK channel.** The BK channel, although classified as part of the 6TM/P channels, is a 7TM/P channels. It is similar to the 6TM/P channels, except that it has an additional transmembrane domain (labeled E) with an extracellular amino terminus. Also, its carboxyl terminus is extended with two additional subdomains known as RCK1 and RCK2 which are involved with calcium sensing (Gonzalez et al., 2012).

Another class of potassium channels are the 4TM/2P channels, also known as the two-pore, or tandem pore, domain channels (K_{2p}). These channels are referred to as background or

leak channels as they are considered voltage- and time-independent and function based on asymmetric K^+ levels. The K_{2p} channels are encoded by 14 genes with six subgroups (TWIK, TREK, TRESK, TASK, TALK, and THIK). Unlike the 2TM/P and 6TM/P channels, K_{2p} channels form dimers (Enyedi and Czirjak, 2010). The last class of potassium channels are the 8TM/2P, which are a hybrid between the first two classes. These channels, thus far, have only been identified in yeast (Tian et al., 2014).

Calcium Channels

Calcium channels can be grouped into three functional groups, voltage-operated calcium channels (VOCCs), receptor-operated calcium channels (ROCCs), and store-operated calcium channels (SOCCs). The VOCCs are found in the cell membrane and mediate influx of calcium in response to changes in the membrane potential. VOCCs can be further classified into five subclasses based on the electrophysiological signature (electrical current): L-type, T-type, P/Q-type, N-type, and R-type. The two main subclasses are the L-type and T-type voltage-dependent calcium channels. The L-type channels are channels that produce large currents through "slow" gating kinetics meaning the channel allows for a long-lasting flow of ions (>500 msec), hence the "L" in L-type. The L-type channels have a high voltage activation with a threshold activation of -30 to -10 mV and an inactivation range of -60 to -10 mV. The L-type channels are labeled as $Ca_V1.x$ such as $Ca_V1.1$, $Ca_V1.2$, $Ca_V1.3$, and $Ca_V1.4$. T-type channels produce small currents and have "fast" gating kinetics (20-50 msec). T-type channels have a low voltage activation with a threshold activation of -70 mV and an inactivation range of -100 to -60 mV. T-type channels are labeled as $Ca_V3.x$ such as $Ca_V3.1$, $Ca_V3.2$, and $Ca_V3.3$ (Bean, 1989; Bourinet et al., 2014; Yamakage and Namiki, 2002).

The ROCCs are channels which respond to a receptor-based agonist stimulating the channel resulting in a flux of calcium. There are two main types of ROCCs, IP_3R (inositol 1,4,5-trisphosphate receptor) and RYR (ryanodine receptor). Both IP_3R and RYR have three isoforms (IP3R1-3 and RYR1-3) and localize in the endoplasmic reticulum to facilitate calcium release from internal stores (Lanner et al., 2010; McFadzean and Gibson, 2002; Striggow and Ehrlich, 1996).

Store-operated calcium entry has been observed in many tissues and processes using electrophysiological means; however, the channels involved were unknown for quite some time. Currently, the channels identified are encoded by three genes, ORAI1, 2, and 3. These channels are also known as calcium release-activated channels (CRAC), with their contributing electrophysiology labeled as CRAC currents. The ORAI channels function by forming a complex with STIM (stromal interaction molecule), which acts as a calcium sensor within the cell. The STIM proteins are encoded by two genes, STIM1 and STIM2. Together, the ORAI-STIM protein complex functions by detecting when calcium from the endoplasmic reticulum is released and induces an influx of calcium through the plasma membrane (McFadzean and Gibson, 2002; Prakriya and Lewis, 2015).

Chloride Channels

Chloride channels are abundantly expressed in a variety of tissues and cell types with their channels grouped by structure or biophysical property. Currently, there are three distinct groups of chloride channels: the CLC family, the cystic fibrosis conductance regulator (CFTR), and ligand-gated GABA- and glycine-receptor chloride channels. There are additional channels that do not neatly fall into a specific class based on structure. Instead, these channels have been

grouped based on biophysical properties. Additionally, there is evidence of several more chloride channels existing based on electrophysiological measurements, but their corresponding proteins or encoding genes have yet to be identified (Jentsch et al., 2002).

The CLC family of chloride channels is one of the more ubiquitous ion channels encoded by nine genes. The CLC proteins are fairly large with only a limited elucidation of its three-dimensional structure. The CLC channels can be placed into three subgroups based on sequence homology, and the CLC family is a mix between channels localized in the plasma membrane and intracellular membranes. Though, during certain processes some of the intracellular membrane channels can translocate to the plasma membrane. The CLC channels are thought to be mostly, if not entirely, gated by voltage. Some of the CLC channels are specific to certain tissues, such as CLC-1 in skeletal muscle and CLC-5, Ka, and Kb in kidney, while others show broad expression, CLC-2, 3, 4, 6, and 7 (Chen, 2005; Jentsch et al., 2005).

The CFTR channel is encoded by a single gene, but is structurally different from other chloride channels, placing it in its own family. It has been well characterized with the structure composed of 6 transmembrane domains and a nucleotide binding fold (NBF) regulated by a domain rich in phosphorylation sites. CFTR is widely expressed and not only functions as a transporter, but also is capable of regulating other ion channels (Cant et al., 2014; Liang et al., 2010).

Sodium Channels

The sodium channel family is comprised of two major types, epithelial sodium channel (ENaC) and voltage-gated sodium channel (VGSC). The ENaC group, a part of the denegrin/ENaC (Deg/ENaC) superfamily, are ligand-gated sodium channels normally found in

the epithelial lining of tissues in the body. The family has nine paralogs which are typically grouped into two families, ENaC and acid-sensing ion channel (ASIC). The sodium selective ENaCs are encoded by four genes in humans (SCNN1A, B, D, and G). These four genes correspond to the four protein subunits which make up the ENaC channel (ENaC alpha, beta, delta, and gamma) (Hanukoglu and Hanukoglu, 2016). The ASICs are encoded by five genes with two splice variants forming seven ASIC subunits (ASIC1a, 1b, 2a, 2b, 3, 4, and 5). It is important to note that although ASICs are part of the ENaC superfamily, they are actually non-selective cation channels permeable to calcium along with sodium (Boiko et al., 2014; Kweon and Suh, 2013). More information about ASICs can be found below in the section on non-selective channels (Section 1.7.5).

The major type of sodium channels are the voltage-gated sodium channels. The VGSCs are encoded by 13 different genes which produce nine pore-forming subunits ($Na_V1.1$-1.9) as well as four beta subunits ($Na_V\beta$1-4) (Kruger and Isom, 2016). VGSCs are important in the electrogenesis in excitable tissues such as muscle and neurons, however, these channels are also expressed in a number of non-excitable tissues. Their functions in non-excitable tissues is not always as an ion channel with the β-subunits capable of functioning as cell adhesion molecules (Brackenbury and Isom, 2008).

Non-selective Channels

Non-selective channels include any channels that are not selective for any specific ion, but instead allow the flow of different anions or cations. The major group of non-selective channels are the transient receptor potential (TRP) channels. The TRP channels have three major subtypes: TRPC, TRPM, and TRPV channels. The TRP channels are a family of cation channels

responsible for a variety of signaling processes and response cascades. The TRP channels were originally cloned in *Drosophila melanogaster* (Montell and Rubin, 1989), and all the closely related channels are referred to as canonical TRP channels or TRP-Canonical (TRPC). The TRPC channels are encoded by seven different genes (TRPC1-7) and are involved in store-operated channels as well as secondary messenger processes (Vazquez et al., 2004; Zheng, 2013). The second major group are the TRPM channels named after the first channel identified in melanocytes named melastatin (Duncan et al., 1998). The TRPM subfamily is encoded by eight different genes (TRPM1-8) with a variety of functions including cold receptors, calcium-activated and magnesium-activated cation channels, and osmo-sensitive channels (Harteneck, 2005; Zheng, 2013). The third subfamily are the vanilloid TRP channels (TRPV) encoded by six different genes (TRPV1-6) capable of forming homomeric and heteromeric complexes. The TRPV1-4 are cation channels that are weakly to moderately selective for Ca^{2+}, while TRPV5 and TRPV6 are cation channels that are strongly selective for Ca^{2+} (Zheng, 2013). The TRPV1-4 channels can be activated by different stimuli, but are mainly thermo-sensitive (Voets et al., 2004). Besides the external stimuli capable of activating TRPV channels, it has been found that TRPV channels are also regulated by intracellular calcium levels through calmodulin binding sites (Holakovska et al., 2011; Lambers et al., 2004; Rosenbaum et al., 2004; Strotmann et al., 2003; Xiao et al., 2008). Of all the TRPV channels, TRPV1 and TRPV4 are able to detect a wide range of stimuli including pH, ATP, mechanical stress, and osmotic swelling/stretch (Pedersen et al., 2005; Zheng, 2013).

Another group, previously mentioned, are the ASIC channels. The ASIC channels are members of the Deg/ENaC superfamily which are paralogous to the sodium channels ENaC. The ASIC channels have seven proteins (ASIC1a, 1b, 2a, 2b, 3, 4, and 5) encoded by five separate

genes with two additional splice variants (Hanukoglu and Hanukoglu, 2016; Kweon and Suh, 2013). Little is known of ASIC4 and ASIC5, but when referring to ASICs, ASIC4 and ASIC5 are not included due to their lack of acid sensitivity in a homo- or hetero-meric channel (Boiko et al., 2014; Schwartz et al., 2015). The ASIC channels are mainly permeable to sodium, though can also allow calcium to pass through. Although calcium permeability is low, extracellular acidosis causes enough calcium to enter the cell to generate transients large enough to induce cell death through apoptosis (Hu et al., 2012; Li et al., 2014). Each ASIC subunit is comprised of two transmembrane domains with an extracellular pore-loop and an intracellular amino and carboxyl terminus with the functional ASIC channel consisting of a homomeric or heteromeric trimer. The different ASICs have different activation pHs, with ASIC1a sensitive to pHs 5.8-6.8, ASIC1b to pHs 6.1-6.2, ASIC2a to pHs 4.5-4.9, and ASIC3 to pHs 6.4-6.6. ASIC2b does not form a functional homomeric channel but modulates channel activity in a heteromeric channel (Wemmie et al., 2013; Zhou et al., 2016). The pH ranges are indicative of the pHs at which the respective channels are half-activated, meaning they are still capable of activity outside their respective ranges.

Ion Channels in Cartilage Maintenance

Chondrocytes are the only resident cells in cartilaginous tissue and are responsible for the production and maintenance of the ECM making up a majority of the tissue. The maintenance is dependent on a multitude of extracellular stimuli such as mechanical forces, growth factors, osmolarity, and pH among others. Other than some of the more traditionally known receptors detecting extracellular growth factors (e.g. TGFβ and BMP receptors), ion channels are capable of detecting a variety of changes in the cell's microenvironment. These ion channels activate,

resulting in the transduction of a signaling cascade commonly invoking changes in the cell's membrane potential, intracellular calcium transients, and ATP fluxes. The downstream effects are changes in the production of new ECM and enzymes which break down the old ECM which help maintain the tissue (Asmar et al., 2016; Barrett-Jolley et al., 2010).

Chondrocytes have very limited mitotic potential in comparison to most other cells, and tissue growth in articular cartilage normally occurs through the addition of ECM causing cells which are in close proximity to become distanced. These islands in a sea of ECM are known as isogenic groups because the clusters of cells come from a single cell which has undergone mitosis over the lifetime of the tissue. The regulation of growth and differentiation has been shown to be influenced by multiple different channels. Specifically, blocking of Ca_V channels by nifedipine and Na_V channels with tetrodotoxin eliminated or significantly reduced the level of differentiation of primary chondrocytes cultured in 3D scaffolds under dynamic mechanical loading (Wu and Chen, 2000). In chicken chondroprogenitor mesenchymal stem cells grown in high density cultures and grown into mature cartilage, blocking of Ca_V channels by nifedipine as well as the non-selective Ca^{2+} cation channels by lanthanum chloride disrupted normal calcium oscillations associated with tissue growth and differentiation resulting in decreased production of ECM (Fodor et al., 2013). Growth of costal cartilage is not a well-known process, but it is assumed to follow the same growth methods as articular cartilage.

Studies on ion channels and disease in cartilage have mainly focused on the development and progression of osteoarthritis (OA). Many different ion channels have been identified as being dysregulated in OA-affected chondrocytes. However, it is not known if the resulting expression changes are the underlying cause of OA, or if the changes were influenced by the change in the osmolarity of the synovial fluid (Lewis and Barrett-Jolley, 2015). Ion channels are also thought

to be involved in other skeletal diseases, though there is limited investigation into their contribution to the pathogenesis of other diseases.

Ion Channels in Mechanotransduction

There are a number of channels which detect biomechanical stimuli and induce mechanotransduction using different methods (Fig. 7). Mainly, it is a based on a mechanical force or stretching causing a shift in the conformation of a channel leading to activation. The responses or ion fluxes vary based on the different channels involved. A common result of mechanotransduction is the formation of a calcium transient. This increase in intracellular calcium induces a calcium positive feedback through activation of calcium-dependent potassium channels which depolarize the membrane and facilitate calcium influx by voltage-activated calcium channels (Steward et al., 2014). The resulting electrophysiological change is known as the mechanically activated (MA) current.

One group of mechanosensitive channels are called Piezo channels which are made up of two channels, Piezo1 and Piezo2. These channels are unique in that they are not related to any other ion channel, but instead were not classified as ion channels nor even known to form transmembrane channels until recently (Coste et al., 2012). The Piezo1 and Piezo2 channels are large proteins (~2500 and ~2800 amino acids, respectively) forming a homotrimer with up to 40 transmembrane domains per subunit. The Piezo channel's mechanotransduction functions mainly by allowing the flow of calcium in response to mechanical stimuli (Lee et al., 2014).

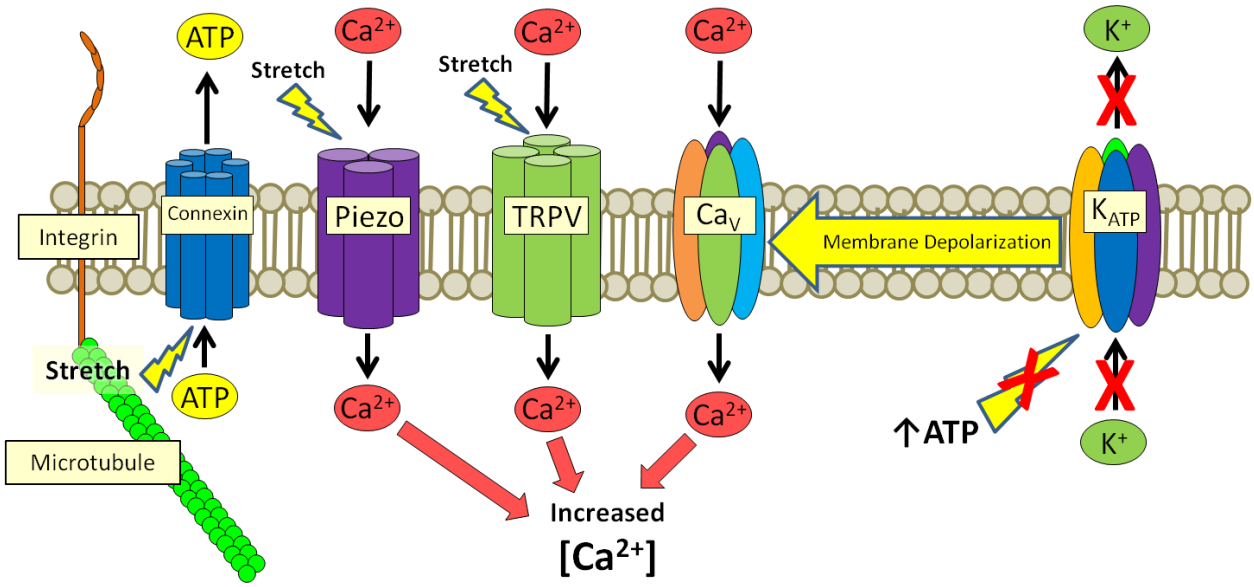

Figure 7. **Schematic showing the multiple channels involved in mechanotransduction in cartilage.** The channels include connexins, Piezo channels, and TRPV channels. Connexins are activated by its interactions with cytoskeletal and adhesion proteins (Giepmans, 2004; Knight et al., 2009). The ultimate result being the formation of a calcium transient which then can cause increases in ATP and blocking K_{ATP} channels further depolarizing the membrane and activating additional calcium influx by Ca_V channels (Mobasheri et al., 2007).

One of the main ion channels involved in mechanotransduction is the TRPV4 channel. TRPV4 is characterized as a "stretch" channel, meaning that the channel is activated due to conformational changes induced by the forces of the membrane, such as swelling which pulls on the channel. TRPV4 is a versatile sensor in that it functions as a mechanosensor, osmosensor, and thermosensor as well as a contributor to normal calcium homeostasis. The activation of TRPV4 causes an influx of calcium and formation of a calcium transient (O'Conor et al., 2014; Pedersen et al., 2005).

Connexins are also capable of playing a role in mechanotransduction. Connexin hemichannels bind to cytoskeletal and adhesion proteins such as actin, microtubules, integrins, and cadherins (Giepmans, 2004). This interactions allows connexins to indirectly detect mechanical stress on a cell and become activated. Mechanical stress-induced integrin signaling is able to activate connexins resulting in ATP released by the cell into the extracellular environment (Batra et al., 2012; Knight et al., 2009). The extracellular ATP, in turn, can activate downstream channels which contribute to increased intracellular calcium (Garcia and Knight, 2010; Plotkin et al., 2015).

A group of mechano-sensitive channels are the voltage-gated sodium channels (Na_V) as these channels are do not properly fit the definition of mechanoreceptors. While these channels are gated by voltage, membrane stretching can significantly accelerate the channel kinetics (Morris and Juranka, 2007). Na_V channels are known to have variable mechanics dependent on lipid bilayer properties. However, $Na_V\beta$ subunits are also able to bind focal adhesion proteins and aid in mechanical stress detection, potentially translating mechanical stress to modulation of Na_V channel kinetics (Isom, 2001; Kruger and Isom, 2016). The role of Na_V channels in mechanotransduction and its contribution to the MA current is still relatively unknown.

Ion Channels in Osmotic Sensing and Response

Most of the ion channels in chondrocytes activate and function depending on changes in the membrane potential. However, the membrane potential is modified by certain channels which activate a cascade of ion channels to help maintain homeostasis. Important examples of this are regulated volume increase (RVI) and regulated volume decrease (RVD). When an osmolar shift occurs, hypertonic or hypotonic conditions cause the cell to shrink or swell due to osmosis. In

response, certain channels become activated and lead to a shift in the membrane potential which causes the activation of other downstream channels. This activation is part of a process to prevent permanent damage caused by the osmolar swelling and shrinking. In order to prevent further swelling or shrinking, ions are pumped out of or into the cell, respectively, which reduces the flow of water into (RVD) or out of the cell (RVI). These processes have been explored at a biophysical level with contributing currents from chloride, sodium, and potassium channels (Lewis et al., 2011a; Lewis et al., 2011b).

Chondrocytes are equipped with a range channels capable of detecting changes in the extracellular osmolarity. Changes in osmolarity occur due to the flow of water and ions from external forces such as compressive forces with the changes commonly resulting in two different situations. One situation is where a decrease in the extracellular concentration of ions results in hypo-osmotic stress on the cell, meaning that the cell will have a driving force to bring water within the cell to match the extracellular osmolarity (Fig. 8). Hypo-osmotic stress results in swelling of the cell, where in situations of an extreme dilute extracellular environment results in the cell bursting. Detection of hypo-osmolarity can result from two main methods, ion stimulation and stretch-activation. The change in extracellular osmolarity combined with the diffusion of water into the cell causes a change in the membrane potential. Changes in the membrane potential activates voltage-gated channels and normally induces the formation of a calcium transient which activates downstream signaling including calcium-activated channels (Lewis et al., 2011a). The second method, stretch activation, involves channels which detect the forces of membrane stretching and then transduces the biomechanical force. The common response by stretch-activated channels are intracellular calcium transients which induces downstream responses. The activation of downstream ion channels causes an efflux of ions,

raising the osmolarity of the immediate extracellular environment while lowering the intracellular osmolarity which reduces the influx of water (Martina et al., 1997; Mobasheri et al., 2010). The ultimate result by both these methods is to reduce the damage caused by cellular swelling. This response is referred to as regulated volume decrease (RVD), pertaining to the controlled mechanism of counteracting the osmotic swelling by reducing the volume increase.

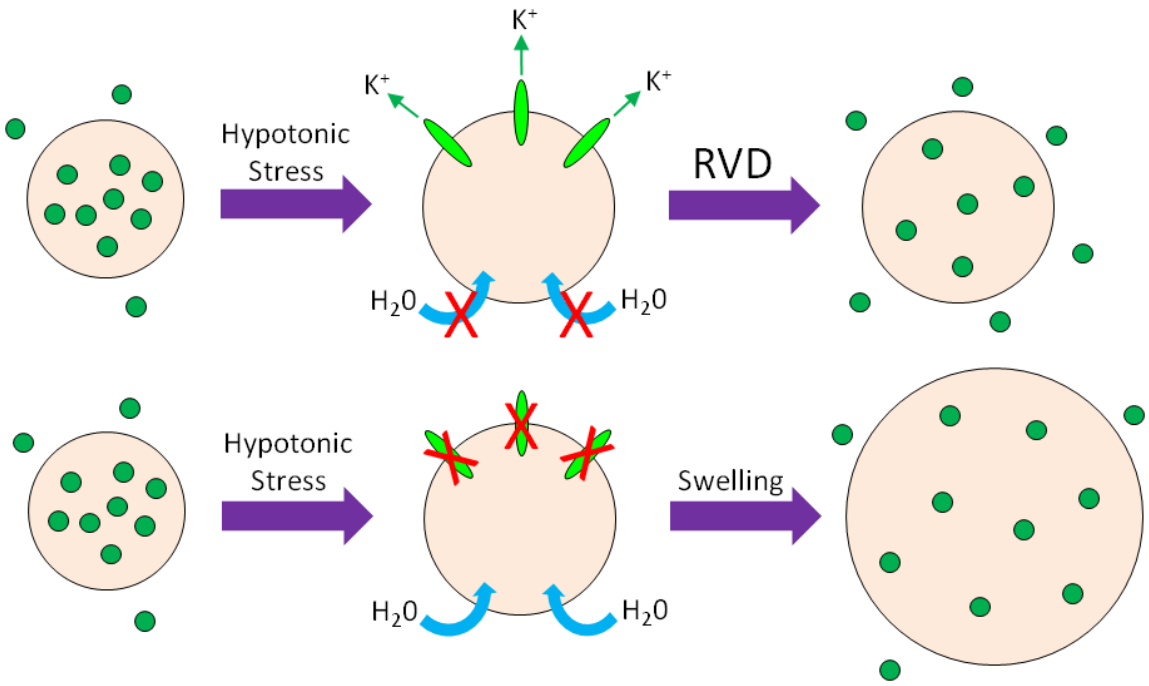

Figure 8. **Schematic of regulated volume decrease (RVD).** As cells are challenged by an environment with a lower osmolarity, a hypo-osmolar stress occurs. This stress causes water to diffuse into the cell; however, flux of ions, mainly potassium, out of the cell offsets the difference in osmolarity and reduces the amount of swelling.

Conversely, hypertonic stress is the elevated extracellular ion concentration which induces the efflux of water from the cell causing the cell to shrink (Fig. 9) (Hall et al., 1996b). In an opposite fashion to RVD, hyperosmolar stress response prevents the shrinking, called regulated volume increase (RVI). However, there is no consistent evidence of RVI occurring *in vivo*, as it has mainly been observed *in vitro* (Lewis et al., 2011b). This could be possible because of the cells being anchored to the surrounding matrix within the tissue which may help mitigate the shrinkage.

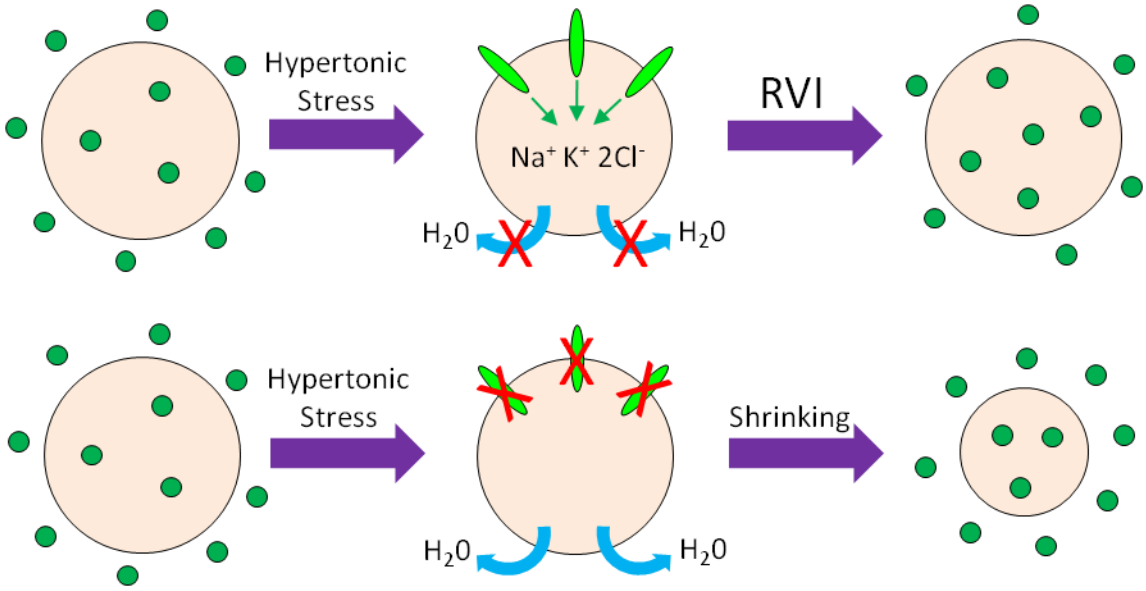

Figure 9. **Schematic of regulated volume increase (RVI).** As cells are challenged by an environment with a higher osmolarity, a hyperosmolar stress occurs. This stress causes water to diffuse out of the cell; however, flux of ions into the cell offsets the difference in osmolarity and reduces the amount of shrinkage.

Ion Channels in pH Sensing and Response

Extracellular acidosis commonly occurs in cartilage due to the flow of water and ions due to different forces experienced within the tissue. The change in pH is mainly detected by the acid-sensing ion channels (Fig. 10). The ASICs are sensitive to changes in pH through extracellular receptors which bind hydrogen ions. Though, other ion channels which have walker loops containing extracellular histidines can be modified by hydrogen ions to become more active in low pH environments. The response through activation of ASICs creates a cascade ultimately dependent on the formation of intracellular calcium transients. The activated ASIC causes an influx of sodium and calcium which increases the intracellular calcium levels as well as depolarization of the membrane. The membrane depolarization can activate voltage-gated calcium channels and increase the influx of calcium. Additionally, the increased intracellular calcium levels can activate calcium-dependent potassium channels, causing the membrane to be further depolarized. The intracellular calcium levels can cause downstream changes in gene expression, though an excessive amount of intracellular calcium will induce cell death through apoptosis in chondrocytes (Li et al., 2014; Rong et al., 2012; Zhou et al., 2015). Low pHs are known to cause a decrease in ECM production (Yuan et al., 2010), however, Kolker et al. (2010) found that ASIC response to acidosis lead to increased hyaluronan production in chondrocytes.

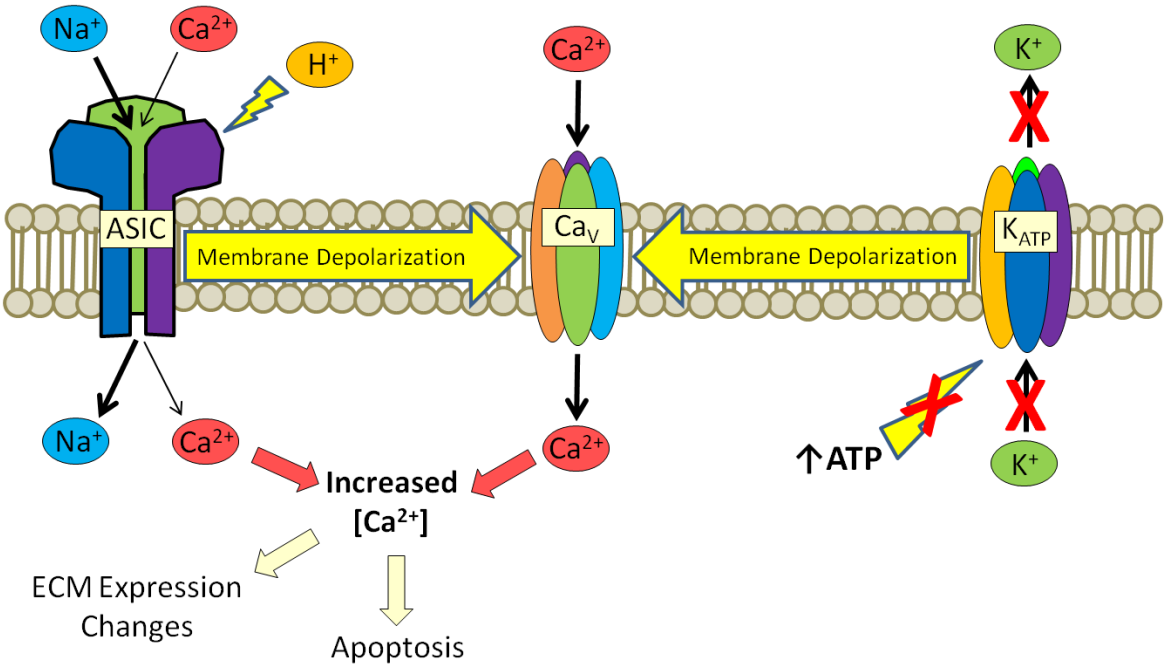

Figure 10. **Schematic of cell response to external acidosis. ASICs are activated by external hydrogen ions and cause a flux of sodium and calcium.** The influx of sodium causes the membrane to become depolarized leading to activation of Ca_V channels which bring in calcium. The calcium transient which then increases in ATP, blocking K_{ATP} channels and further depolarizing the membrane (Mobasheri et al., 2007). The resulting calcium transient leads to downstream changes in ECM expression, though in cases of high calcium influx, apoptosis is induced.

1.8 Connexins

Connexins are a type of channel that have been studied for their involvement in direct cell-cell communication and electrophysiology but have garnered increasing attention for their involvement in other processes. Connexins are proteins subunits capable of forming homomeric or heteromeric transmembrane channels called connexons (or hemichannels). A gap junction is

when two connexons from opposing cells join to form a cell-cell channel (Fig. 11) (Evans and Martin, 2002). Much of the focus is on gap junctions, however, there has been an expansion in research focusing on the function of the hemichannels individually.

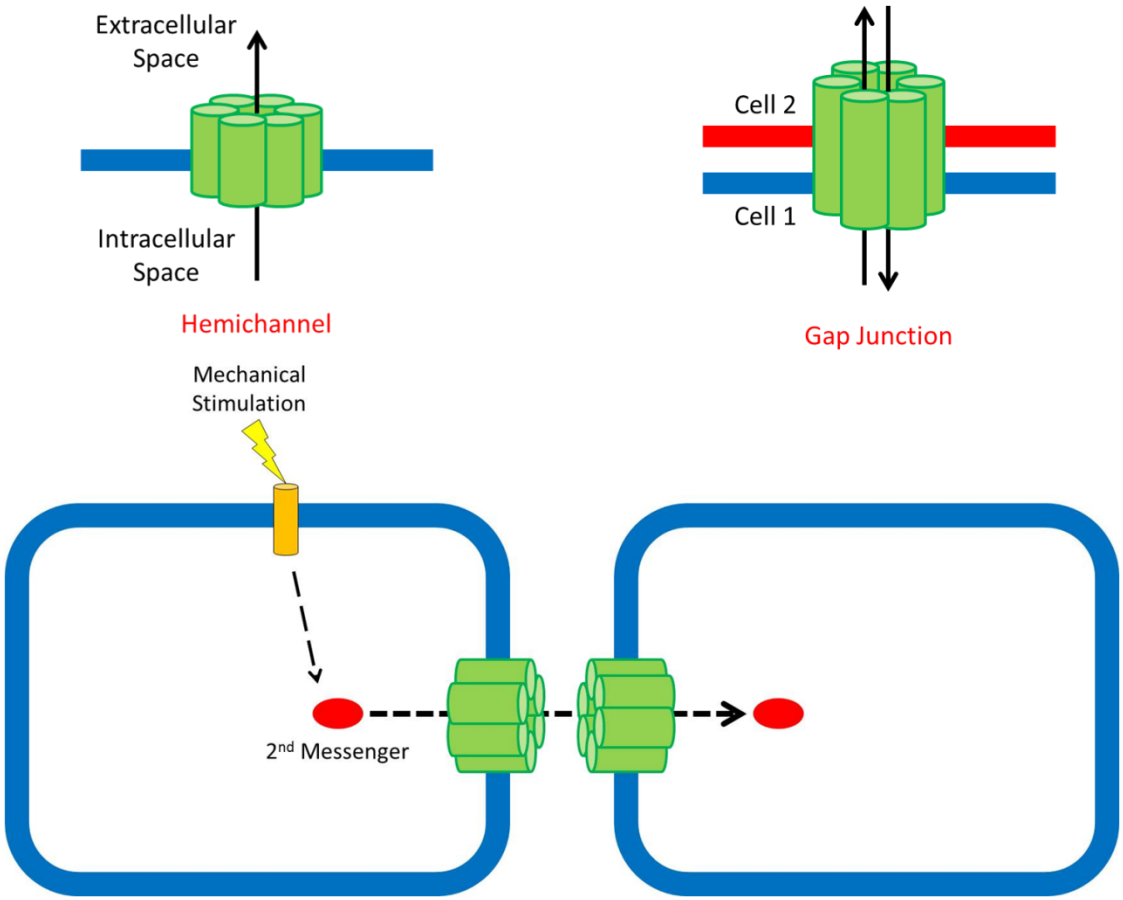

Figure 11. **Schematic of connexins and their function.** Connexins arrange as a homo- or heteromer of six subunits to form a hemichannel allowing for transfer of molecules from within the cell to the extracellular space. Two hemichannels from adjacent cells can bind together to form a bidirectional channel known as a gap junction. The gap junctions are important for the transfer of secondary messengers to other cells following cell stimulation.

Connexins and Gap Junctions

Gap junctions are connections between adjacent cells formed by the joining of individual connexin hemichannels from each cell which enable intercellular communication crucial for signal propagation in the nervous, cardiac, and vascular systems among many others. The junction allows for the passage of ions and metabolites between cells. Gap junctions are the main components involved in signal propagation by electrical synapses in nerves (Evans and Martin, 2002). As opposed to chemical synapses, electrical synapses can have much shorter delay times for signal transfer from one cell to the next. These types of synapses are common in motor neurons in vertebrates and almost exclusive in invertebrates (Szczupak, 2016). In cardiac myocytes, gap junctions are the main mode of signal propagation for contraction in the heart, caused by the diffusion of calcium through gap junctions (Bernstein and Morley, 2006). The vascular system relies on gap junctions for smooth muscle signaling for vasoconstriction and vasodilatation (Martinez et al., 2009).

Connexin Hemichannels

Connexin hemichannels are homomeric or heteromeric transmembrane proteins. Originally thought to be inactive unless as a gap junction, bound to an opposing connexon on another cell, hemichannels are now known to be involved in the transportation of small molecules such as glutamate, ATP, and noncoding RNAs. The hemichannel has garnered increasing interest due to the structural nature of connexins. Connexins have a large carboxyl terminus (CT) containing multiple binding sites for a variety of different proteins as well as multiple phosphorylation sites. Proteins which directly or indirectly bind to the connexin CT include microtubules, filamentous actin, cadherins, and calmodulin (Giepmans, 2004).

Connexin and Ion Channel Association

Sequencing and studies into the connexin 43 carboxyl terminus (Cx43-CT) has found that the Cx43-CT is capable of binding to actin, microtubules, and other structural proteins (Fig. 12). Binding to structural proteins has been linked to the method of connexons linking with adjacent cell connexons. These binding sites also allow for colocalization with ion channels. Connexin 43 can indirectly interact and colocalize with $Na_V1.5$ through N-cadherin and the Na_V beta subunit (Brackenbury and Isom, 2008). The interaction with N-cadherin may be linked to an ability for connexins to be involved in mechanotransduction.

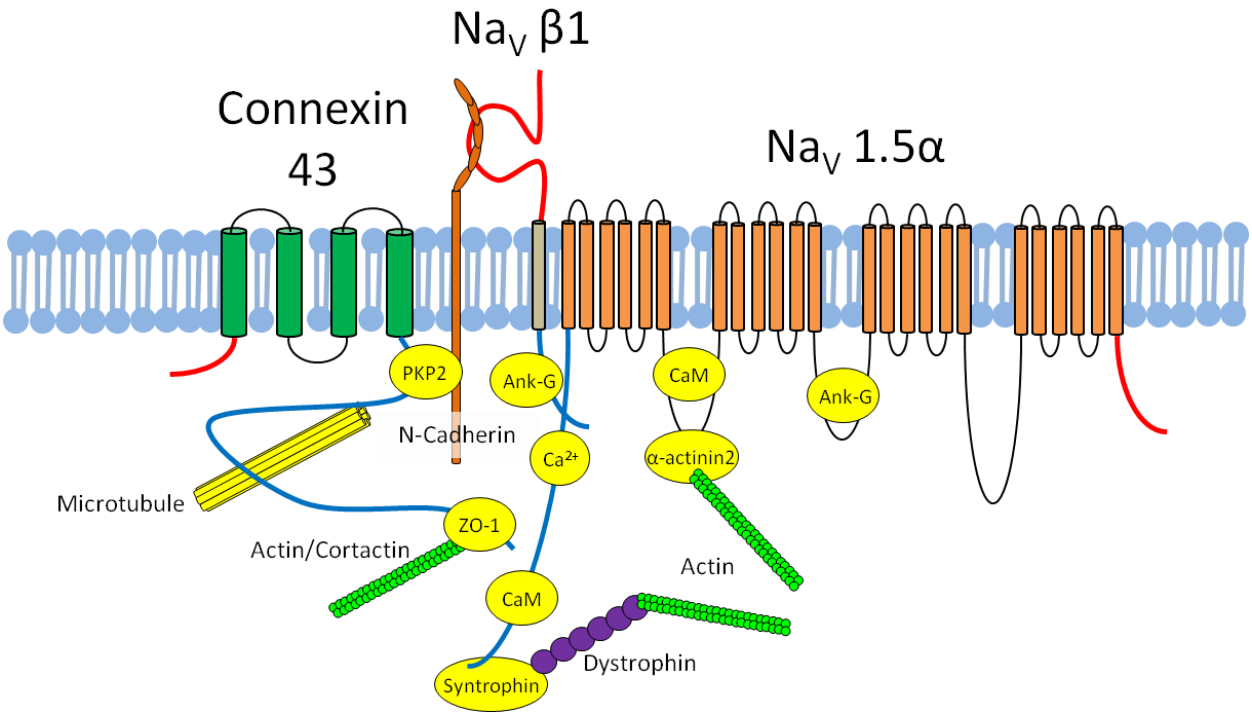

Figure 12. **Illustration of connexin 43 and its association with cytoskeletal proteins, adhesion proteins, and ion channels.** The C-terminus of connexin has multiple binding sites for direct binding of microtubules as well as a PDZ motif for ZO-1 binding which links it to actin/cortactin (Giepmans, 2004). PKP2 also allows for binding to N-cadherin which allows for

indirect association with $Na_V\beta1$ and its alpha subunit (Brackenbury and Isom, 2008). The $Na_V1.5\alpha$ also has multiple binding sites allowing interactions for channel regulation and associations (Rook et al., 2012).

Connexins and the Cell Cycle

Connexins are able to impact the cell cycle through its carboxyl terminus (CT) (Fig. 13). The connexin CT is able to be cleaved and translocate to the nucleus and surrounding area (Dang et al., 2003) where the internalized CT can bind to heat shock cognate protein 70 (Hsc70). This association with Hsc70 has been implicated with failure of cell cycle progression from G1 to S phase (Hatakeyama et al., 2013). The Hsc70-Cyclin D1-CKD4-p27 complex forms close to the nucleus, and then translocates into the nucleus, leading to the progression of the cell cycle from G1 to S phase. Cyclin D1 and CDK4 are required to phosphorylate other proteins within the nucleus to trigger the transition to S phase from G1. The CDK inhibitor, p27, decreases the translocation of the Cyclin D1 complex into the nucleus unless Hsc70 is also present. The internalized connexin CT sequesters Hsc70 which prevents Hsc70 from binding to the Cyclin D1 complex. Cyclin D1 complex is required for G1-to-S phase progression and requires Hsc70 to be present in order to prevent p27 inhibition of CDK4 (Hino et al., 2015). Additionally, the connexin CT has a Cyclin A binding motif which allows it to sequester Skp2, a protein necessary for p27 ubiquitination and G1/S phase progression (Shi et al., 2015).

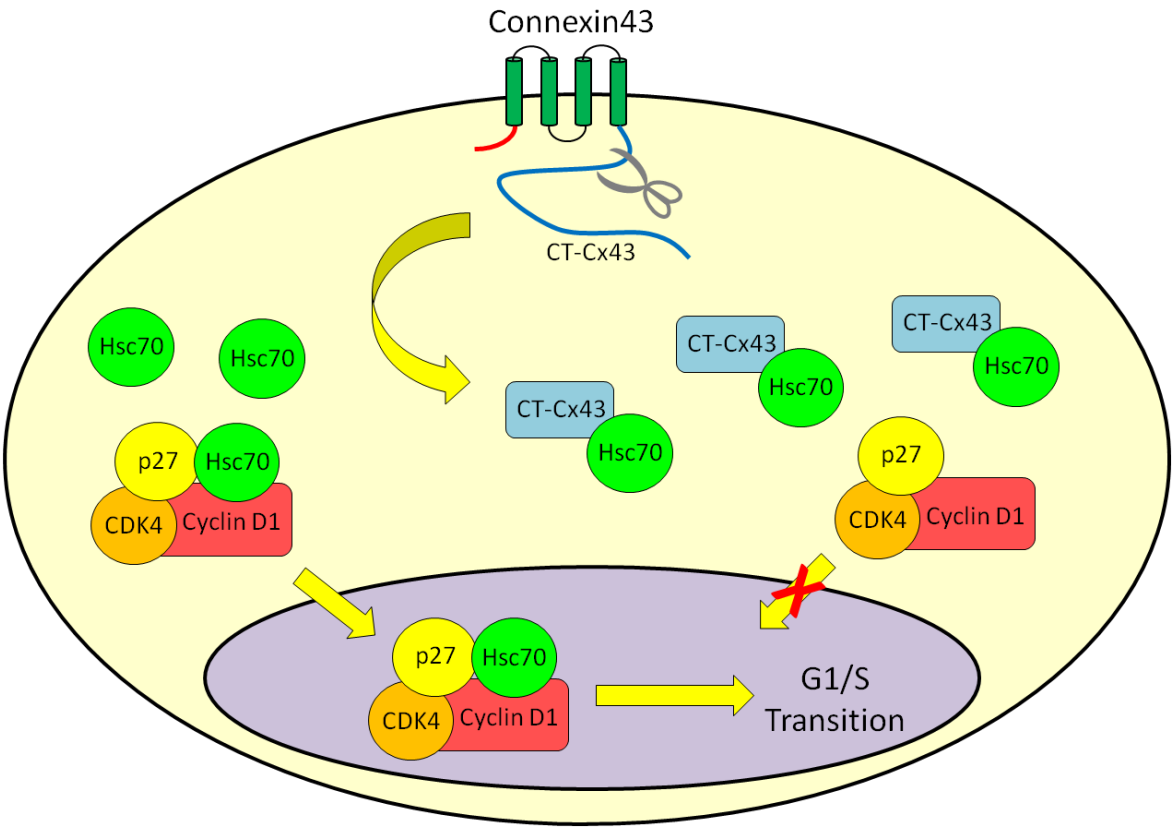

Figure 13. **Diagram of connexin and cell cycle inhibition by Hsc70 sequestration.** The connexin carboxyl terminus (CT) is able to translocate to the nucleus and nuclear region where it can bind to Hsc70. Hsc70 is necessary for G1/S phase transition by allowing for translocation of the Cyclin D1 complex into the nucleus. The sequestration prevents the translocation and inhibits the cell cycle at the G1/S transition.

1.9 MicroRNAs

MicroRNAs are short, stable RNAs of around 20 nucleosides in length and are considered to be a post-transcriptional regulator of protein expression classified as an RNA interfering (RNAi) molecule. They mainly interfere with the translation of an mRNA transcript through complementary binding to a specific sequence of around seven nucleosides, normally in

the 3' untranslated region (3'UTR). The short length and relative non-specificity of microRNAs allows them to bind to a large number of different mRNAs, as opposed to siRNAs targeting a specific mRNA target (Fig. 14). Another difference is that siRNAs cause endonucleolytic cleavage of mRNA, while microRNAs mainly suppress translation through their binding. MicroRNAs are also able to induce mRNA cleavage if the microRNA sequence is highly complementary to the mRNA (Lam et al., 2015; Shukla et al., 2011).

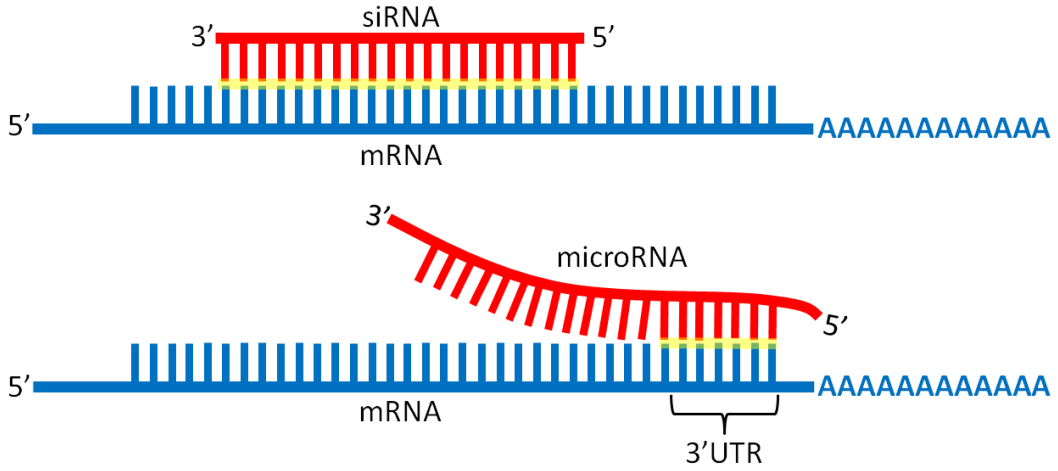

Figure 14. **Complementary binding of siRNAs and microRNAs to mRNA.** SiRNAs and microRNAs are around the same size, however, (A) siRNAs bind to mRNAs which are fully complementary while (B) microRNAs are partially complementary to the 3' untranslated region of a target mRNA.

MicroRNA Structure and Production

MicroRNAs are transcribed by RNA polymerase II to produce primary microRNAs (pri-

miRNA) from non-coding intronic regions. A single intron can produce a single microRNA or multiple microRNAs referred to as clusters. The pri-miRNAs is a single RNA strand which folds and pairs with itself resulting in a mainly double strand-like transcript with a loop structure at one end and free, unpaired 5' and 3' overhands on the other end. While still in the nucleus, the pri-miRNA is processed by Drosha to remove the unpaired ends leaving a transcript folded and paired with itself with a loop structure known as the pre-miRNA. Exportin 5 binds with the pre-miRNA which is then processed by DICER to remove the loop structure resulting in a short double-stranded microRNA. A key feature in the structure is a 3' overhang of 2 nucleosides of either UU or TT which is used as an identifier for by the AGO-RISC complex. The double-stranded microRNA forms a complex with RISC and AGO and discards its passenger strand to make a functional microRNA-RISC-AGO complex, known as miRISC, capable of binding to target mRNA (Fig. 15) (Chendrimada et al., 2005; Lam et al., 2015; Shukla et al., 2011).

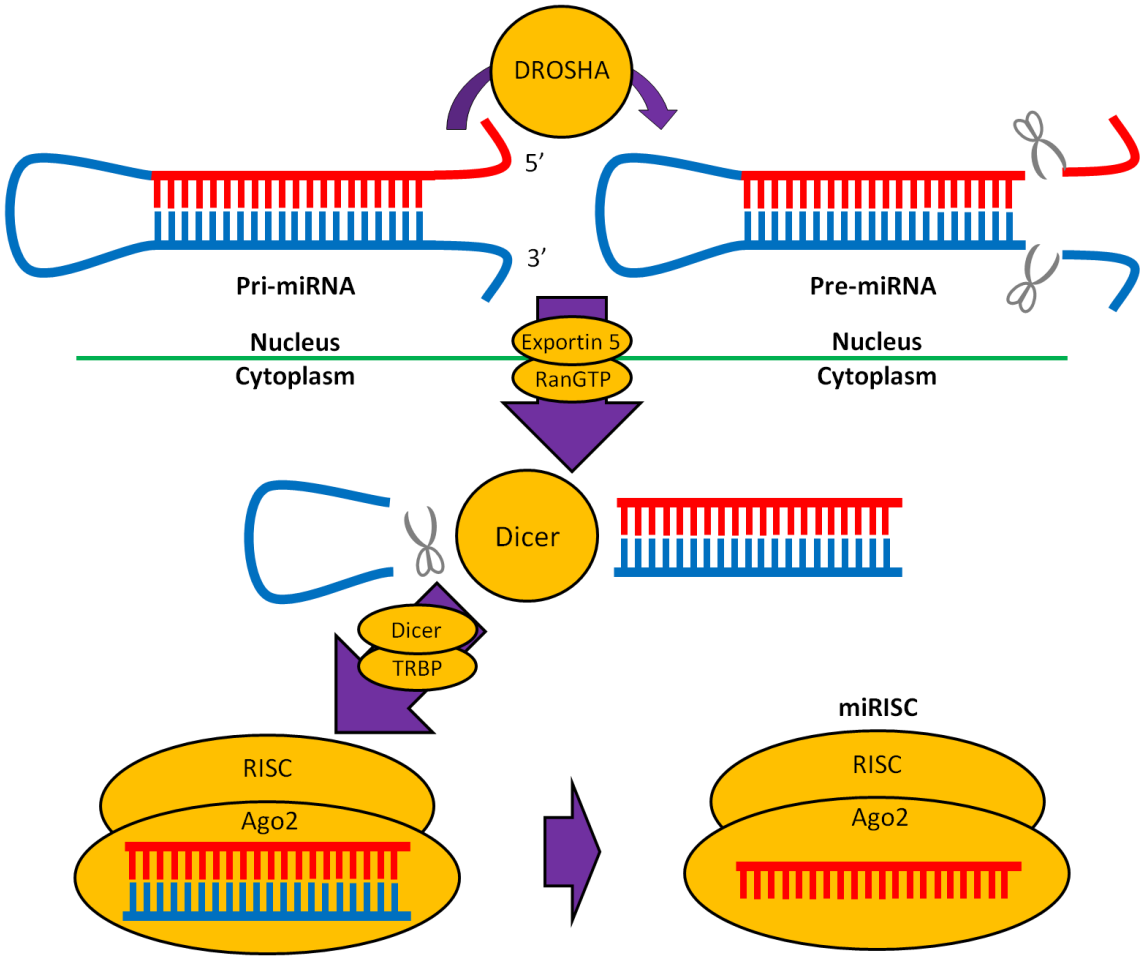

Figure 15. **Diagram of microRNA processing.** The pri-miRNA is transcribed in the nucleus from the intronic regions of genomic DNA. The product after removal of 5' and 3' overhangs is known as pre-miRNA. After exportation from the nucleus, the loop structure is removed by Dicer and the microRNA forms a complex with RISC and Ago2. The passenger strand is removed and the final product is the miRISC complex. Adapted from Chendrimada et al. (2005) and Lam et al. (2015).

MicroRNAs in Post-Transcriptional Regulation

The miRISC partially binds to the 3'UTR of the target mRNA with complimentary binding as low as five nucleosides can result in interrupted translation of the mRNA. This partial complimentary binding also allows for a single miRNA to regulate multiple different mRNAs as opposed to siRNAs requiring full complementary binding (~20 nucleosides) to a single specific mRNA. The partial complementary binding as well as imperfect base pairing can result in a single miRNA sequence binding to over 100 different mRNAs one such example is Mir-124 which is capable of downregulating 174 different genes (Karginov et al., 2007).

Over 60% of protein-coding genes contain conserved miRNA binding sites with the presence of multiple non-conserved sites suggests that most protein-coding genes are able to be regulated by miRNAs. These sites are commonly referred to as microRNA regulatory elements (MRE), and although MREs are normally present in the 3'UTR, there are instances of MREs being present in the 5'UTR or even in the coding sequence. Interestingly, when cells are proliferating, the 3'UTR is shorter with reduced MREs and is likely a process to increase the efficiency of protein translation during proliferation (Bassett et al., 2014; Shukla et al., 2011). Methods of regulation can be categorized as translational repression or mRNA degradation. Translational repression is associated with decapping of the 5' and or 3' ends while degradation can occur by endonucleaic cleavage by miRISC or by deadenylation of the mRNA 3' poly-A tail. Additionally, the miRISC being present in the 5' or 3' MREs may physically block translation of the mRNA by ribosomes. The 3' MRE binding is capable of this due to the mRNA folding to form a loop during translation (Djuranovic et al., 2012; Wilczynska and Bushell, 2015).

CHAPTER 2

METHODS

2.1 Samples

Cartilage samples were obtained from seven human subjects. Informed consent was obtained following Institutional Review Board (IRB) approval of the protocol at Eastern Virginia Medical School (#05-01-EX2027) and ODU (#12-093) and Institutional Biosafety Committee approval at ODU (#13-008). Patients also signed release forms for the disclosure of images for use in scientific publications. Normal costal cartilage was obtained from a 15-year-old male (CON8) and two 17 year old males (CON9 and CON10) and processed within 24 hours. Femoral head articular chondrocytes from a 57-year-old male were purchased from PromoCell (Heidelberg, Germany). Pectus excavatum samples (PE1, PE2, and PE3) were acquired from adolescent patients (17, 14, and 14 years old, respectively) undergoing corrective surgery. Pectus carinatum samples (PC1, PC2, PC3, PC4, and PC5) were acquired from adolescent patients (21, 17, 13, 16, and 15 years old, respectively) undergoing corrective surgery. All cells were cultured in Chondrocyte growth medium (PromoCell). Three fetal samples of costal cartilage were obtained, one from a 37 weeks gestation, live born to an eclamptic mother that died of severe acidosis (F1), a second from a 21 week gestation (F2) born prematurely due to severe chorioamnionitis and funisitis, and a third from a 15 week gestational male with severe congenital cardiac disease (F3). Fetal cells were grown in DMEM/F12 (HyClone, Logan, Utah, USA) supplemented with 10% FBS (Atlanta Biologicals, Norcross, GA, USA), 2 mM L-glutamine (Invitrogen, Carlsbad, CA, USA), 50 IU/mL penicillin (Invitrogen), and 50 mg/mL streptomycin (Invitrogen) at 37°C with 5% CO_2 in air. For experiments, chondrocytes were maintained in suspension culture to maintain their differentiated phenotype, and briefly expanded

in tissue culture flasks. All experiments used cells that had been passaged less than 4 times. Cardiomyocytes were used as controls since their ion channel phenotype is extensively characterized; cardiomyocytes were from a 24 year old Caucasian male (PromoCell) and used as a positive control for cells known to express ion channel genes.

2.2 RNA Extraction and PCR Analysis

RNA was directly isolated from cells in tissue culture dishes, and genomic DNA eliminated using a Direct-zol™ RNA MiniPrep (Zymo Research, Irvine, CA, USA). Complimentary DNA (cDNA) was generated using an RT-First Strand Kit (Qiagen, Valencia, CA, USA). Polymerase chain reactions (PCRs) were performed using SYBR green detection (Qiagen) and customized ion channel array plates (Qiagen) in a BioRad CFX96 system (BioRad, Hercules, CA, USA). These customized plates provide gene expression data on 84 different ion channel-related genes. Manufacturer guidelines were used for PCR reaction volumes and cycle parameters. The cycling parameters were 95°C for 10 minutes, then 40 cycles of 95°C for 15 seconds and 60°C for 60 seconds. Reaction specificities were assessed with a melt curve of 65°C to 95°C in 0.2°C increments. The data was standardized to 5 (*ACTB, B2M, GAPDH, HPRT1* and *RPLP0*) reference gene expression values for all samples using the ΔCq method. Gap junction gene expression was determined using a connexin and pannexin gene array (Qiagen CA, USA), with data standardized to the 5 reference genes described above. Aggrecan and COMP gene expression was by RT-PCR using commercially available primers (Qiagen) and data standardized against 2 reference genes (*GAPDH* and 18srRNA). Gene expression was calculated as $2^{-(Cq_{GOI} - Cq_{Ref})}$, where Cq_{GOI} is the Cq value of the gene of interest and Cq_{Ref}, is the Cq value for the averaged reference genes. The assay range using the RT^2 profiler array

(Qiagen) is 6.8–35 Cq with constant concentration of total cDNA in all reactions, and a raw Cq cutoff of 30 was used.

2.3 Western Blotting

Protein was extracted using a fast, single-step direct lysis method (Philipson et al., 1995). Laemmli buffer (62.5mM Tris-HCL, 25% glycerol, 5% β-mercaptoethanol, 2% SDS, 0.01% Bromophenol Blue, pH 6.8) was added to directly to confluent tissue cultures and allowed to lyse the cells by mixing by pipette. The total homogenates were then boiled at 95°C for 5 minutes and were ready for loading into gels for SDS-PAGE. The sample mixture were loaded into a precast 12.5% Mini-PROTEAN TGX gel (Bio-Rad) and run at 100V constant voltage in running buffer (25mM Tris, 192mM Glycine, 0.1% SDS, pH 8.3). After running the samples, the gel was removed and the protein transferred to a 0.45µm nitrocellulose membrane (Bio-Rad) using a Mini Trans-Blot Electrophoretic Transfer apparatus (Bio-Rad) in chilled transfer buffer (25mM Tris, 192mM Glycine, 20% methanol, pH 8.3) at 100V constant voltage for 1 hour. The nitrocellulose membrane was washed with phosphate buffered saline (PBS), blocked in 5% boiled goat serum (BGS) for 1 hour, incubated with primary antibodies (ASIC2, GAPDH, and Actin purchased from Santa Cruz, Santa Cruz, CA, USA) overnight at 4°C, and then stained using Odyssey IRDye fluorescent secondary antibodies (LI-COR) for 45 minutes. The stained membrane was imaged using the Odyssey Infrared Imaging System (LI-COR).

2.4 Calcium Imaging

Intracellular calcium imaging was performed on Con and PC cells using procedures previously described (Semenov et al., 2013). Cells were cultured on glass coverslips, loaded with

Fura-2/AM dye (Sigma-Aldrich, St. Louis, MO, USA), and placed into a vacuum perfusion chamber mounted on an IX71 microscope (Olympus, Center Valley, PA, USA) while being maintained using a physiological solution consisting of 5.4 mM KCl, 140 mM NaCl, 2 mM CaCl2, 1.5 mM MgCl2, 10 mM glucose, and 5 mM HEPES. The cells were recorded in the physiological solution for 60 seconds before the physiological solution at pH 5.5 was perfused and washed out with the physiological solution after 3 minutes. Alternating excitation at 340 and 380 nm was performed using a Lambda DG4 switcher (Sutter, Novato, CA, USA), and emission at 510 nm was recorded with a C9100-02 electron multiplication CCD digital camera (Hamamatsu Photonics, Hamamatsu, JPN). The intracellular calcium concentration was calculated using a calibration kit (Life Technologies, Carlsbad, CA, USA) and the equation:

Eq. 1 $[Ca^{2+}]_i = (\frac{R-R_{min}}{R_{max}-R}) \times K_D \times \beta$

where the recorded ratios are R, zero calcium ratio is R_{min}, ratio at calcium saturation is R_{max}, the effective dissociation constant is K_D, and the ratio of free:bound dye is β (Grynkiewicz et al., 1985).

2.5 Metabolic Assay

The metabolic activity of cells was evaluated using an MTT (3-(4,5-dimethylthiazol-2-yl)-2,5-diphenyltetrazolium bromide) Cell Proliferation Assay Kit (ATCC) following manufacturer guidelines. In brief, the assay works by adding a yellow tetrazolium reagent that is reduced by dehydrogenase enzymes, yielding a purple formazan dye. The dye can be solubilized by lysing the cells and measured using a spectrophotometer. Cells were cultured in 96-well plates, then treated with different mediums, and evaluated at different time points. All experiments were performed in triplicate.

2.6 microRNA Microarray

MicroRNA (miRNA) was isolated from cultured cells using a miRNeasy Mini Kit (QIAGEN). The miRNeasy Mini Kit uses phenol-chloroform extraction followed by phase separation and subsequent washes using spin columns. As miRNAs are stable RNAs, cDNA synthesis using reverse transcriptase is unnecessary. Following manufacturer guidelines, the miRNA is loaded onto Affymetrix miRNA microarrays which target over 6000 miRNAs. The loaded microarrays are then run using an Affymetrix microarray processor. The machine hybridizes the sample to the probes and analyzes the resulting signal. The expression levels are produced by normalizing the signals using a robust normalization method. For relative sample comparisons, expression changes are calculated using Tukey's Biweight method.

2.7 Microarray Analysis

Preprocessing of data to organize and produce a binary adjacency matrix using an miRNA predicted target database (miRDB) is written in Python (version 2.7). The STRING database was used to pull gene-gene interactions for select genes. The output data from the STRING database was converted to a binary adjacency matrix using Python. For the gene-miRNA matrix, the most current miRNA target database from miRDB was used. The database was imported into a Pandas dataframe in Python, then used to find matches between all expressed miRNAs and genes of interest. The miRNA-gene interactions with target scores less than 50 were omitted from analysis (Wang and El Naqa, 2008; Wong and Wang, 2015). The gene and miRNAs are weighted using their expression values, however, the interactions are in a binary adjacency matrix. For the creation of a binary matrix (also known as a sparse matrix), any interaction that meets the cutoff is assigned a value of 1, otherwise it has a value of 0 allowing

for faster computing times. The matrix factorization is run in Python 2.7 on an Intel i7 3.6GHz quad core processor (overclocked at 4.4GHz) with 16GB of DDR3 RAM. The NumPy library is used for basic numerical matrix processing due to the implementation of Python commands in C, allowing for faster computation speeds than Python matrices or dictionaries. Pandas, which builds off of the NumPy and SciPy libraries, allows for easy multidimensional matrix manipulation including mixed datatypes while reducing computation time through C implementation.

Using the gene and miRNA expression profiles, a clustering analysis can be performed for gene-gene and miRNA-gene interactions. This would allow for the identification of possible miRNAs functioning as key regulators in membrane channel maintenance. The method for clustering is known as MCODE (molecular complex detection algorithm). The MCODE method first calculates the weights of the vertices based on the core clustering coefficient. Next, the highest weighted vertex is used as a cluster seed and iteratively grows the cluster by adding vertices with weights larger than the given threshold (Wang et al., 2010). Using the interaction matrices from preprocessing, edge weight tables can be produced for both gene-gene interactions and gene-miRNA interactions. These edge weight tables can be plotted in Cytoscape (ver. 3.3.0) to produce a visual interaction network.

2.8 Immunocytochemistry

Confirmation of *KCNMA1* ($K_{Ca}1.1\alpha$), *KCNA2* ($K_V1.2$), *SCN9A* ($Na_V1.7$), and *GJA1* (Cx43) gene expression were made by immunocytochemistry. Cells were grown on cover slips and fixed in 4% paraformaldehyde for 20 minutes then permeabilized with PBS + 0.5% TRITON-X100 for 10 minutes. Washes with PBS were performed after both steps and cells were

then blocked in 10% boiled goat serum (BGS) for 1 hour. Incubation with primary antibodies was performed in 5% BGS at 4°C overnight then washed 3 times in PBS + 0.1% Tween-20 (PBS-T) for 5 minutes each. Rabbit polyclonal primary antibodies were purchased from Santa Cruz Biotechnology (Santa Cruz, CA, USA) for $K_{Ca}1.1\alpha$ (sc-25686), $K_V1.2$ (sc-292447), $Na_V1.7$ (sc-130096), and Cx43 (sc-9059). Negative controls were produced using normal rabbit IgG (Santa Cruz). Secondary staining was with goat anti-rabbit Alexa Fluor 488 (Life Technologies, Carlsbad, CA, USA) in 5% BGS for 45 minutes at room temperature then washed 3 times in PBS-T for 5 minutes each. The nuclei were counterstained using 1 μg/ml DAPI (4′,6-diamidino-2-phenylindole; Sigma) in PBS-T for 5 minutes followed by 3 PBS-T washes for 5 minutes each. After a brief rinse in PBS, the coverslips were mounted on slides using VECTASHIELD antifade mounting medium (Vector Labs, Burlingame, CA, USA). Electronic fluorescent images were captured using an Olympus DP70 CCD camera through an Olympus BX51 microscope (Olympus America Inc., Center Valley, PA, USA).

2.9 ATP Measurements

Chondrocytes were preincubated in Hank's balanced salt solution (HBSS) with the addition of 10% fetal bovine serum (FBS) for 1 hour at 37°C (no CO_2). As we have previously shown, a buffered salt solution alone causes a significant decrease in cell metabolism/viability (assessed using an MTT assay), however the addition FBS results in a significant recovery of metabolism/viability (Sabuncu et al., 2015). After 1 hour, the medium was replaced with HBSS+FBS at pH 7.4 or HBSS+FBS at pH 5.5, and the extracellular ATP was measured at 1 minute and 10 minutes. After 10 minutes, the extracellular medium was aspirated and the intracellular ATP was extracted using boiling ddH_2O (Yang et al., 2002). The cells, plated in

small wells, were treated, then the extracellular medium collected and measured for ATP release by luciferin-luciferase bioluminescence assay following manufacturer's guidelines (Molecular Probes). In brief, first, a reaction solution containing a reaction buffer mixed with DTT (dithiothreitol), D-luciferin, and recombinant firefly luciferase is prepared. The DTT is used to prevent the formation of disulfides which reduce the enzyme efficiency. When the solution is added to a sample containing ATP, the D-luciferin and oxygen react with ATP in the presence of luciferase and magnesium resulting in the oxidation of D-luciferin to oxyluciferin in an ATP-dependent manner. This oxidation reaction, catalyzed by luciferase, produces a chemiluminescence which can be measured at 560nm. The standards were measured and the relative luminescence values were fit using a quadratic fit (Wolfram) to extrapolate the equivalent ATP concentrations. Multiple fitting methods were tested and compared based on their adjusted R^2 values. The tested fitting methods included linear, logarithmic, power, and polynomial fitting of different degrees with second degree polynomials yielding the highest R^2 values.

2.10 Statistical Analysis

P-values were generated using Student's T-test with a minimum of n=3. P-values <0.05 were considered to be statistically significant.

CHAPTER 3

RESULTS AND DISCUSSION

3.1 Ion Channels in Normal Cartilage

Using qPCR with an 84 ion channel gene array, expression profiles for normal costal cartilage (n=3), normal articular cartilage (n=3), and fetal costal cartilage (n=3) were produced (Appendix 1-15). The detection using SYBR Green based arrays on 6.8-35 Cq's. Averaging the samples for each sample type and using 30 Cq's as a cutoff, a Venn diagram was produced to show the shared and individually expressed ion channels genes (Fig. 16).

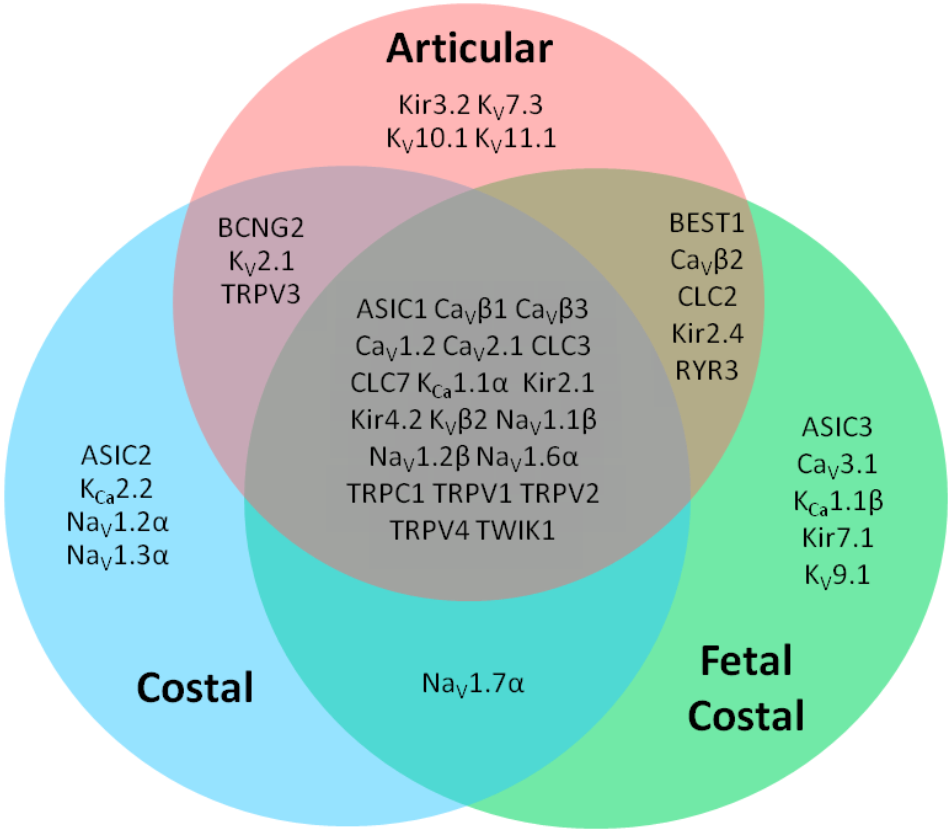

Figure 16. **Venn diagram of ion channels in normal chondrocytes.** Venn diagram depicting ion channel genes showing significantly detectable levels of expression in chondrocytes from normal costal cartilage, costal cartilage from fetal samples, and normal articular cartilage.

Potassium Channels in Normal Cartilage

Potassium channels, mainly voltage-gated potassium channels (K_V), are the most abundant ion channel. Interestingly however, our analysis did not find any consistently expressed K_V channels in adolescent and fetal costal chondrocytes and articular chondrocytes other than Kvβ2, suggesting that K_V channels are important for the functional differences and possibly be used as a phenotypic marker between the different tissues. K_Vβ2 is known to be a non-pore-forming subunit of K_V channels which modulates the channel's activity, though the function in

chondrocytes is unknown. Articular chondrocytes highly express more K_V channels which may be important for regulating the membrane potential from the type of highly compressive forces experienced in joints in contrast to the more mild compressive and tensile forces in costal cartilage from breathing. Multiple K_V channels were identified in articular chondrocytes (K_V7.3, K_V10.1, and K_V11.1), with only one expressed in adolescent costal chondrocytes which was also detected in articular chondrocytes (K_V2.1) and another expressed only in fetal chondrocytes (K_V9.1).

This expression profile is indicative of the main regulating processes in each different cartilage type. The potassium channels themselves are an integral part of membrane potential homeostasis and osmotic stress response among other processes. K_V channel-related currents have been observed through biophysical analyses and have similar conductances and activation midpoints to the K_V1.x and K_V4.x channels (Barrett-Jolley et al., 2010). The conductance cannot be attributed to any specific/single channel and is suggestive of heteromultimeric channels or a heterotypic population. In equine and elephant articular cartilage, K_V1.4 was identified by immunohistochemical analysis (Mobasheri et al., 2005). In chondrocytes isolated from mouse articular cartilage, K_V1.6, K_V2.1, and K_V3.3 expression was observed (Clark et al., 2010). Our analyses also found expression of K_V2.1, however, we had no detectable expression of K_V1.6 in any adolescent costal or articular chondrocytes. Two of the fetal samples also had no detectable expression of K_V1.6, but a single fetal costal cartilage samples showed significant expression. In chicken mesenchymal stem cells undergoing chondrogenesis, K_V1.3 and K_V4.1 were identified by qPCR and western blotting (Varga et al., 2011). However, our assays did not have primers for both K_V1.3 and K_V4.1, but we did also find expression of Kv7.3 in adult articular chondrocytes and Kv7.1 in fetal costal chondrocytes. The K_V7.3 channel is known to be a major contributor to

the M-current in neurons (Stewart et al., 2012). Additionally, K_V7.x channels are known to have a calcium-sensitive site as well as having its voltage-sensitive domain, meaning that the channel not only plays a role in RMP maintenance, but also in response to calcium-dependent stimuli (Delmas and Brown, 2005). The K_V9.1 channel function is unknown in chondrocytes and relatively unknown in neurons with down-regulation linked to neuronal misfiring and possible role in chronic neuronal pain (Tsantoulas et al., 2012). K_V11.1 is a delayed rectifier potassium channel with expression in a range of tissue types including neuronal, cardiac, and endocrine tissues. It is not classified as producing a pacemaker current, but does play a contributing role to amplifying the oscillations as well as stabilizing the frequency in the sinoatrial and atriventricular node cells of the heart (Vandenberg et al., 2012). Overall, the different K_V channels are thought to cumulatively maintain the RMP and contribute to the regulation of differentiation and calcium signaling.

The K_{ir} channels have not been properly investigated in chondrocytes due to the limited selectivity of channel inhibitors. A predicted K_{ir} channel was the K_{ir}6.x which was shown to be expressed in chondrocytes. Additionally, Clark et al. (2011) found expression of K_{ir}2.2 in mouse articular chondrocytes. Our investigation has revealed high expression of multiple K_{ir} channels with a mixture of some commonly expressed and others specific to their respective cartilage types. K_{ir}2.1 and 4.2 were found to be commonly expressed with adolescent costal chondrocytes showing significantly higher expression of K_{ir}2.1 (+8.93-fold, $p<0.001$) versus articular chondrocytes. K_{ir}4.2 expression was higher in articular chondrocytes versus adolescent costal (+5.18-fold, $p<0.05$) and fetal costal (+7.03-fold, $p<0.01$) chondrocytes. Fetal costal chondrocytes showed expression of K_{ir}7.1, including K_{ir}2.4 which was also found in articular chondrocytes. K_{ir}3.2 expression was observed in articular chondrocytes but not in costal

chondrocytes which is interesting because it is a known G-protein coupled ion channel found in neurons and cardiac tissue, but has not yet been observed in chondrocytes (Inanobe et al., 1999; Marionneau et al., 2005). The function in excitable tissues is producing a slow inhibitory postsynaptic potentials, though evidence shows that it has an agonist-independent basal current. However, its function in chondrocytes remains to be elucidated.

An important and well characterized channel in chondrocytes is the BK channel ($K_{Ca}1.1\alpha$) known to play a crucial role in cell homeostasis by maintaining the membrane potential in response to intracellular calcium sensing. We confirmed high expression of the BK channel in articular chondrocytes as well as similar levels of expression in adolescent and fetal costal cartilage. SK channels have been shown to be expressed in chondrosarcomas, though only SK1 and SK3 were detected (Funabashi et al., 2010). However, we did not observe expression of SK1 or SK3 in any of the samples, but instead, found expression of SK2 ($K_{Ca}2.2$) in adolescent costal cartilage. This discrepancy is likely due the differences between chondrocytes and chondrosarcomas.

Explorations into chondrocyte K^+ efflux in response to hypo-osmotic stress in the presence of a range of channel inhibitors found that the main contributors were likely to be the K_{ir} channels, BK channels, and SK channels. Pimozide, a known inhibitor for K_{ir} channels, was found to be a potent inhibitor of K^+ efflux during hypotonic challenge of chondrocytes (Hall et al., 1996b). The BK channel response to hypotonic challenge was blocked using REV5901 and inhibited RVD. Additionally, apamin also showed some reduction in K^+ efflux during hypotonic challenge suggesting involvement of SK channels in RVD (Lewis et al., 2011a). Fold differences of expressed potassium ion channels relative to adult articular chondrocytes were calculated (Fig. 17).

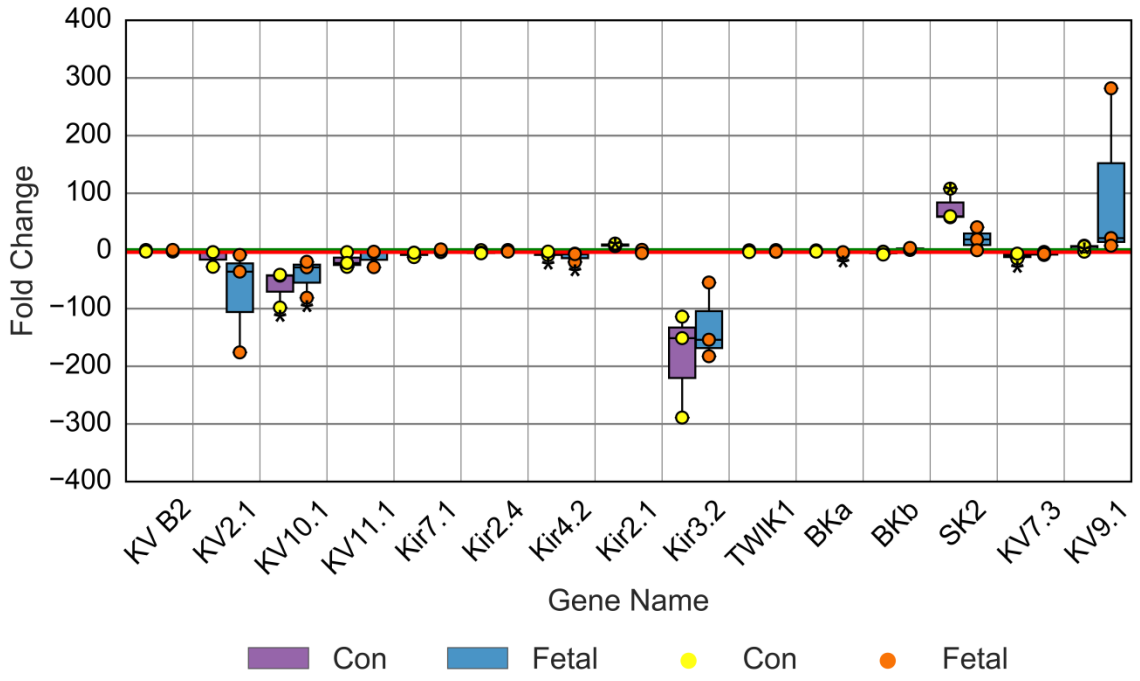

Figure 17. **Fold changes in potassium ion channels in normal chondrocytes.** Fold changes in potassium ion channel gene expression using qPCR in adolescent and fetal costal chondrocytes relative to articular chondrocytes. Each sample was analyzed with an n=3 and significant changes ($p<0.05$) relative to normal costal cartilage are indicated (*). The green and red horizontal lines indicated a +2 or -2 fold change, respectively.

Sodium Channels in Normal Cartilage

An unexpected class of sodium transporters are the voltage-gated sodium channels (Na_V) which were found to be expressed in all our samples. We found expression of $Na_V\beta1$ and $Na_V\beta2$ as well as $Na_V1.2$, $Na_V1.3$, $Na_V1.6$, and $Na_V1.7$. Fold differences of expressed sodium ion channels relative to adult articular chondrocytes were calculated (Fig. 18). Previously, in chicken MSCs undergoing chondrogenesis $Na_V1.4$ was shown to be expressed (Varga et al., 2011).

However, the RMP in chondrocytes is too depolarized for the Na_V channels to function as traditional sodium transporters, suggesting alternative roles for these proteins. Though the alpha-subunits have no known alternative roles, the auxiliary subunits not only function in modulating the channel activity, but also as cell adhesion molecules with involvement in mechanotransduction (Brackenbury and Isom, 2008).

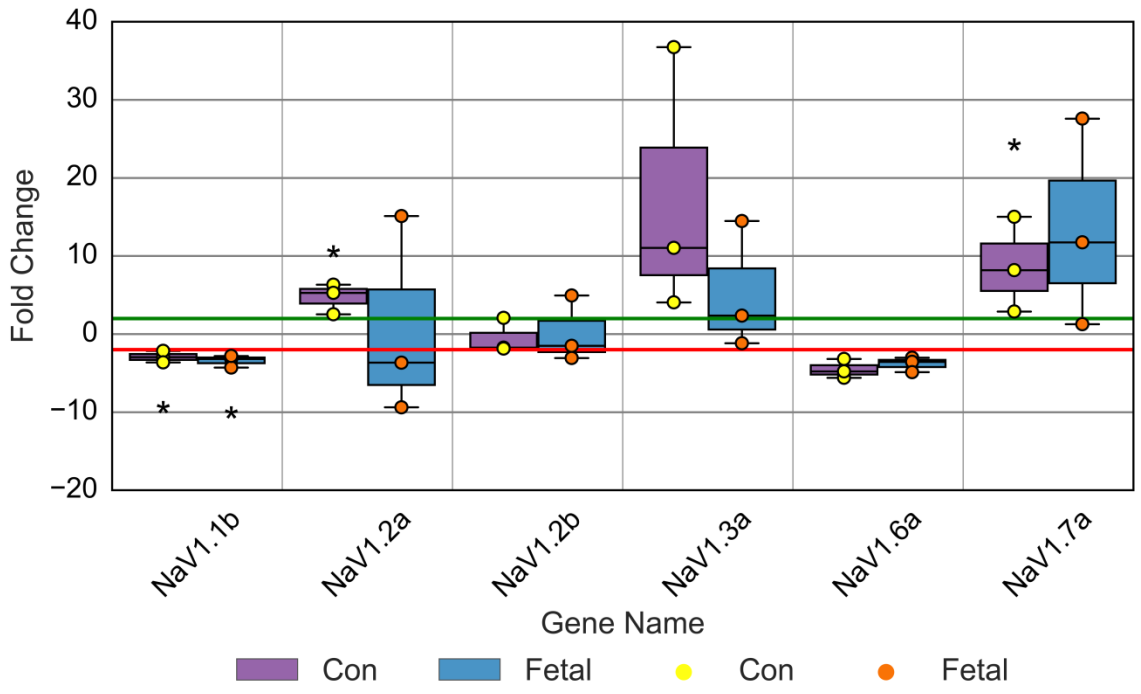

Figure 18. **Fold changes in sodium ion channels in normal chondrocytes.** Fold changes in sodium ion channel gene expression using qPCR in adolescent and fetal costal chondrocytes relative to articular chondrocytes. Each sample was analyzed with an n=3 and significant changes ($p<0.05$) relative to normal costal cartilage are indicated (*). The green and red horizontal lines indicated a +2 or -2 fold change, respectively.

Calcium Channels in Normal Cartilage

PCR analysis of calcium transporters identified the expression of several voltage-gated calcium channels (Ca_V or VGCCs). The $Ca_V1.2$, $Ca_V2.1$, $Ca_V\beta1$, and $Ca_V\beta3$ channels appear to be commonly expressed in all hyaline cartilage types tested. Additionally, $Ca_V\beta2$ was expressed in articular and fetal costal chondrocytes while fetal costal chondrocytes also expressed $Ca_V3.1$. Ryanodine receptor 3 (RYR3) was found to be expressed in articular and fetal costal chondrocytes, but not in adolescent costal chondrocytes. Fold differences of expressed calcium ion channels relative to adult articular chondrocytes were calculated (Fig. 19). Studies using chondrogenic progenitor cells from articular cartilage found expression of all isoforms of IP_3R, ORAI, and STIM while RYR was not detected (Matta et al., 2015a). Electrophysiological investigation using mandibular chondrocytes from rabbit found that intracellular calcium release due to mechanical stimulation was dependent solely on IP_3R (Zhang et al., 2006), making it unclear whether RYR are present and/or functional at the protein level in our samples. Chicken mesenchymal stem cells undergoing chondrogenesis were found to express ORAI and STIM as well as several VGCCs ($Ca_V1.2$, $Ca_V1.3$, $Ca_V2.3$, $Ca_V3.1$, $Ca_V3.2$, and $Ca_V3.3$). The calcium oscillations during chondrogenesis was found to be reliant on both SOCCs and VGCCs (Fodor et al., 2013).

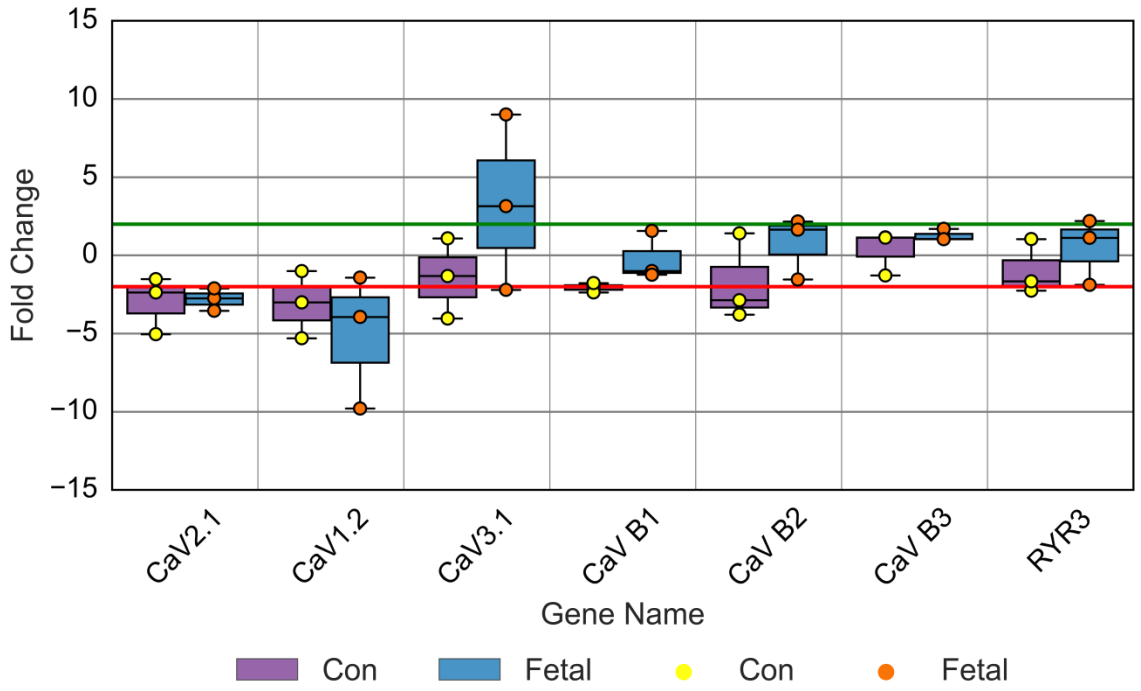

Figure 19. **Fold changes in calcium ion channels in normal chondrocytes.** Fold changes in calcium ion channel gene expression using qPCR in adolescent and fetal costal chondrocytes relative to articular chondrocytes. Each sample was analyzed with an n=3 and significant changes ($p<0.05$) relative to normal costal cartilage are indicated (*). The green and red horizontal lines indicated a +2 or -2 fold change, respectively.

Voltage-gated L-type calcium channels have been identified as functional in chondrocytes using patch clamp physiology combined with the inhibitors nifedipine and verapamil (Fodor et al., 2013). VGCCs were implicated in being involved in chondrogenesis (Fodor et al., 2013; Matta and Zakany, 2013), mechanical loading (Chao et al., 2006; Han et al., 2012), and RMP homeostasis (Fodor et al., 2013; Matta and Zakany, 2013). Using the VGCC inhibitors, disruption of several signaling cascades have been identified, revealing the previously

unknown importance of VGCCs in chondrocytes. Blocking of VGCCs interrupted protein kinase C (PKC) signaling in growth plate chondrocytes and interfered with chondrocyte differentiation (Boileau et al., 2006). Blocking was also found to reduce the RMP by 18%, ultimately affecting chondrocyte proliferation and also producing a cytotoxic effect (Matta et al., 2015b). A study on chicken costal chondrocytes found that inhibition of VGCCs eliminated the proliferative and differentiational effect of mechanical loading, indicating that VGCCs are also involved in mechanotransduction in chondrocytes (Wu and Chen, 2000). Applying electrical fields (20mV/cm at 60Hz) to articular chondrocytes has been shown to increase the production of the ECM proteins collagen type II and aggrecan as well as reducing IL-1β-dependent MMP production. However, blocking of VGCCs using verapamil completely negated the effects (Xu et al., 2009). Although chondrocytes have a relatively depolarized RMP, VGCCs are still functional and contribute to different regulatory processes. Though we were surprised to see expression of RYR3, albeit somewhat low, it is still unknown if the channel is functional or even present at the protein level.

Chloride Channels in Normal Cartilage

In chondrocytes, CLC-dependent currents have been observed by electrophysiological means, however, expression of CLC channels were not confirmed until recently. Sugimoto (1996) first measured a Cl^- dependent current in rabbit articular chondrocytes. Using the chloride channel blocker SITS (4-acetamido-4’-isothiocyanato-stilbene-2,2’-disulfonic acid) (Sugimoto et al., 1996; Tsuga et al., 2002), DIDS (4,4-diisothiocyanatostilbene-2,2-disulfonate) (Kurita et al., 2015; Okumura et al., 2009), NFA (niflumic acid) (Funabashi et al., 2010), and DCPIB (4-(2-butyl-6,7-dichloro-2-cyclopentyl-indan-1-on-5-yl)oxobutyric acid) (Okumura et al., 2009), Cl^-

currents were found to be involved in regulating the membrane potential in chondrocytes as well as response to osmotic swelling and pH stress. The specific chloride channel genes expressed in chondrocytes were unknown until Kurita et al. (2015) found significant expression of genes for CLC-3, 4, and 7 in OUMS-27 cells (chondrosarcoma cells). Liang et al. (2010) found expression of the CFTR gene and protein as well as confirmed its function through biophysical measurements; however, their analysis was performed on mouse chondrocytes with no indication of the specific type of cartilage source. Our PCR analysis found expression of CLC-3 and CLC-7 in all cartilage types, as well as expression of CLC-2 and BEST1 in both articular and fetal costal chondrocytes. Fold differences of expressed chloride channels relative to adult articular chondrocytes were calculated (Fig. 20). Although the CLC family of chloride channels have been predicted and observed in chondrocytes-like cells, this is the first description of bestrophin 1 in chondrocytes. Bestrophin functions as an important calcium-activated Cl^- channel in retinal epithelial cells. Also, bestrophin functions as a VRAC (volume-regulated anion channel) in certain cells and tissues. Although bestrophin was originally predicted to not be a VRAC in mammals (Chien and Hartzell, 2008), it was later discovered to be a major contributor to the VRAC current in human retinal pigment epithelium as well as in mouse sperm (Milenkovic et al., 2015). It is important to note that although bestrophin is normally characterized as a chloride channel, it is actually a non-selective channel under certain conditions permeable to sodium, potassium, and cesium (Yang et al., 2014).

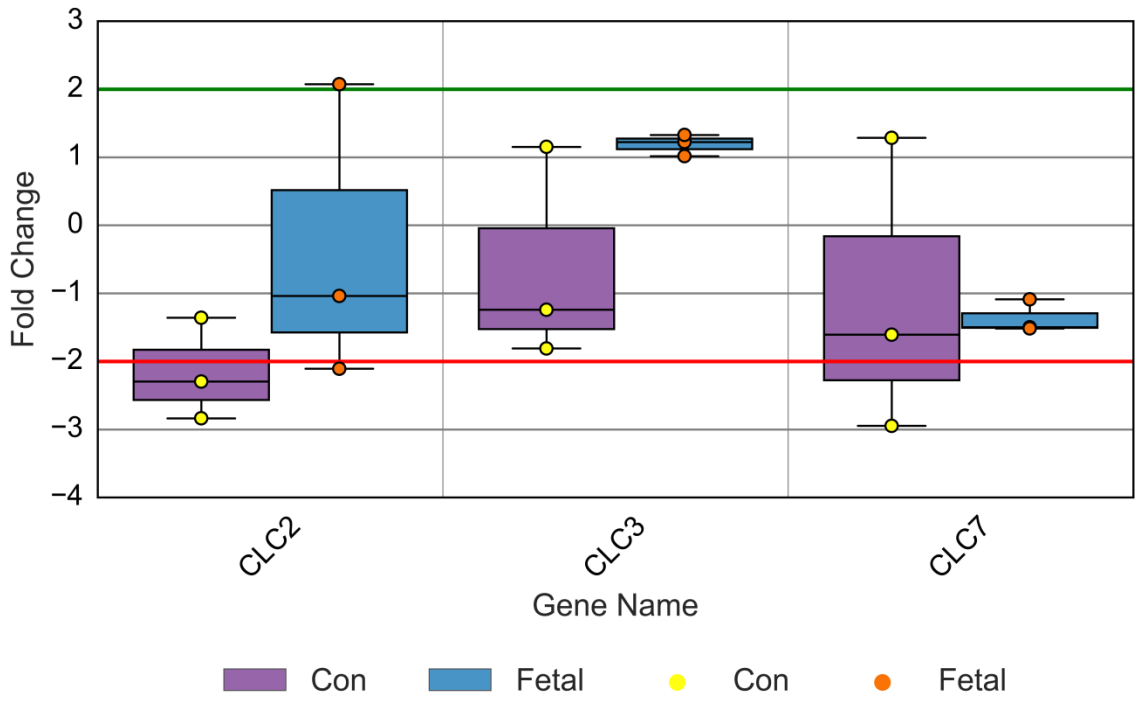

Figure 20. **Fold changes in chloride channels in normal chondrocytes.** Fold changes in chloride ion channel gene expression using qPCR in adolescent and fetal costal chondrocytes relative to articular chondrocytes. Each sample was analyzed with an n=3 and significant changes ($p<0.05$) relative to normal costal cartilage are indicated (*). The green and red horizontal lines indicated a +2 or -2 fold change, respectively.

Non-Selective Channels in Normal Cartilage

Non-selective channels are mainly cation channels that are permeable to multiple different ions. However, most channels normally have a higher permeability for certain ions while others are only non-selective under certain conditions (e.g. bestrophin 1). Several different non-selective ion channels were detected in chondrocytes and their fold changes relative to articular chondrocytes are shown in Fig. 21. A major non-selective channel are the ion channels

sensitive to decreases in extracellular pH known as ASICs. In articular cartilage, ASIC1 is the main ASIC expressed (Yuan et al., 2010), which is consistent with our results. Interestingly, our adolescent costal cartilage showed significant expression of both ASIC1 and ASIC2, while fetal costal cartilage showed expression of ASIC1 and ASIC3. Fold differences of expressed ASICs and other non-selective ion channels relative to adult articular chondrocytes were calculated (Fig. 21). Experiments in rat articular chondrocytes found that acid-induced intracellular calcium transients were dependent on ASIC1 where transient peaks were significantly reduced when the ASIC1-specific blocker PcTX (Psalmotoxin) was used while controlling for other calcium sources by blocking VGCCs, intracellular store release, and glutamate receptors (Yuan et al., 2010). Using the ASIC blocker amiloride without the presence of any other blockers, calcium transients were significantly reduced in a dose-dependent manner suggesting that although ASICs are mainly permeable to sodium, they are significant contributors to acid-induced calcium response in chondrocytes (Hu et al., 2012). ASICs are important for pH sensing and the different ASICs activate a different pHs. The presence of ASIC2 and ASIC3 may be an indicator that costal cartilage is subjected to different pHs than articular cartilage.

The TRPV channels are likely considered one of the most influential ion channels in chondrocytes. All our samples showed expression for TRPC1, TRPV1, TRPV2, and TRPV4 while adolescent costal and adult articular cartilage both showed expression for TRPV3. TRPC1 is a non-selective channel permeable to Ca^{2+} which is capable of associating with BKα and although has been identified in chondrocytes, its function in chondrocytes is unknown (Gavenis et al., 2009). Gavenis et al. (2009) also identified TRPV1 and TRPV2 before with TRPV3 only recently being detected in high density chicken cultures undergoing chondrogenesis (Somogyi et al., 2015). Although these different TRP channels have been identified as being expressed and

present in chondrocytes or chondrocyte-like cells, it remains to be known what their functions are within the cell or tissue. TRPV4 is expressed in a number different tissues while functioning in a variety of roles as a thermosensor, osmosensor, and mechanosensor. TRPV4 also plays a role in regulating the basal levels of intracellular calcium (O'Conor et al., 2014; Pedersen et al., 2005). Unlike the other TRP channels in chondrocytes, TRPV4 has been well studied and is known to play a vital role in mechanotransduction and response in osmotic swelling (O'Conor et al., 2013; O'Conor et al., 2014; Phan et al., 2009). Lastly, we are the first to report expression of HCN2 (BCNG2) which was detected in adolescent costal and adult articular cartilage. BCNG2 is an non-selective cation channel with an unknown permeability known to be involved in the pacemaker potential of the heart and thought to be involved in nocioception (Emery et al., 2012; Macri et al., 2012). BCNG2's function is unknown in chondrocytes, and it is difficult to speculate the possible functionality as it is activated at very low membrane potentials (-60mV to -90mV).

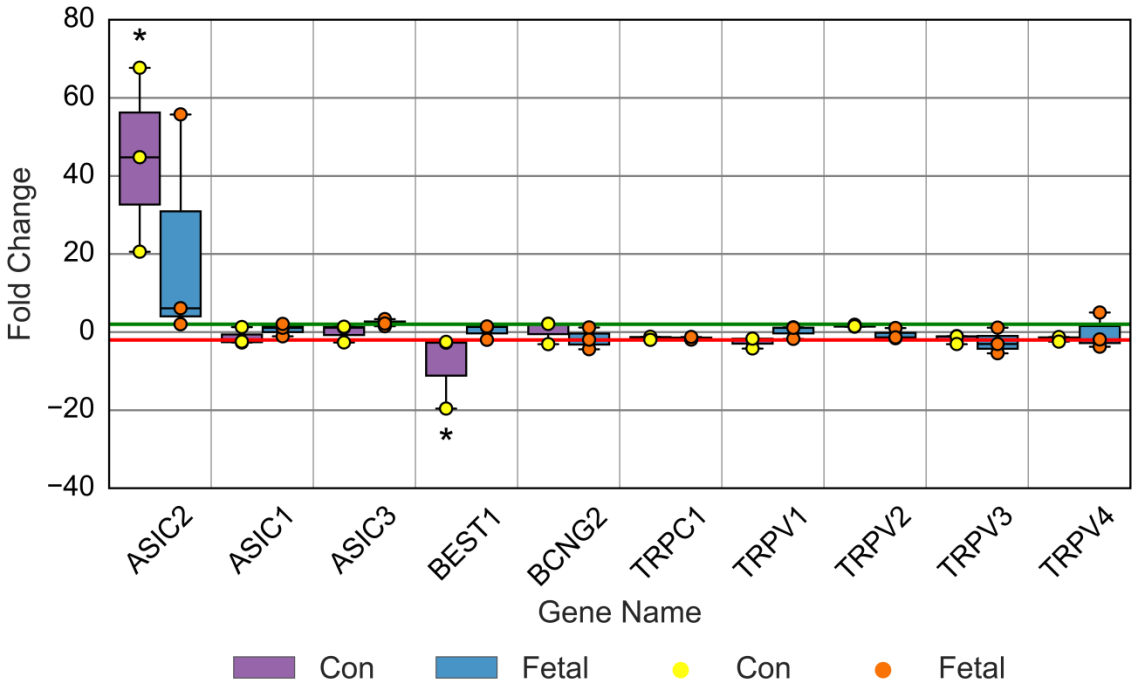

Figure 21. **Fold changes in non-selective ion channels in normal chondrocytes.** Fold changes in non-selective ion channel gene expression using qPCR in adolescent and fetal costal chondrocytes relative to articular chondrocytes. Each sample was analyzed with an n=3 and significant changes ($p<0.05$) relative to normal costal cartilage are indicated (*). The green and red horizontal lines indicated a +2 or -2 fold change, respectively.

3.2 Ion Channels in Pectus Deformities

Similarly to the previous section, an expression profiles for chondrocytes derived from pectus excavatum (n-3) and pectus carinatum (n=3) were produced (Appendix 16-30). Averaging the samples for each sample type and using 30 Cq's as a cutoff, a Venn diagram was produced to show the shared and individually expressed ion channels genes between normal, PC, and PE chondrocytes (Fig. 22). Using delta-delta Cq comparison of PC and PE relative to normal costal

chondrocytes, relative fold changes were calculated and plotted based on ion channel type. Fold changes greater than 2-fold up or down were considered a significant change. Interestingly, two genes were consistently down-regulated in both PC and PE versus normal costal chondrocytes. KCNN2 (SK2) was down-regulated in PC (-13.73, $p<0.01$) and PE (-10.04, $p<0.05$) (Fig. 22). Also, ACCN1 (ASIC2) was down-regulated in PC (-6.41-fold, $p<0.01$) and PE (-9.17-fold, $p<0.05$) (Fig. 23). Additionally, PC samples showed significant changes in HCN2 (BCNG2; -3.36-fold, $p<0.05$), SCN3A ($Na_V1.3$; +5.20-fold, $p<0.05$), SCN9A ($Na_V1.7$; +5.76-fold, $p<0.01$), TRPV2 (-2.09-fold, $p<0.001$), and TRPV3 (-2.34-fold, $p<0.05$); while PE showed significant changes in SCN1B ($Na_V\beta1$; +2.45-fold, $p<0.05$).

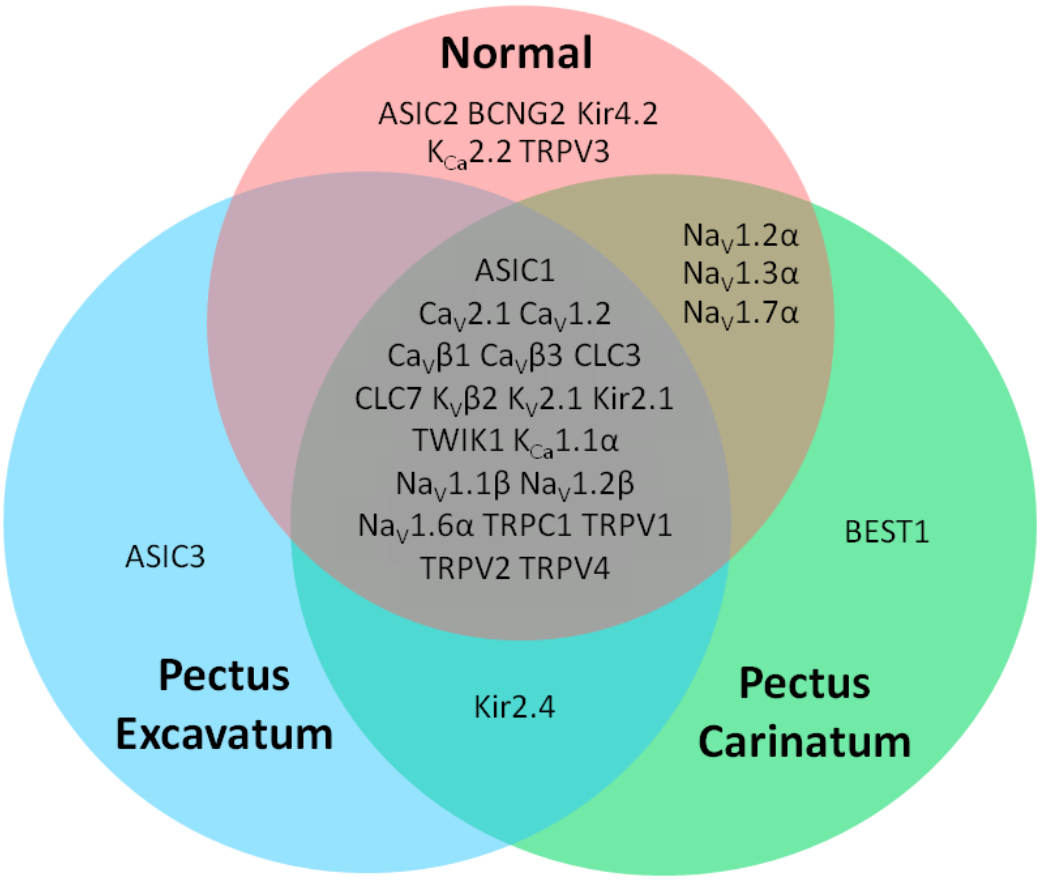

Figure 22. **Venn diagram of ion channels in normal and pectus chondrocytes.** Venn diagram depicting ion channel genes showing significantly detectable levels of expression in chondrocytes from normal costal cartilage and costal cartilage from patients with pectus excavatum and pectus carinatum.

Potassium Channels in Pectus Deformities

Normal costal chondrocytes and chondrocytes from patients with pectus deformities express similar levels of potassium channels with the main exception being SK2 (Fig. 23). The SK2 downregulation was consistent down-regulated in both PC and PE samples. SK2 is a calcium-activated potassium channel (K_{Ca}) involved in the formation of intracellular calcium

transients induced by mechanical stimuli. Normally, the initial increase of intracellular calcium is detected by the K_{Ca} channels causing their activation and efflux of K^+ which hyperpolarizes the membrane. The mechanism by which SK channels contribute to intracellular calcium transient formation is unknown, though there is evidence that it may function through a histamine-mediated (Funabashi et al., 2010) and/or α5β1-integrin-mediated pathway (Wright et al., 1997). Interestingly, Western blot analysis did not detect decreases in SK2 protein levels, but instead we observed increases in protein levels of SK2 (Fig. 24).

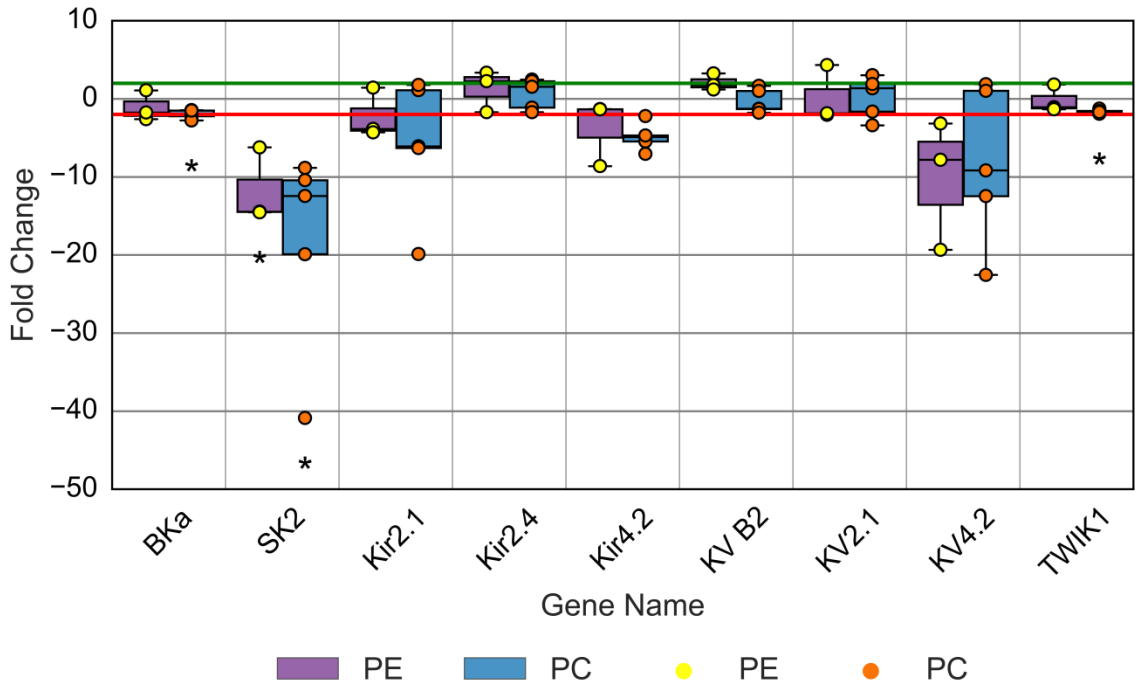

Figure 23. **Fold changes in potassium ion channels in pectus chondrocytes.** Fold changes in ion channel gene expression using qPCR in chondrocytes in pectus excavatum and pectus carinatum relative to normal costal cartilage. Each sample was analyzed with an n=3 and

significant changes ($p<0.05$) relative to normal costal cartilage are indicated (*). The green and red horizontal lines indicated a +2 or -2 fold change, respectively.

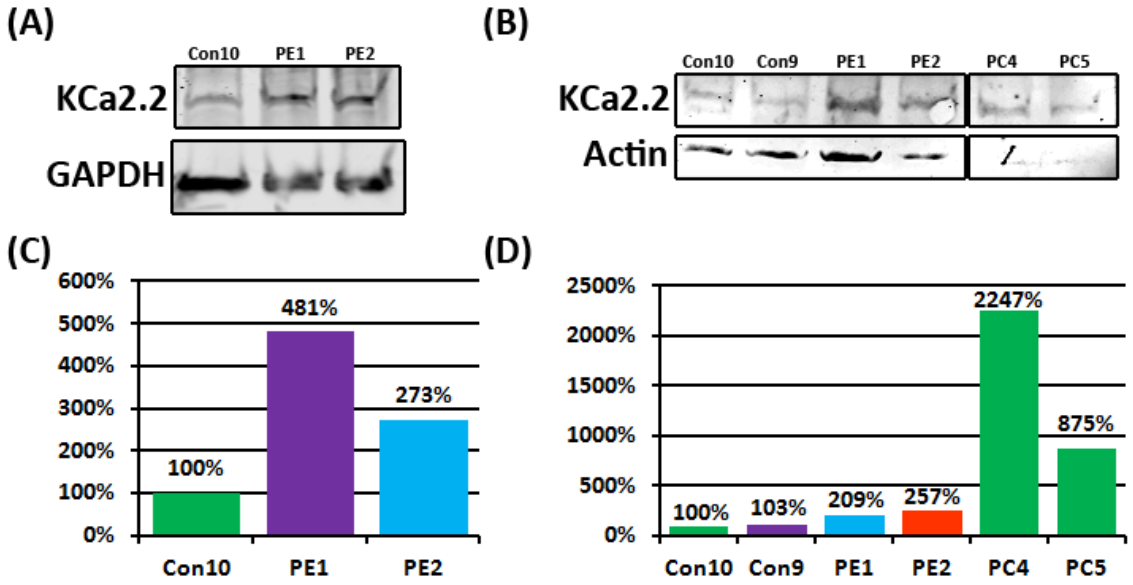

Figure 24. **Western blot of SK2. Western blot of $K_{Ca}2.2$ (SK2) in protein extracts from chondrocytes from normal costal cartilage and patients with pectus deformities.** (A) Protein blotting for chondrocytes from normal and two pectus excavatum costal cartilage samples was performed staining for $K_{Ca}2.2$ and GAPDH. (B) The median $K_{Ca}2.2$ band signals were normalized to the median GAPDH band signals and then the normalized signals were calculated relative to the control sample. (C) Protein blotting for chondrocytes from two normal, two pectus excavatum, and two pectus carinatum costal cartilage samples was performed staining for KCa2.2 and Actin. (D) The median KCa2.2 band signals were normalized to the median Actin band signals, and then the normalized signals were calculated relative to the control sample.

Sodium Channels in Pectus Deformities

Gene expression analysis of normal costal chondrocytes and chondrocytes from patients with pectus deformities for sodium ion channels revealed a few differences (Fig. 25). Pectus excavatum showed a minor, but statistically significant increase in $Na_V\beta1$ (+2.45-fold, $p<0.05$). Meanwhile, pectus carinatum showed significant increases for both $Na_V1.3$ (+5.20-fold, $p<0.05$) and $Na_V1.7$ (+5.76-fold, $p<0.01$). Due to the highly depolarized state of the resting membrane potential in chondrocytes, the Na_V channels are not able to be activated, and their function in chondrocytes remains a mystery.

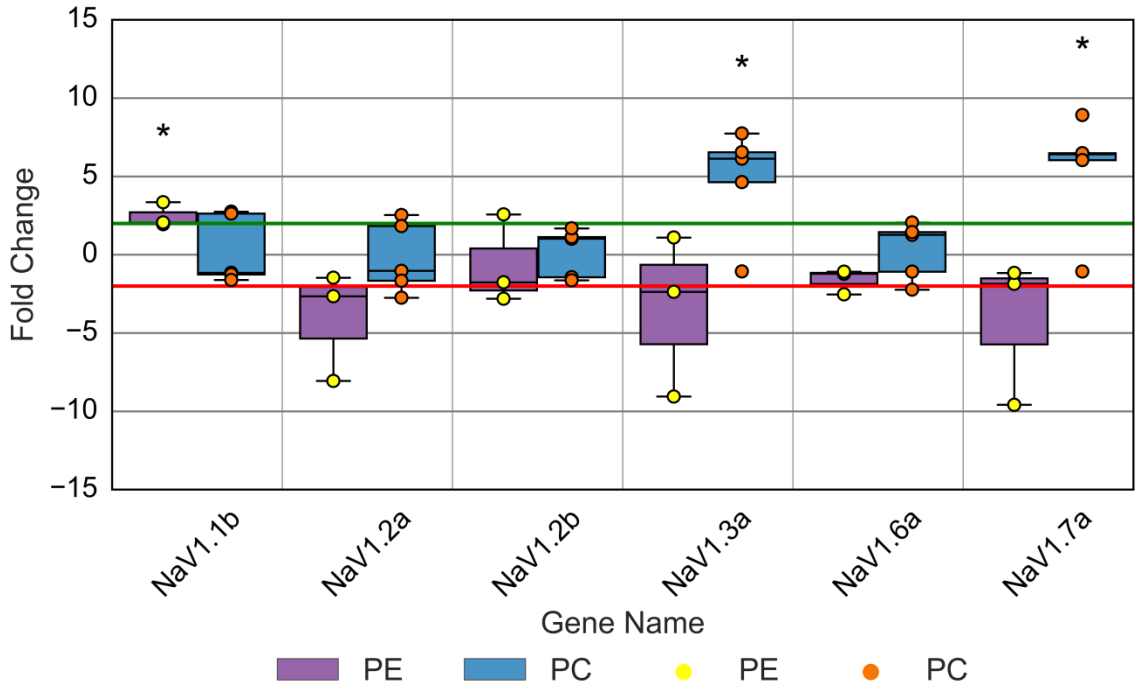

Figure 25. Fold **changes in sodium ion channels in pectus chondrocytes.** Fold changes in ion channel gene expression using qPCR in chondrocytes in pectus excavatum and pectus carinatum relative to normal costal cartilage. Each sample was analyzed with an n=3 and significant

changes ($p<0.05$) relative to normal costal cartilage are indicated (*). The green and red horizontal lines indicated a +2 or -2 fold change, respectively.

Calcium Channels in Pectus Deformities

Gene expression analysis of calcium ion channels for normal and pectus deformity-affected costal chondrocytes did not yield any statistically significant differences (Fig. 26).

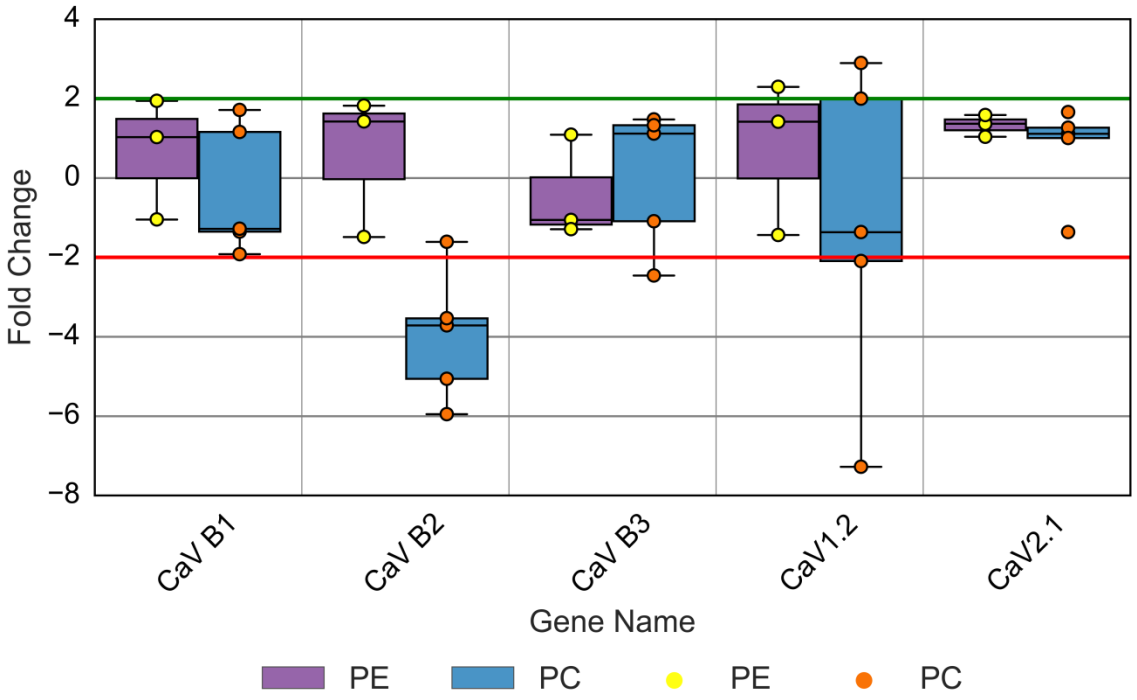

Figure 26. **Fold changes in calcium ion channels in pectus chondrocytes.** Fold changes in ion channel gene expression using qPCR in chondrocytes in pectus excavatum and pectus carinatum relative to normal costal cartilage. Each sample was analyzed with an n=3 and

significant changes ($p<0.05$) relative to normal costal cartilage are indicated (*). The green and red horizontal lines indicated a +2 or -2 fold change, respectively.

Chloride Channels in Pectus Deformities

Gene expression analysis of chloride ion channels fin chondrocytes from normal and pectus deformity-affected costal chondrocytes did not yield any statistically observable differences (Fig. 27).

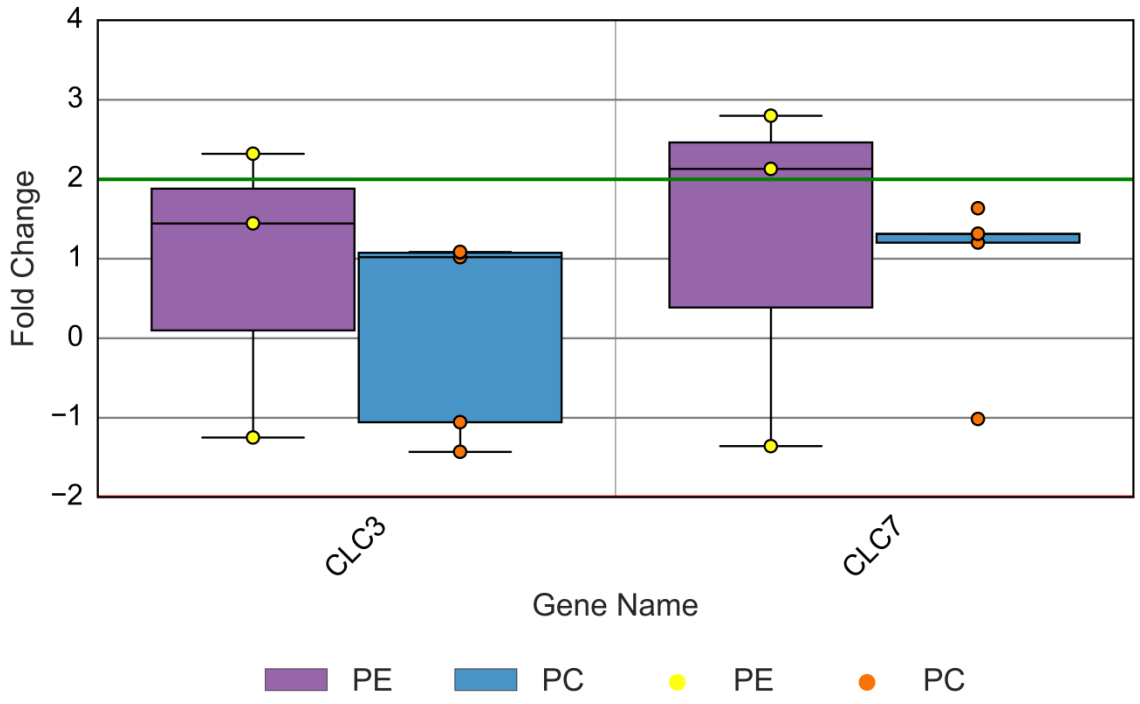

Figure 27. **Fold changes in chloride channels in pectus chondrocytes.** Fold changes in ion channel gene expression using qPCR in chondrocytes in pectus excavatum and pectus carinatum relative to normal costal cartilage. Each sample was analyzed with an n=3 and significant

changes ($p<0.05$) relative to normal costal cartilage are indicated (*). The green and red horizontal lines indicated a +2 or -2 fold change, respectively.

Non-Selective Channels in Pectus Deformities

Our gene expression analysis of non-selective ion channels in PC and PE versus normal costal chondrocytes showed a few statistically significant different ion channels (Fig. 28). In PC samples, TRPV2, TRPV3, and BCNG2 were all down-regulated. However, TRPV2 (-2.09-fold, $p<0.001$) and TRPV3 (-2.34-fold, $p<0.05$) were minor while BCNG2 was more pronounced (-3.36-fold, $p<0.05$). The interesting result is ASIC2 exhibited considerable downregulation in both PC (-6.41-fold, $p<0.01$) and PE (-9.17-fold, $p<0.05$) samples. Western blot analysis found decreased levels of ASIC2 in both PC and PE costal chondrocytes relative to control costal chondrocytes, though not as substantial as expected (Fig. 29). Protein extractions were performed on Con10, PE1, PE2, PC4, and PC5 and immunoblotted with antibodies specific to ASIC2a. PE1 and PE2 showed slight decreases (77.61% and 61.39%, respectively) while PC4 and PC5 showed a more reduced level of protein (43.68% and 64.50%, respectively) relative to Con10.

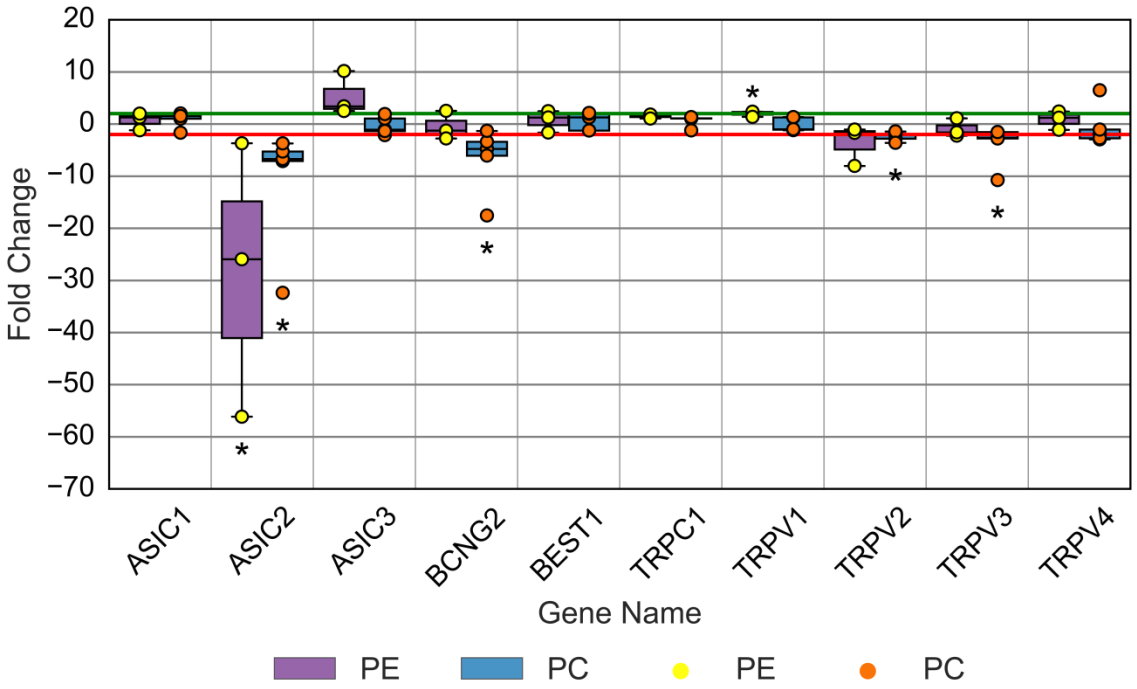

Figure 28. **Fold changes in non-selective ion channels in pectus chondrocytes.** Fold changes in ion channel gene expression using qPCR in chondrocytes in pectus excavatum and pectus carinatum relative to normal costal cartilage. Each sample was analyzed with an n=3 and significant changes ($p<0.05$) relative to normal costal cartilage are indicated (*). The green and red horizontal lines indicated a +2 or -2 fold change, respectively.

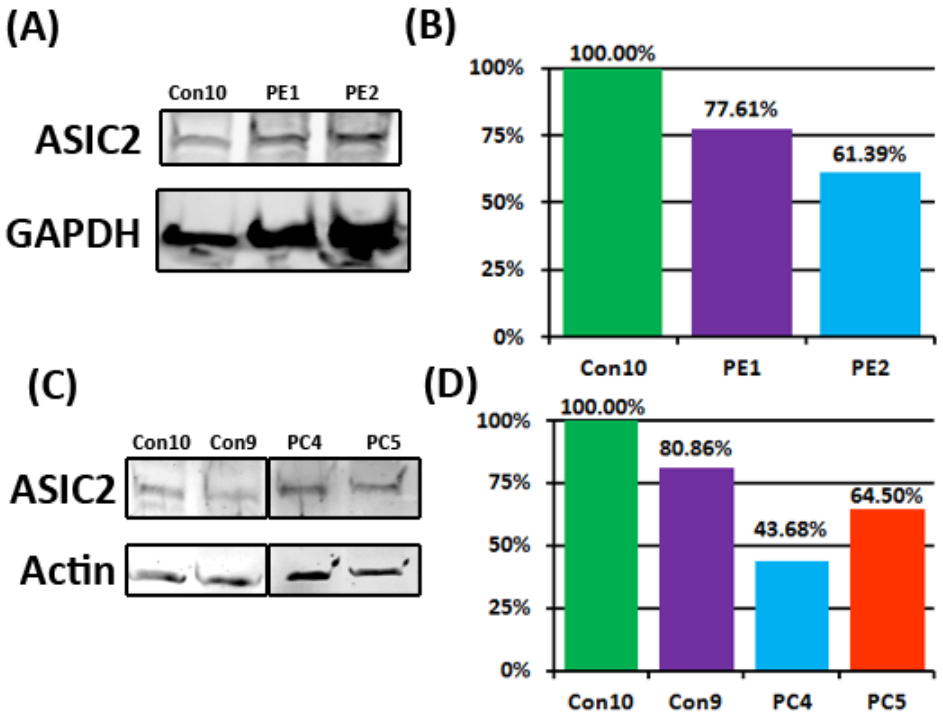

Figure 29. **Western blot of ASIC2.** (A) Protein blotting for chondrocytes from normal and two pectus excavatum costal cartilage samples was performed staining for ASIC2 and GAPDH. (B) The median ASIC2 band signals were normalized to the median GAPDH band signals, and then the normalized signals were calculated relative to the control sample. (C) Protein blotting for chondrocytes from two normal and two pectus carinatum costal cartilage samples was performed staining for ASIC2 and Actin. (D) The median ASIC2 band signals were normalized to the median Actin band signals, and then the normalized signals were calculated relative to the control sample.

Downregulation of ASICs has been attributed to increased cell survival by prevention of acid-induced injury in rat articular chondrocytes. Acid-induced cell death in chondrocytes is thought to occur through a mitochondrial-dependent pathway, and it was found that ASIC-

induced calcium transients cause increased production of calpain and calcineurin leading to induction of caspase 3-mediated apoptosis (Hu et al., 2012). Another study in rat articular chondrocytes has also shown reduced cellular death using ASIC blockers during external acidosis. The cell death in rat articular chondrocytes was found to occur by apoptosis through a mitochondrial pathway where external acidosis resulted in increased expression of *Bax*, increased levels of caspase 3 and caspase 9, and decreased mitochondrial membrane potential (Rong et al., 2012). Although the downregulation of ASICs should increase cell viability under pH stress, it also causes the cell to become more desensitized to extracellular acidosis. The shifts in pH, which occur regularly in the tissue, are crucial to the proper maintenance of cartilage, so the desensitization could impair or modify the development and growth of the tissue. Based on our observation of down-regulated ASIC expression and previous ASIC studies in chondrocytes, we hypothesized that chondrocytes affected by pectus deformities will have decreased intracellular calcium levels when subjected to external acidosis in comparison to unaffected chondrocytes.

3.3 Acid Sensitivity in Costal Chondrocytes

The downregulation of *ACCN1* which encodes for acid sensing ion channel 2 (ASIC2), led to the question of whether PC and PE chondrocytes are desensitized to external acidosis. Normally, ASICs respond to external acidosis by influx of calcium which leads to the formation of intracellular calcium transients. Using live cell ratiometric monitoring of intracellular calcium, measurements of normal costal and PC chondrocytes were performed (Fig. 30). We had predicted that the peak levels of the transient in PC cells would be reduced. To our surprise, we observed a delayed formation of calcium transients in PC cells. Measurements were taken for 60

seconds in normal physiological buffer before low pH buffer (pH 5.5) was added using a vacuum perfusion system. Comparison of transients from Con and PC cells were calculated (Table 1 and Fig. 31 and 32) and found that the transient began to form at around 68.09 (±10.23) seconds and peaked at 103.03 (±15.36) seconds in control cells (n=8); while in PC cells, the transient began at 160.81 (±12.72) seconds and peaked at 200.54 (±2.32) seconds (n=3). Both averaged transients peaked between 0.9 and 0.7 µM $[Ca^{2+}]_i$. Normal cells peaked at 0.892 (±0.152) µM and PC cells peaked at 0.715 (±0.0714) µM. The peak levels were reduced in PC cells, and the differences are marginally increased when accounting for PC levels having slightly higher basal levels of intracellular calcium than control cells (PC: 0.156 ± 0.00747 µM, Con: 0.121 ± 0.00937 µM). Intracellular calcium levels are not well characterized for pH response in chondrocytes with previous recordings of calcium transient levels to be mainly in response to hypo-osmotic stress response showing inconsistent peak levels and total time of intracellular calcium transients (Dascalu et al., 1996; Edlich et al., 2001; Kurita et al., 2015; Parvizi et al., 2002; Sanchez et al., 2003; Sanchez and Wilkins, 2004; Yellowley et al., 2002).

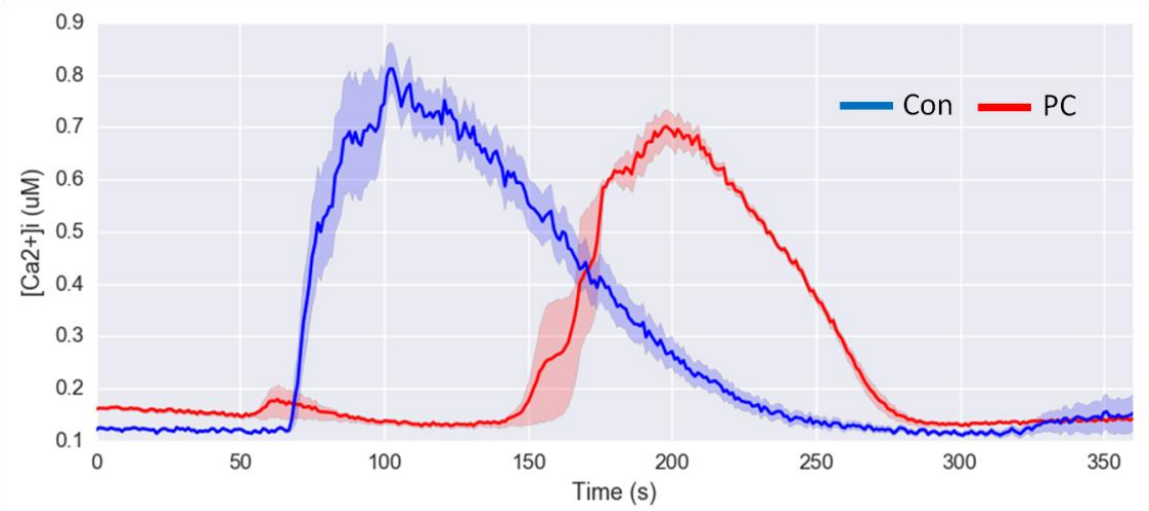

Figure 30. **Intracellular calcium transients in control and PC chondrocytes following pH challenge.** Live imaging of intracellular calcium levels using Fura2-AM with ratiometric imaging. Cells were allowed to equilibriate in a physiological buffer at pH 7.4 and measured for 60 seconds before the buffer was replaced with physiological buffer at pH 5.5 using a vacuum perfusion system and imagining continued for an additional 2 minutes. Individual cell measurements for Con and PC are shown in light blue and light red, respectively. Averaged values for Con and PC are shown as dark blue and dark red traces, respectively.

Table 1. **Summary of transient curve properties following pH challenge**

Property	Control	PC	p-Value
Time of Transient Start (s)	72.68 ± 4.03	160.81 ± 12.7	0.00542
Transient Rise Time (s)	30.36 ± 11.7	39.73 ± 10.4	0.267
Time of Peak (s)	103.04 ± 15.4	200.54 ± 2.32	1.64E-07
Time of Transient End (s)	236.80 ± 31.4	271.76 ± 2.65	0.0161
Transient Fall Time (s)	133.76±35.4	71.22±4.88	0.00209
Total Transient Time (s)	164.12 ± 32.2	110.95 ± 15.2	0.00607

Table 1 Continued

Property	Control	PC	p-Value
Cell Basal Level (µM)	0.121 ± 0.00937	0.156 ± 0.00747	0.00172
Transient Peak Level (µM)	0.892 ± 0.152	0.715 ± 0.0714	0.0310
Transient Increase (µM)	0.771 ± 0.155	0.559 ± 0.0694	0.0135

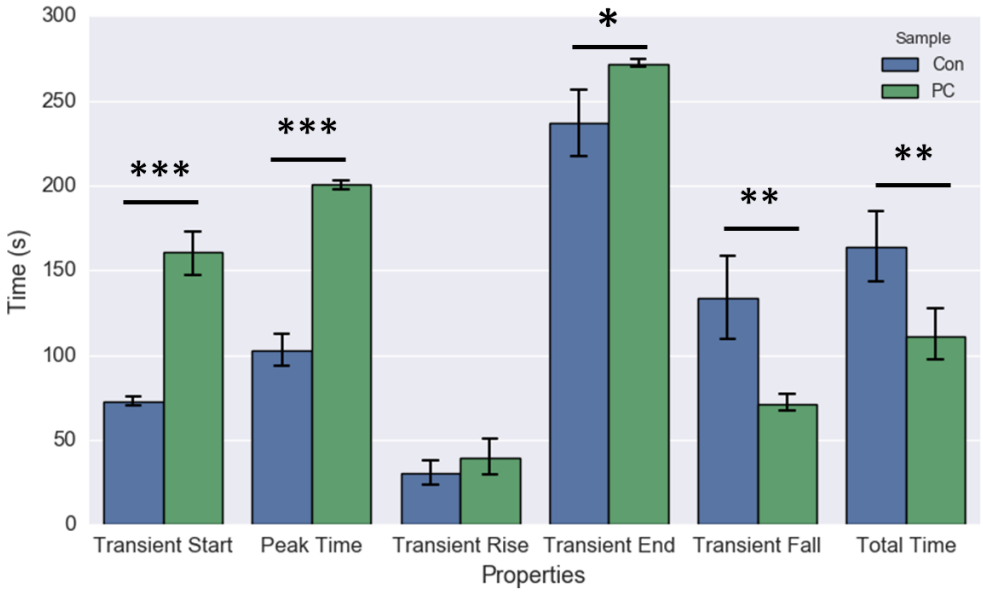

Figure 31. **Graphical display of intracellular calcium transient time properties following pH challenge.** Bar graph representation of summarized transient properties in table 1. The transients analyzed are displayed in Fig. 30. Significant differences ($p < 0.05$, < 0.01, and < 0.001) are indicated by asterisks (*,**, and ***, respectively). P-values are displayed in Table 1.

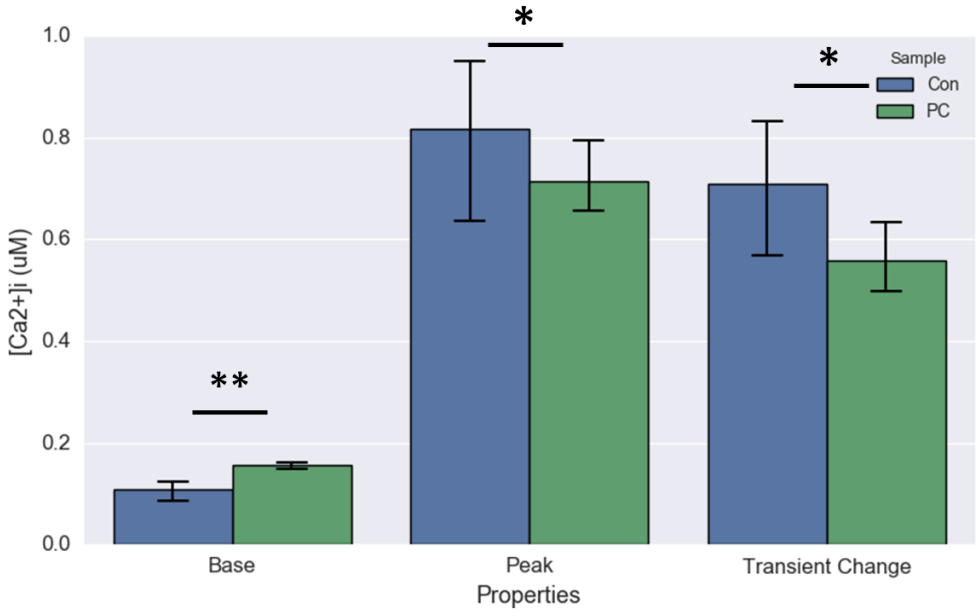

Figure 32. **Graphical display of intracellular calcium transient concentration properties following pH challenge.** Bar graph representation of summarized transient properties in table 1. The transients analyzed are displayed in Fig. 30. Significant differences ($p < 0.05$ and < 0.01) are indicated by asterisks (* and **, respectively). P-values are displayed in Table 1.

The delayed transient formation has not been commonly observed in the literature (to the author's knowledge). A thorough search did not yield any studies where transient formation was delayed to this extent. The only study found where calcium transient formation was delayed was in rat cardiomyoblasts following ultrasonic sonoporation (Fan et al., 2010). The delays observed ranged from 6s-42s (n=4), however the mechanism is unknown and the conditions are not comparable to our study. In a different study, Cheng et al. (2015) looked at the effect of PICK1-knockout in mouse cortical neurons. PICK1 (protein interacting with PRKCA1) is a protein which binds with Protein Kinase C (PKC) and associates with ASICs, assisting with subcellular

localization. The PICK1-knockouts and knockdowns resulted in eliminated or decreased calcium transient peak levels though delays in transient formation following stimulation were not observed. A problem with our observations is that we do not have total elimination of ASIC2 at the protein level, unless there are some modifications causing inactivation. Additionally, expression levels of ASIC1 in PC and PE samples were similar to control samples, though the protein levels have not been confirmed. This poses the question of whether the aberrant calcium transient is a result of decreased ASIC expression, altered functionality, or another mechanism involving other ion channels.

We also analyzed the cell metabolism by MTT assay in normal, PC, and PE costal chondrocytes following acid challenge (n=2 for all sample types; Fig. 33). Due to the expression changes in ASIC2 as well as the abnormal calcium transient, we expected to see decreases in cell metabolism in normal cells while PC and PE cells would be less sensitive or have a delayed response. At pH's 6.5 and 6.0, we saw very similar levels of cell metabolism at almost all time points (0, 5, 10, 30, 60 minutes and 24 hours). Unexpectedly, challenge with media at pH 5.5 lead to consistent decreases in both PC and PE cells, while control samples had a mixed response. The results showing that the pH response by PC and PE cells may only be different at pHs lower than 6.0 may suggest certain ASIC heteromeric combinations (e.g. ASIC1a + ASIC2a) in costal chondrocytes. The variable composition of the ASIC heteromer is known to shift the half-maximal activation pH. Baron et al. (2002) found that the half-maximal activation pHs for ASIC1a and ASIC2a are 6.4 and 4.4, respectively; however, a heteromeric association of ASIC1a and ASIC2a resulted in a channel with a half-maximal activation pH of 5.1. Additionally, the instantaneous response by PC and PE cells and gradual response by control cells may be indicative of regulation of cell response by other pathways being compromised in

pectus-affected cells. This compromised response could be due to the external acidosis at pH 5.5 causing the triggering of downstream signals which would otherwise be blocked by the fast calcium transient formation. Another critical piece of information missing in the literature, other than calcium response to external acidosis, are short-term temporal studies on cell response to external acidosis. Although the hypoxic nature of cartilage creates a slightly acidic environment, the mechanical changes of the tissues are what produce the low pH environments for short periods. Analyzing the literature yields only studies monitoring chondrocyte response to external acidosis for time points greater than 1 hour (Collins et al., 2013; Li et al., 2014; Rong et al., 2012; Yuan et al., 2010; Zhang et al., 2016). Many of the studies monitored the changes over days, but none immediately following pH challenge. It is unknown what mechanisms by which chondrocytes typically respond to pH stress, including short-term downstream effects.

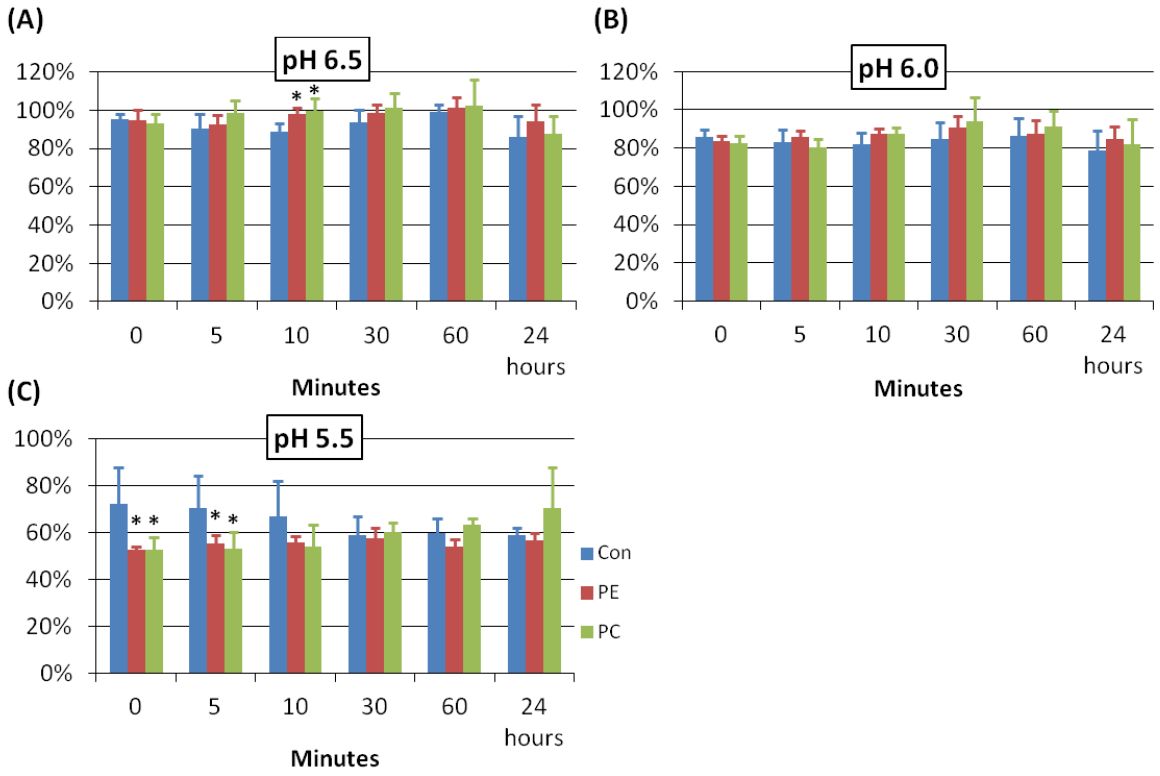

Figure 33. **Metabolic levels of costal chondrocytes after pH challenge.** Metabolic levels of cells from normal costal cartilage (Con), pectus carinatum (PC), and pectus excavatum (PE) were measured after being subjected to low pH (6.5, 6.0, and 5.5). Cell metabolism was measured using an MTT assay at different time points (0, 5, 10, 30, and 60 minutes and 24 hours) after the addition of medium at different pHs. Metabolic levels displayed are relative to the levels of cells treated with normal media at each time point. Significant differences ($p < 0.05$) between Con and both PC and PE are indicated (*).

3.4 Osmotic Sensitivity in Costal Chondrocytes

We tested to see if pectus-affected chondrocytes respond differently from normal chondrocytes when subjected to hypotonic and hypertonic stress (Fig. 34 and 37, respectively).

Analyzing the intracellular calcium response, normal chondrocytes exhibited a mixed calcium transient response to hypotonic (110 mOsm) challenge. PC cells also responded in a similar manner with a mixed response (Fig. 34); however, some cells showed persistently high concentrations of calcium as well as a secondary, but smaller transient. It is difficult to explain the strange transient response by PC cells to hypotonic challenge. One possibility is that the increased expression of Na_V channels in PC cells could be intensifying the hypotonic stress response through their auxiliary functions. Comparison of transients from Con and PC cells were calculated (Table 2 and Fig. 35 and 36) but did not yield any statistically significant differences except for a slight delay in transient formation (Con: 89.20 ± 0.70 and PC: 97.68 ± 1.10, p=2.74E-09).

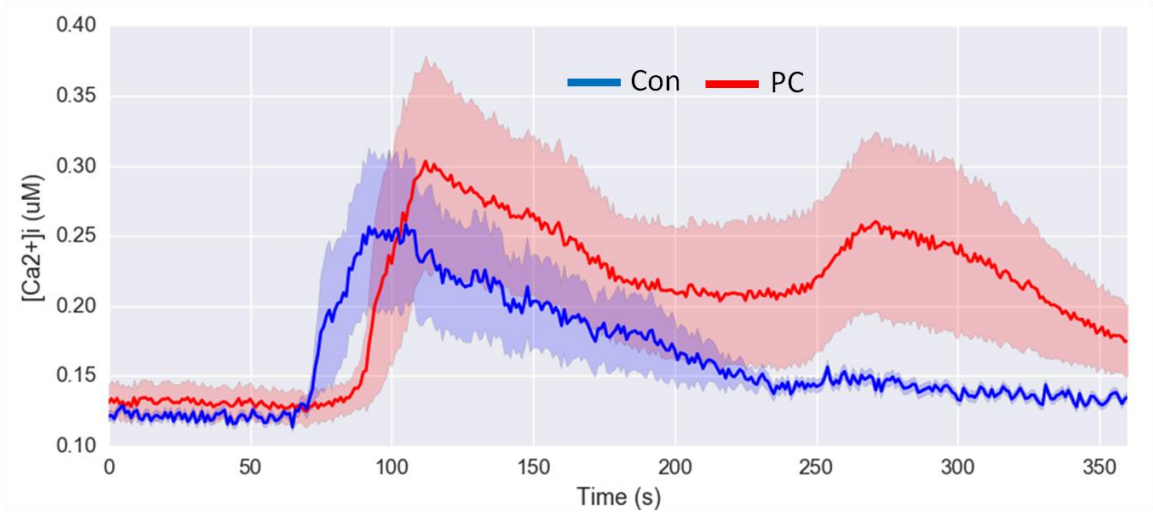

Figure 34. **Intracellular calcium transients in control and PC chondrocytes following hypo-osmolar challenge.** Live imaging of intracellular calcium levels using Fura2-AM with ratiometric imaging. Cells were allowed to equilibriate in a physiological buffer at 280 mOsm and measured for 60 seconds before the buffer was replaced with physiological buffer at 110

mOsm using a vacuum perfusion system and imagining continued for an additional 2 minutes. The confidence interval of cell measurements for Con and PC are shown in light blue and light red, respectively. Averaged values for Con and PC are shown as dark blue and dark red traces, respectively.

Table 2. **Summary of transient curve properties from hypo-osmolar stress**

Property	Control	PC	p-Value
Time of Transient Start (s)	89.20 ± 0.70	97.68 ± 1.10	2.74E-09
Transient Rise Time (s)	67.02 ± 100.10	60.22 ± 86.59	0.903
Time of Peak (s)	156.2 ± 100.5	157.9 ± 86.9	0.976
Time of Transient End (s)	273.5 ± 117.8	321.4 ± 92.4	0.458
Transient Fall Time (s)	117.3 ± 120.1	163.5 ± 109.7	0.501
Total Transient Time (s)	184.3 ± 117.1	223.7 ± 93.3	0.539
Cell Basal Level (µM)	0.121 ± 0.012	0.131 ± 0.029	0.388
Transient Peak Level (µM)	0.299 ± 0.195	0.335 ± 0.204	0.755
Transient Increase (µM)	0.178 ± 0.188	0.204 ± 0.180	0.810

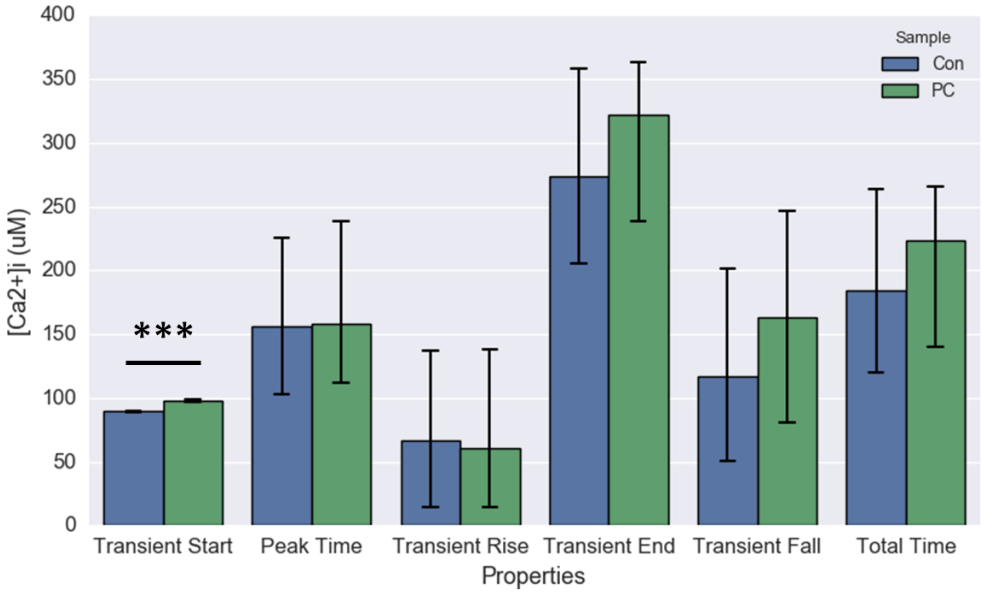

Figure 35. **Graphical display of intracellular calcium transient time properties following hypo-osmolar challenge.** Bar graph representation of summarized transient properties in Table 2. The transients analyzed are displayed in Fig. 33. Significant differences ($p < 0.05$, < 0.01, and < 0.001) are indicated by asterisks (*,**, and ***, respectively). P-values are displayed in Table 2.

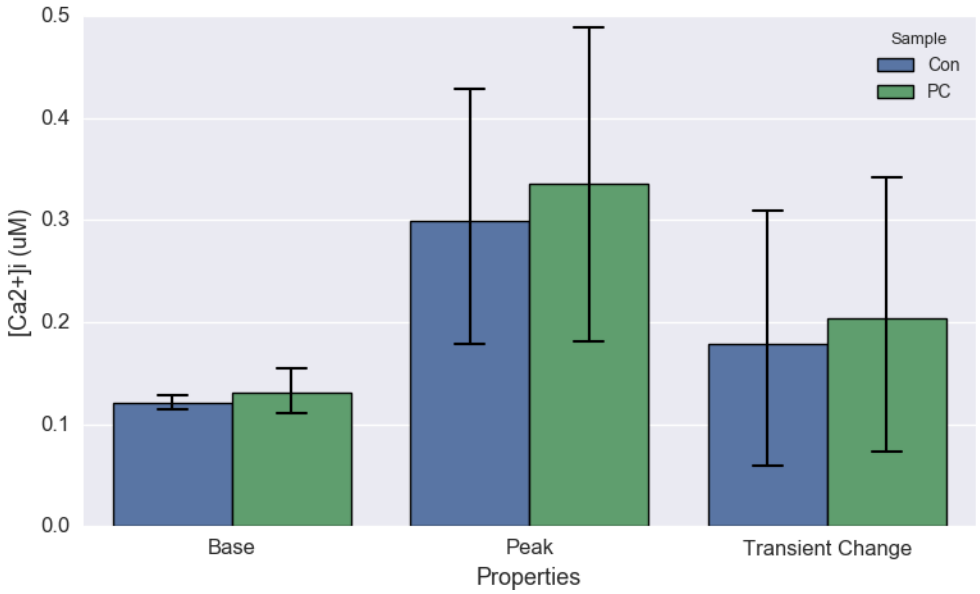

Figure 36. **Graphical display of intracellular calcium transient concentration properties following hypo-osmolar challenge.** Bar graph representation of summarized transient properties in Table 2. The transients analyzed are displayed in Fig. 33.

When challenged with a hyperosmolar solution (400 mOsm), neither control nor PC cells exhibited any response (Fig. 37). Although there were quick spikes in fluorescence in PC cells, it was determined to be from debris during perfusion. This supports previous findings that hypertonic environments does not normally invoke regulated volume increase response (Lewis et al., 2011b).

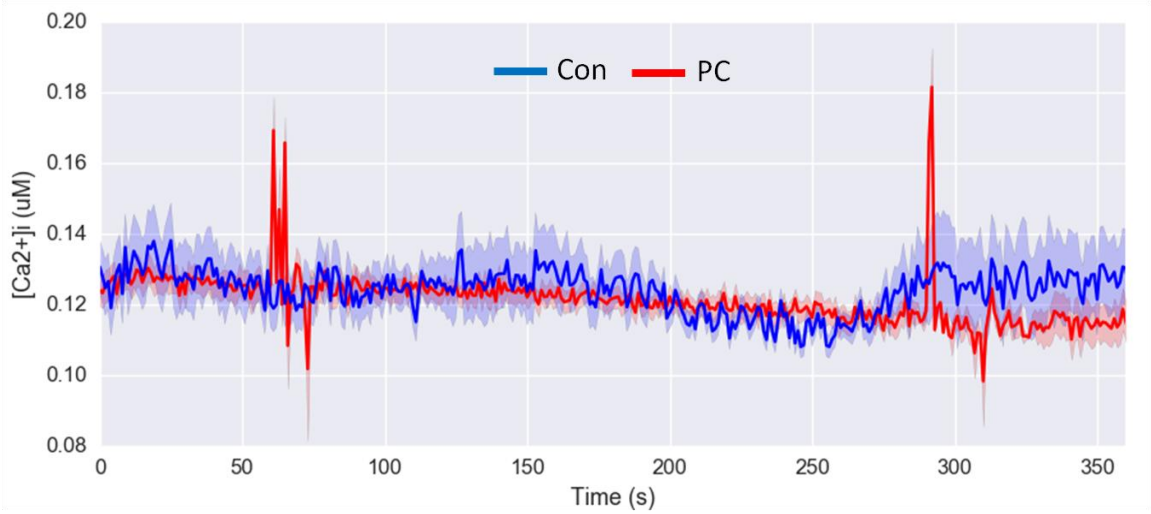

Figure 37. **Intracellular calcium transients in control and PC chondrocytes following hyper-osmolar challenge.** Live imaging of intracellular calcium levels using Fura2-AM with ratiometric imaging. Cells were allowed to equilibriate in a physiological buffer at 280 mOsm and measured for 60 seconds before the buffer was replaced with physiological buffer at 400 mOsm using a vacuum perfusion system and imagining continued for an additional 2 minutes. The confidence interval of cell measurements for Con and PC are shown in light blue and light red, respectively. Averaged values for Con and PC are shown as dark blue and dark red traces, respectively.

The metabolic levels were also measured under both hypotonic and hypertonic challenge (Fig. 38). The response by control, PC, and PE cells were all fairly similar with PC showing a slight increase in metabolism under hypotonic stress. Overall, the differences between Con, PC, and PE cells were unremarkable.

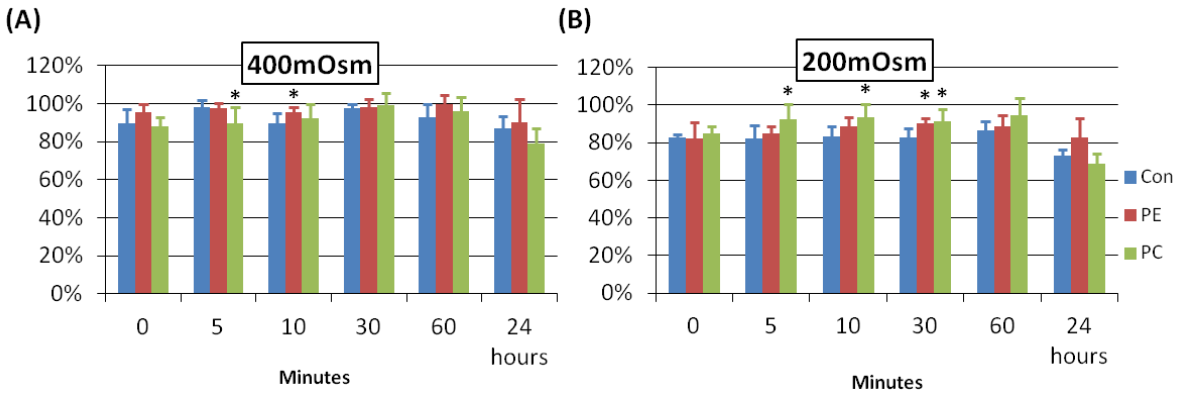

Figure 38. **Metabolic levels of costal chondrocytes after osmolar challenge.** Metabolic levels of cells from normal costal cartilage (Con) and pectus carinatum (PC) when subjected to hypertonic and hypotonic medium. Cell metabolism was measured using an MTT assay at different time points (0, 5,10, 30, and 60 minutes and 24 hours) after the addition of hypertonic medium at (A) 400 mOsm and (B) 200 mOsm. Metabolic levels displayed are relative to the levels of untreated cells at each time point. Significant differences ($p < 0.05$) between Con and PC are indicated (*).

3.5 Connexins

Connexins are transmembrane proteins that form a homo- or hetero-meric channel, known as hemichannels, which are capable of binding hemichannels on adjacent cells to form a direct passage for multicellular communication known as a gap junction. In chondrocytes, there has been previous evidence of connexins being present at the mRNA and protein level, though their functionality remains unknown (Gago-Fuentes et al., 2014). Most of the previous investigations focused on the formation of multicellular communication by gap junctions, however, more recently, explorations into the function of the hemichannels has become more frequent. Hemichannels were originally thought to be inactive until a gap junction is formed,

though now it is known they are capable of transporting several small molecules including microRNAs, ATP, and glutamate. Chondrocytes are known to release ATP in response to different stimuli, which has been speculated to be through a connexin-mediated process (Knight et al., 2009).

Connexin-mediated ATP Release

As connexins are predicted to be involved in ATP signaling, we decided to test ATP signaling in response to pH stress. We originally tested whether ATP is released in a connexin-dependent manner in chondrocyte-related cells (Fig. 39). Using the chondrosarcoma cell line, JJ012, with and without the presence of the connexin blocker, carbenoxolone, we found that basal levels of extracellular ATP to be reduced at all dosages. Additionally, we stimulated the cells using a single nanosecond pulsed electric field (60 kV/cm, 60 ns). Using an ultrashort pulsed electric field (<1 μs) causes changes to internal structures leading to increases in intracellular calcium (Beebe et al., 2004). The stimulation by pulsed electric field resulted in an increase of extracellular ATP in untreated cells with a significant reduction in cells using higher dosages of carbenoxolone supporting the claim that chondrocytes release ATP through connexins in response to external stimuli.

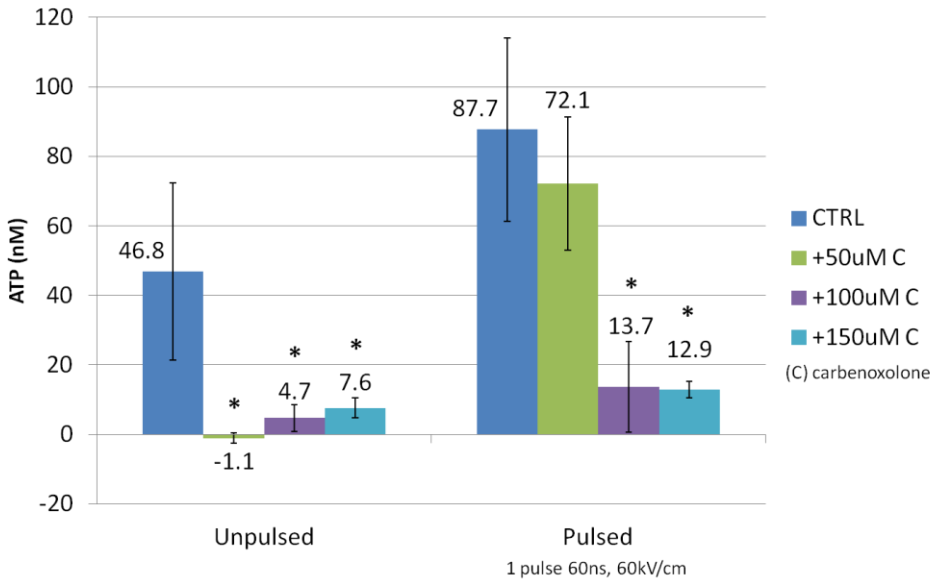

Figure 39. **ATP release in chondrosarcoma cells.** Levels of extracellular ATP measured in chondrosarcoma cells stimulated by a pulsed electric field with and without the addition of the connexin blocker, carbenoxolone. Cells were stimulated with a single 60 nanosecond pulsed electric field with a field strength of 60kV/cm in the presence of four different concentrations of carbenoxolone (0µM, 50µM, 100µM, and 150µM). Levels of ATP are displayed in nanomolars.

ATP release has been shown to occur in chondrocytes when stimulated by mechanical loading (Garcia and Knight, 2010), but no study has looked at ATP release from pH challenge in chondrocytes, though there is evidence that external acidosis causes increases in extracellular ATP in other cell/tissue types (Bergfeld and Forrester, 1992; Kluess et al., 2005; Wildman et al., 1997). The release of ATP is presumed to occur through connexin hemichannels with the extracellular ATP causing activation of P2X and P2Y receptors resulting or assisting in intracellular calcium transients (Fig. 40). P2X receptors are sensitive to extracellular ATP and become permeable to Ca^{2+} and Na^{+}. The influx of calcium increases the cytosolic calcium

concentration while the influx of sodium contributes to membrane depolarization and subsequent activation of voltage-activated calcium channels (Garcia and Knight, 2010). The P2Y channels are quite different in that they are not channels, but G-protein coupled receptors (GPCRs). External ATP activation causes activation of the phospholipase C (PLC) pathway resulting in downstream IP_3-mediated calcium release (Glaser et al., 2013; Puchalowicz et al., 2014).

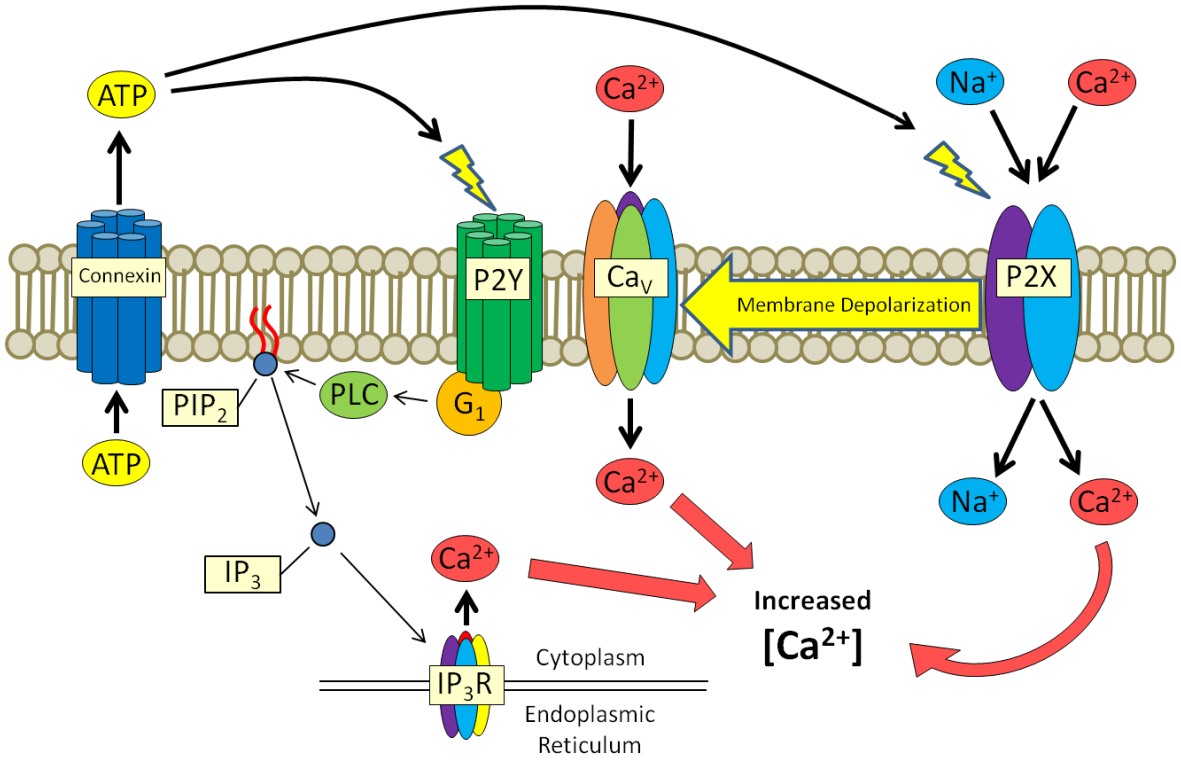

Figure 40. **Diagram of connexin-P2X-P2Y-mediated calcium transient formation.** Stimulation of connexins results in the release of ATP into the extracellular space which activates the ATP-gated P2X channels and P2Y GPCR. The P2X activation causes an influx of Na^+ and Ca^{2+} contributing to the intracellular calcium concentration and depolarizing the membrane to activate Ca_V channels. The P2Y activation causes G-protein-related downstream activation of IP_3R and release of calcium from internal stores.

Although intracellular ATP fluctuations have been seen in changing pH and hypoxic challenges in chondrocytes; this response may be dependent on the type and/or species of the chondrocytes. Milner et al. (2006) found that ATP levels were not affected by hypoxia and changes in pH in equine articular cartilage of metacarpolphalangeal origin. However, human osteoarthritic chondrocytes grown in a 3-dimensional alginate system showed hypoxia- and pH-induced decreases in intracellular ATP levels (Collins et al., 2013). It is important to note that in the Collins et al. (2013) study, normal articular cartilage was not tested. An important consideration for the experimental setup was that the pH studies were done under normoxia which is also a possible cause of the lack of response. In Das et al. (2010), gene expression changes of ECM genes were significantly different at different pH's in a hypoxic environment, while under normoxia, the changes at different pH's were relatively muted.

We measured the ATP release (Fig. 41 and 42) and intracellular ATP levels (Fig. 43) in chondrocytes following challenge with low pH. Although we had expected constitutive release of ATP as in JJ012 cells, both human normal costal and pectus costal chondrocytes showed no constitutive release of ATP into the extracellular medium with the exception of PC4 which seemed to release ATP at both 1 minute and 10 minutes. Additionally, the release was significantly reduced with the addition of 150 µM carbenoxolone suggesting a hemichannel-mediated process. Furthermore, no release of ATP was observed following acid challenge which was unexpected as chondrocytes exhibit ATP released following mechanical stress while ATP release occurs in other tissues when challenged with acid. The preincubation was eliminated as a possible confounding factor as challenge was also tested with no preincubation before the addition of acidic growth medium or the addition of acidic HBSS. There was worry that the

preincubation may have caused release of ATP and led to desensitization to the acid challenge, but in both cases without preincubation, no response was observed (data not shown).

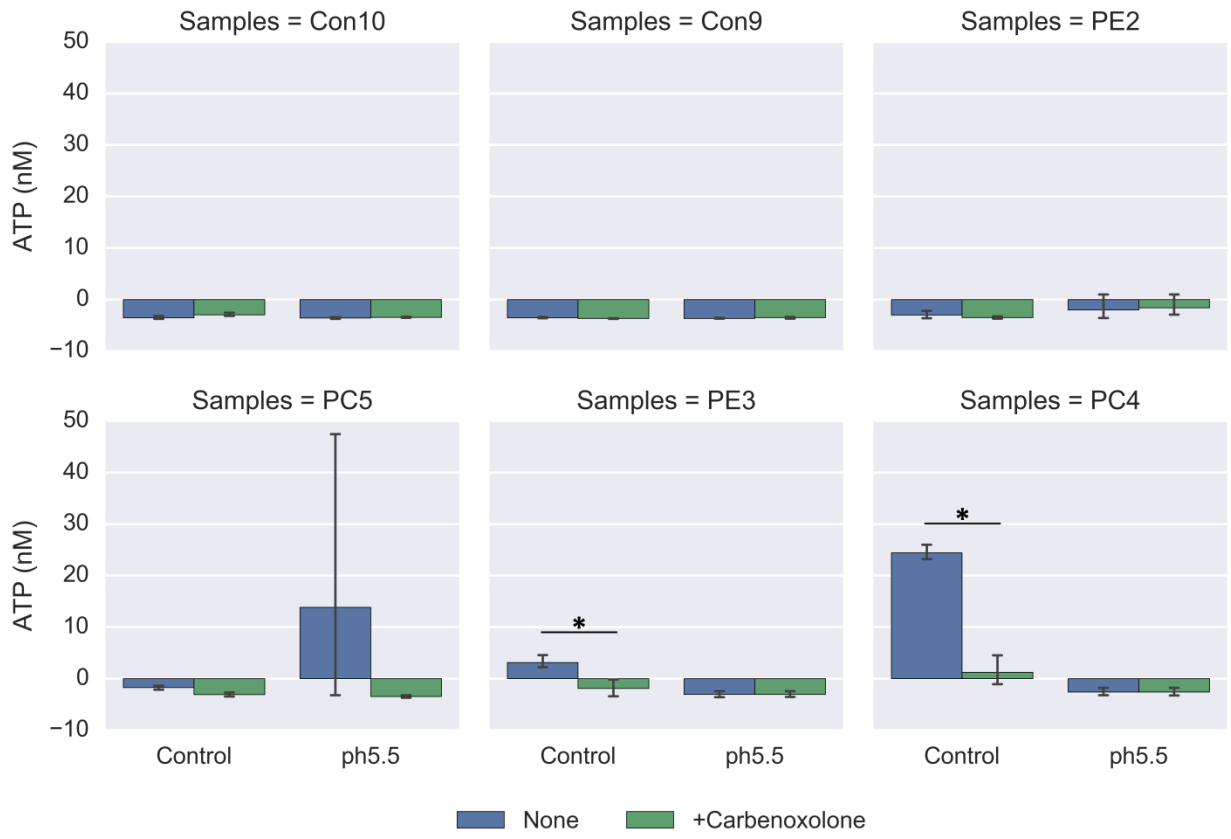

Figure 41. **ATP release from normal and pectus-affected chondrocytes following acid challenge for 1 minute.** Extracellular ATP was measured in normal, PC, and PE cells (n=2 for each) where cells were challenge with HBSS at pH 5.5 with and without the presence of 150µM carbenoxolone. P-values < 0.05 are represented by an asterisk (*).

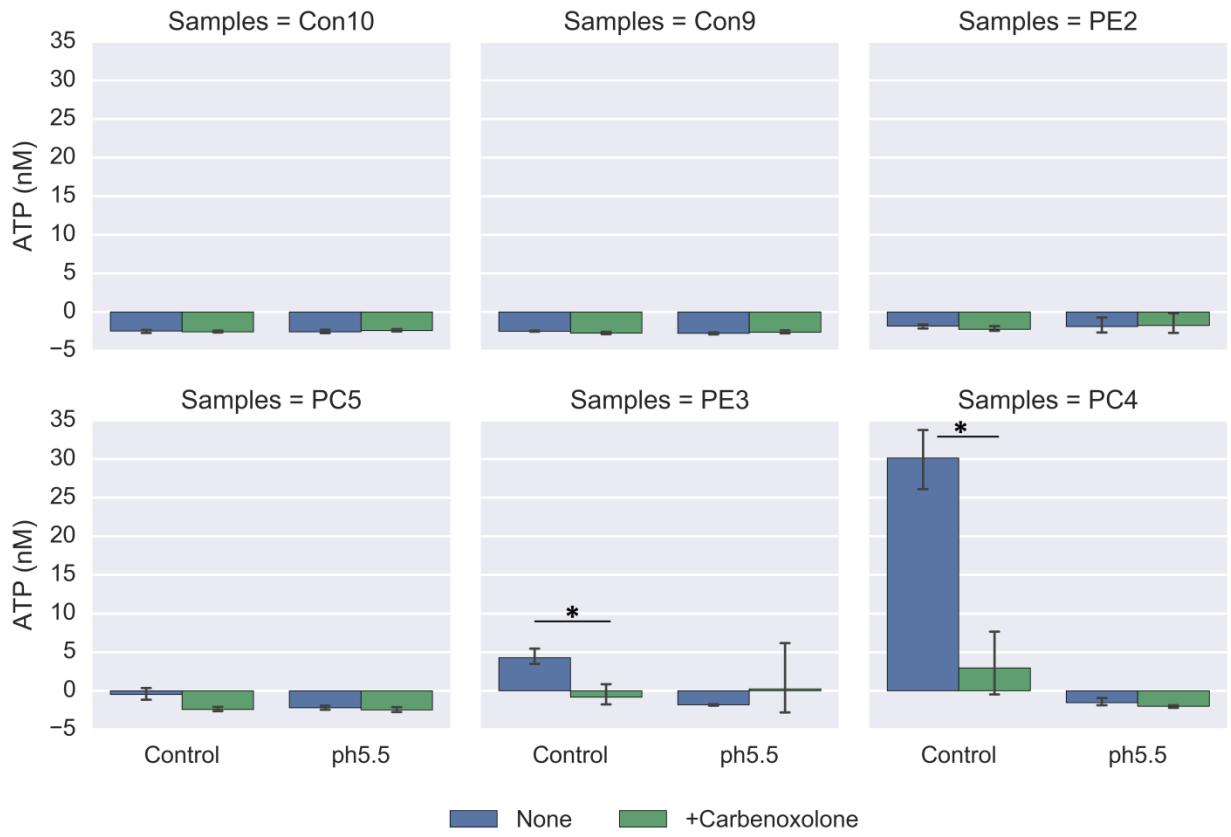

Figure 42. **ATP release from normal and pectus-affected chondrocytes following acid challenge for 10 minutes.** Extracellular ATP was measured in normal, PC, and PE cells (n=2 for each) where cells were challenge with HBSS at pH 5.5 with and without the presence of 150µM carbenoxolone. P-values < 0.05 are represented by an asterisk (*).

The intracellular ATP levels are difficult to interpret, though we had expected to see a reduction after the addition of the acidic HBSS. However, we did observe increases in some samples with the addition of carbenoxolone having varying effects on the intracellular levels. We had expected to see increases due to the reduction of ATP release, however, the amount of ATP release seems to be insignificant in comparison to the basal levels of ATP within the cells (nM vs. µM levels, respectively).

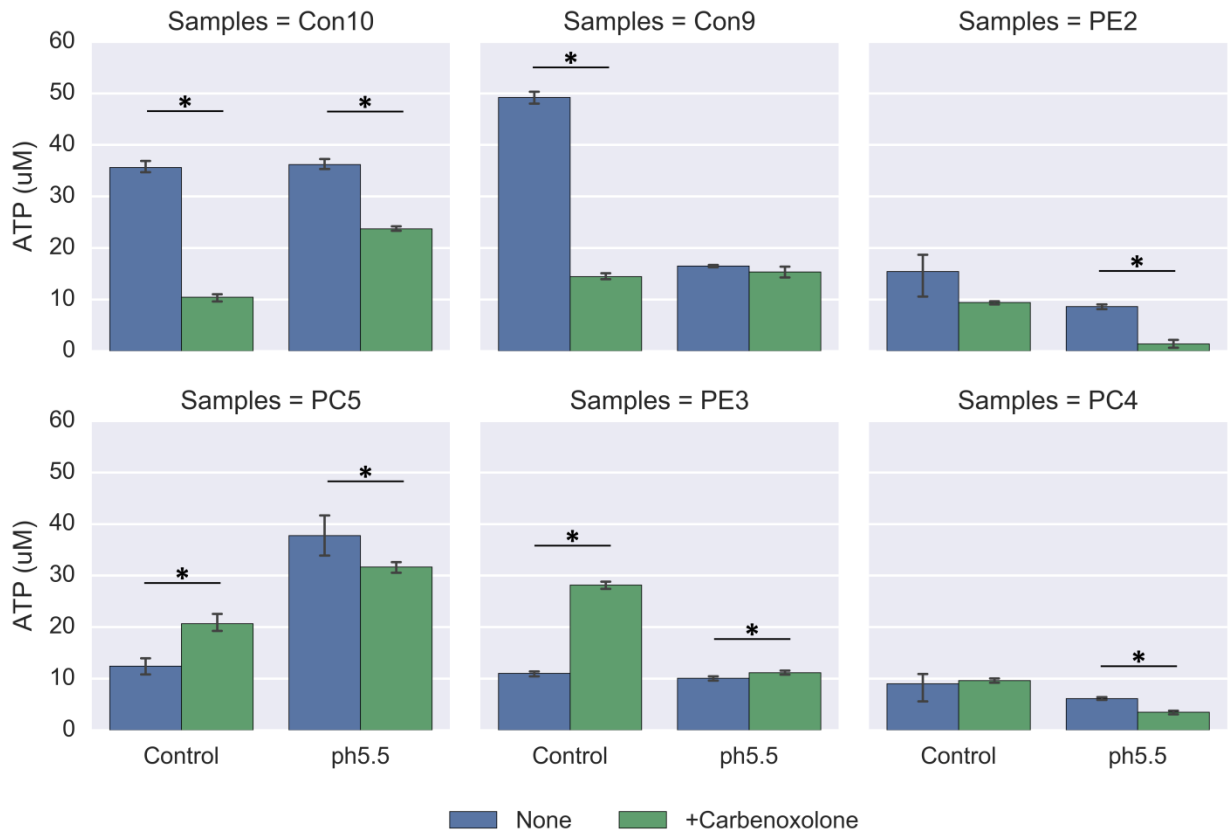

Figure 43. **Intracellular ATP levels in normal and pectus-affected chondrocytes following acid challenge for 10 minutes.** Intracellular ATP was measured in normal, PC, and PE cells (n=2 for each) where cells were challenge with HBSS at pH 5.5 with and without the presence of 150µM carbenoxolone. P-values < 0.05 are represented by an asterisk (*).

Connexins in Chondrocytes

Although we see gene expression of connexins in our chondrocytes, we used immunofluorescent staining to confirm their presence. We observed the presence of Cx43 with multiple foci as well as diffuse staining (Fig. 44). The diffuse staining is expected as connexins have a high turnover rate with a half-life of 1-3.5 hours. The connexins are quickly internalized and recycled and are referred to as annular junctions (Jordan et al., 2001). Additionally, we

analyzed the presence of phosphorylated Cx43 (p-Cx43) and observed an unexpected result of localization in and around the nucleus (Fig. 45).

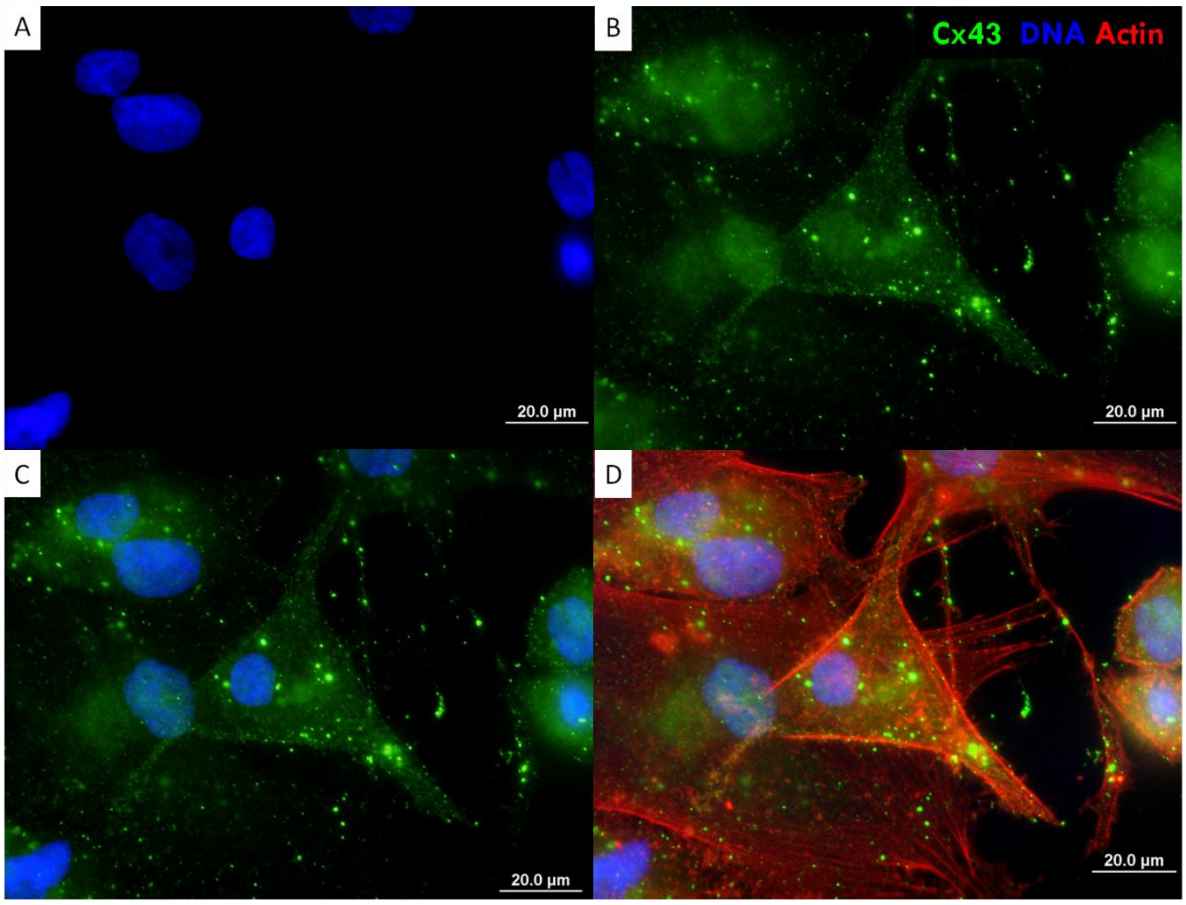

Figure 44. **Immunofluorescent staining for connexin 43 (Cx43) in normal costal chondrocytes.** Nuclei (blue) and Cx43 (green) are displayed individually (a and b, respectively), a merge of nuclei and Cx43 (c), and a merge of filamentous actin (red), nuclei, and Cx43 (d) are displayed. Images were taken at 40X, and scale bars represent 20µm.

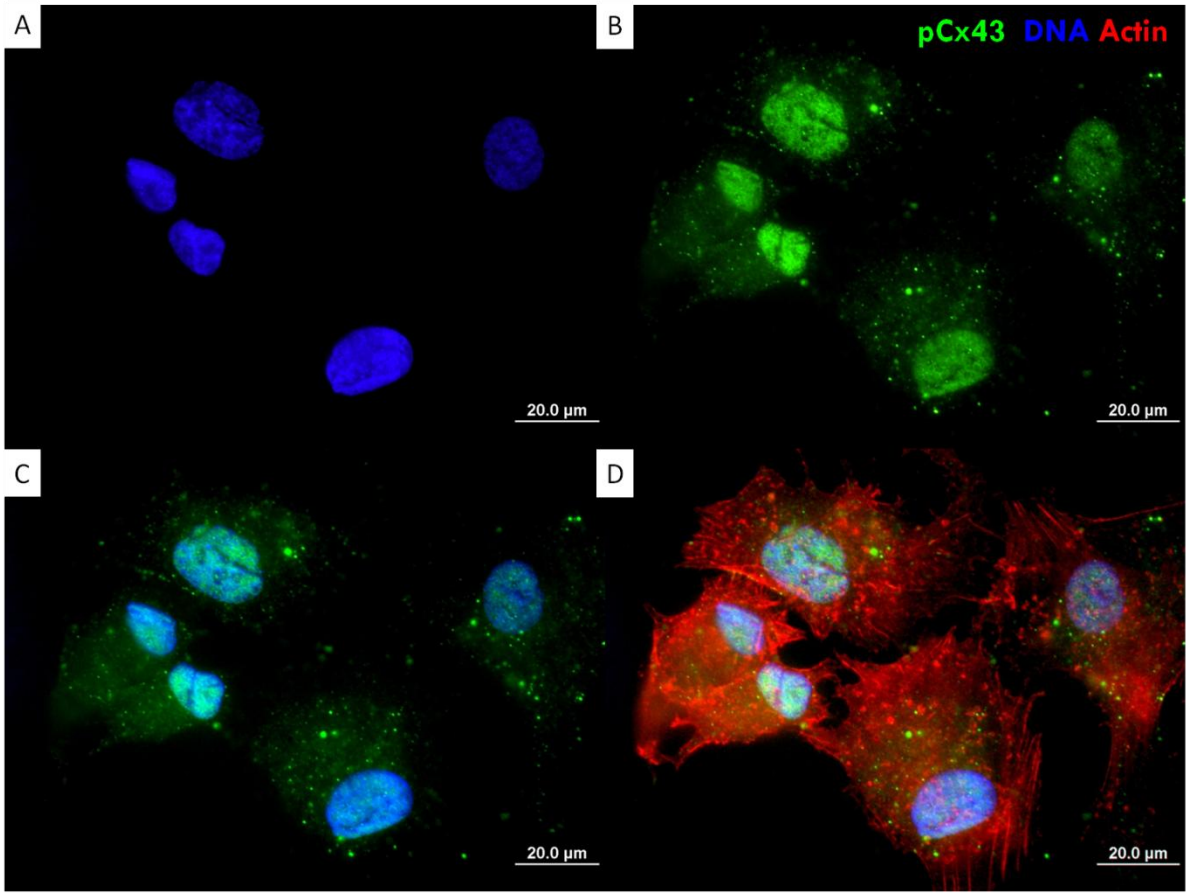

Figure 45. **Immunofluorescent staining for phosphorylated connexin 43 (p-Cx43) in normal costal chondrocytes.** Nuclei (blue) and p-Cx43 (green) are displayed individually (a and b, respectively), a merge of nuclei and p-Cx43 (c), and a merge of filamentous actin (red), nuclei, and p-Cx43 (d) are displayed. Images taken at 40X, and scale bars represent 20um.

One explanation of the nuclear localization of p-Cx43 is that connexins have been connected to controlling cell cycle progression. The mechanism by which this occurs is through sequestration of certain proteins key to cell cycle progression. Dang et al. (2003) found that a truncated form of Cx43 consisting of the carboxyl terminus (CT) internalizes into the cytoplasm and is capable of inhibiting cell growth. Hino et al. (2015) found that cell cycle disruption is due

to the Cx43-CT binding to heat shock cognate protein 70 (Hsc70). Hsc70 normally forms a complex with Cyclin D1 along with p27 and CDK4 resulting in translocation of the complex into the nucleus and triggering G1-to-S phase transition. Using fluorescent microscopy, we have observed the presence of Cx43 in the cell as well as in the nucleus. Interestingly, using an antibody for a phosphorylated form of the Cx43, we see a mainly nuclear localization suggesting that the phosphorylation of Cx43 is what induces the internalization of the carboxyl terminus. What remains unknown is whether the phosphorylation event causes just the cleavage of the CT fragment from Cx43 while it is still localized in the plasma membrane, or if it is a downstream event after the internalization and recycling of the protein. Additional questions we pose are whether the annular junctions are a result of CT phosphorylation or cleavage, or if the cleavage and phosphorylation occur after the internalization. However, what is clear, is that the phosphorylated Cx43 CT is consistently localized in and around the nucleus.

3.6 MicroRNAs

MicroRNAs are short (~20 nucleosides), stable RNAs capable of binding to mRNAs and preventing translations through a number of mechanisms. Similar to siRNAs, miRNAs are considered to be post-transcriptional regulators as they regulate protein production after transcription but before translation. MicroRNAs are a growing field of protein and gene regulation which have been found to play important roles in disease pathogenesis. Using microarray analysis for all known human microRNAs, we analyzed microRNAs extracted from a single control and PC sample (Con8 and PC1). The results were analyzed with upregulated and down-regulated microRNAs plotted versus our expressed ion channels. The interaction plots were created by examining the interactions between our different expressed ion channels using

STRING analysis. The expressed microRNAs were then matched with their target ion channels using a custom matching script in Python and a miRNA database (miRDB) with a high cutoff for target probability. The results were created into an edge table and plotted as an interaction network. An upregulation of microRNAs should supposedly result in decreased proteins levels, even though the mRNA levels are not changed. Conversely, decreased miRNA levels will result in increased protein levels. Different cancers and diseases have specific modifications in miRNA levels which can provide an identifying pattern or "signature." Unfortunately, the current data is limited by the number of samples tested, as well as replications to assess variability, but our microarray analysis of microRNAs showed significant changes in the levels of multiple microRNAs between control and PC costal chondrocytes.

A large number of miRNAs (49 miRNAs) were upregulated in PC2 samples versus Con8 (Table 3 and Fig. 46). Many of the expressed ion channels were targeted by 1-3 miRNAs, but KCNAB2, SCN8A, SCN2A, CLCN3, and ACCN2 all had 4+ associated miRNAs. Having multiple targets may mean that although there is no difference in the gene expression between both sample types, the protein levels may vary due to mRNA degradation or translational repression. Upregulation of miR-196 is associated with early development and differentiation of tissue development including cartilage (Hornstein et al., 2005; Yueh et al., 1998). Additional miRNAs involved in differentiation and development include miR-1915 (Sallustio et al., 2013), miR-637 (Huang et al., 2012), miR-4708 (Kato et al., 2014) and miR-611 (Baglio et al., 2013). Upregulation of most of the listed miRNAs is associated with the development, progression, and metastatic potential of several forms of cancer and include miR-196a and miR196b (Guan et al., 2010), miR-199b (Mudduluru et al., 2011), miR-137 (Xiu et al., 2014), miR-373 and miR-371a (Sanchez-Jimenez et al., 2013), miR-214 (Wang et al., 2014), miR-1208 (Bienertova-Vasku et

al., 2013), and miR-374a (Cai et al., 2013). Conversely, upregulation of other miRNAs may act as tumor suppressors through increased cell senescence such as miR-128 (Palumbo et al., 2013), miR-34c (Cannell et al., 2010), miR-148b (Zhao et al., 2013), miR-218 (Tie et al., 2010), and miR-186 (Li et al., 2013). Some miRNAs are upregulated as part of a response mechanism indicative of increased inflammation such as miR-4455, miR-574, miR-3935 (Miyata et al., 2015; Wang et al., 2016), miR-8071 (Du et al., 2016). The number of upregulated genes is difficult to interpret and suggests that there could be multiple processes and pathways which are dysregulated. The upregulation of tumor-associated miRNAs could suggest that PC cells have an increased proliferative or migratory potential while upregulation of tumor suppressor miRNAs is indicative of higher levels of cellular senescence. Variable states of differentiation and dedifferentiation are also inferred with possible inflammatory processes occurring within the cells.

Table 3. **Upregulated miRNAs and their target ion channels**

miRNA	Con9 Avg Signal	PC2 Avg Signal	Fold Change	Targets	Weight
hsa-miR-196a-5p	4.93	0.63	19.6	CLCN3	92.60863
hsa-miR-199b-5p	4.63	0.86	13.68		
hsa-miR-137	3.28	0.17	8.64		
hsa-miR-5572	3.83	1.07	6.75	TRPV3	71.89545
hsa-miR-128-3p	3.83	1.1	6.67		
hsa-miR-214-5p	5.31	2.62	6.47		
hsa-miR-34c-3p	3.72	1.07	6.28	KCNJ14	55.1709
hsa-miR-2277-3p	3.77	1.24	5.81		

Table 3 continued

miRNA	Con9 Avg Signal	PC2 Avg Signal	Fold Change	Targets	Weight
hsa-miR-373-5p	3.09	0.59	5.67	CLCN3	52.24017
				KCNJ14	80.9857
				SCN2A	53.7676
				SCN9A	91.26496
				TRPV1	74.836
hsa-miR-8064	3.91	1.44	5.54	KCNMA1	87.4121
hsa-miR-34b-5p	2.44	0.12	5.02	CACNA1A	76.7628
hsa-miR-1208	2.38	0.08	4.94		
hsa-miR-148b-3p	3.64	1.35	4.91	ACCN2	50
				CLCN3	60.24487
				SCN8A	68.28949
				SCN9A	77.2726
hsa-miR-374a-5p	2.81	0.57	4.73		
hsa-miR-1202	3.87	1.63	4.73	KCNAB2	69.7576
hsa-miR-637	4.42	2.22	4.59	CLCN7	53.4002
hsa-miR-4479	3.49	1.32	4.5		
hsa-miR-218-5p	2.89	0.72	4.47		
hsa-miR-186-5p	1.88	-0.27	4.43	SCN2A	71.8486
				SCN8A	69.19664
				SCN9A	98.03267
				TRPV1	59.63427
hsa-miR-30b-3p	3.26	1.13	4.39	CACNB1	57.14806
				KCNAB2	79.59724
				TRPV1	53.38016
hsa-miR-6887-5p	3.08	0.98	4.27		

Table 3 continued

miRNA	Con9 Avg Signal	PC2 Avg Signal	Fold Change	Targets	Weight
hsa-miR-8071	2.74	0.65	4.27		
hsa-miR-628-3p	3.2	1.13	4.19		
hsa-miR-1199-5p	3.49	1.43	4.15		
hsa-miR-6826-5p	2.98	0.98	4.02		
hsa-miR-93-3p	4	2.03	3.93		
hsa-miR-4708-3p	2.78	0.81	3.92	SCN8A	56.2813
hsa-miR-650	2.26	0.32	3.84	ACCN2	63.7352
hsa-miR-611	3.23	1.29	3.82		
hsa-miR-3935	2.39	0.49	3.74		
hsa-miR-4525	2.95	1.05	3.74		
hsa-miR-6742-5p	2.99	1.11	3.69		
hsa-miR-3177-5p	2.3	0.46	3.58	ACCN2	73.089
hsa-miR-34c-5p	4.52	2.69	3.56	ACCN1	93.66192
				CACNA1C	54.14347
				CACNB3	88.3234
				CLCN3	83.7212
				KCNAB2	52.70092
				SCN2B	95.73297
hsa-miR-4510	2.57	0.74	3.56	ACCN2	79.14097
				CACNB1	84.8505
hsa-miR-342-5p	3.33	1.52	3.51	CLCN7	62.1237
				KCNAB2	64.51599
hsa-miR-6772-5p	3.2	1.39	3.51	SCN9A	78.9997
hsa-miR-4695-3p	2.18	0.4	3.44		
hsa-miR-596	1.75	-0.02	3.4	CLCN3	61.9444

Table 3 continued

miRNA	Con9 Avg Signal	PC2 Avg Signal	Fold Change	Targets	Weight
hsa-miR-196b-5p	2.34	0.58	3.38		
hsa-miR-431-5p	2.53	0.77	3.38	KCNJ2	84.97203
hsa-miR-4286	2.02	0.28	3.33	TRPV3	84.99304
hsa-miR-6080	5.47	3.74	3.3	SCN2A	76.9705
hsa-miR-3944-3p	2.51	0.79	3.29		
hsa-miR-4306	3.37	1.66	3.27	CACNB1	85.1505
				CLCN3	98.15213
				KCNAB2	89.5872
hsa-miR-574-5p	4.1	2.41	3.23	SCN8A	93.62649
hsa-miR-371a-5p	2.12	0.48	3.12	KCNJ15	60.2885
				SCN2A	69.5943
				SCN9A	87.6327
hsa-mir-1915	2.63	1.03	3.03		
hsa-miR-4455	2.23	0.64	3.01	CACNA1A	66.55729
				CACNA1C	76.75659
				KCNAB2	79.8804
				SCN2B	92.96523
				TRPV3	71.05157
				TRPV4	52.2945

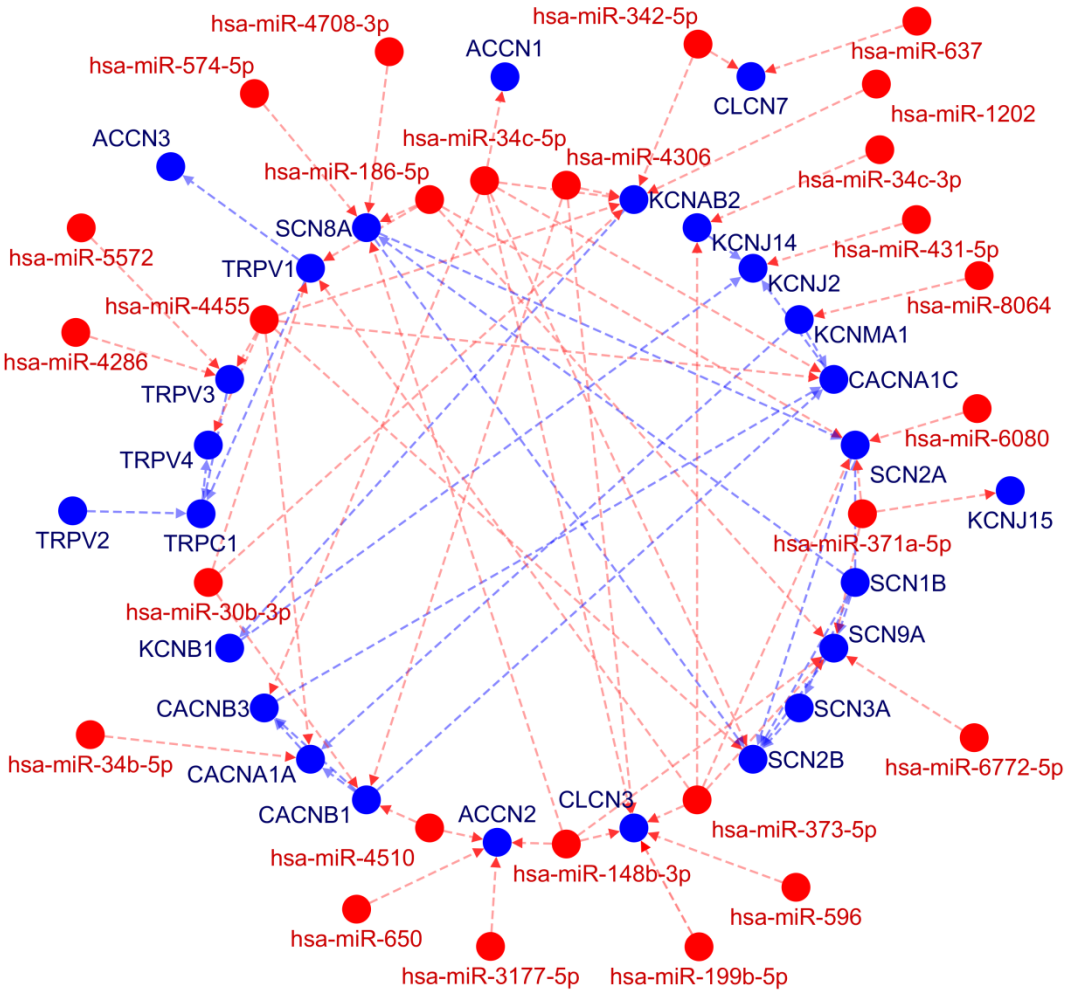

Figure 46. **Network interaction map of miRNAs upregulated in pectus carinatum.** All miRNAs (red nodes) found to be upregulated by 3-fold or more are shown as well as their ion channel targets (blue nodes). Interactions between miRNA and ion channel targets are indicated by a dotted red line and arrow. Ion channel interactions with other ion channels are indicated by a dotted blue line and arrow.

There were less than half as many miRNAs (21) down-regulated in PC2 versus Con8 chondrocytes compared to the number upregulated (Table 4 and Fig. 46). Although there are 21

down-regulated miRNAs, two seem to stand out as possible major regulators of ion channel signaling as they target several different ion channels. Down-regulation of these two miRNAs, miR-195-5p and miR-497-5p, are both part of the same intronic cluster and were found to be methylated in triple-negative breast cancer (Chang et al., 2015) leading to upregulation of *Raf-1* and *Ccnd1* in breast cancer (Li et al., 2011). Down-regulation of both these miRNAs is also associated with osteogenic differentiation and angiogenesis through growth factor regulation (Almeida et al., 2016). It is difficult to say what effect these miRNAs have and whether any effects are from ion channel regulation or from other miRNA targets.

Table 4. **Down-regulated miRNAs and their target ion channels**

miRNA	Con9 Avg Signal	PC2 Avg Signal	Fold Change	Target	Weight
hsa-miR-6766-3p	1.38	2.96	-3.01		
hsa-miR-3651	2.76	4.4	-3.12		
hsa-miR-411-5p	2.93	4.6	-3.18		
hsa-miR-29b-3p	3.56	5.28	-3.28	*CACNA1C*	61.81874
hsa-miR-3921	2.34	4.07	-3.32		
hsa-miR-455-5p	0.36	2.1	-3.33	*KCNJ2*	76.4345
hsa-miR-6813-3p	0.39	2.14	-3.37		
hsa-miR-514b-5p	1.43	3.21	-3.44	*SCN8A*	61.70945
hsa-miR-296-5p	-0.29	1.58	-3.67	*CACNB1*	91.39019
hsa-miR-195-5p	4.85	6.74	-3.69	*CACNB1*	59.2203
				CLCN3	58.8451
				KCNJ2	79.86623
				SCN2A	50.7198

Table 4 continued

miRNA	Con9 Avg Signal	PC2 Avg Signal	Fold Change	Target	Weight
hsa-miR-195-5p	4.85	6.74	-3.69	*SCN3A*	79.2063
				SCN8A	96.29279
				TRPC1	62.25408
				KCNJ15	62.2519
hsa-miR-935	-0.31	1.62	-3.81		
hsa-miR-140-5p	4.72	6.67	-3.87	*ACCN2*	90.16745
				KCNB1	89.0295
				SCN9A	88.208
hsa-miR-299-5p	0.97	3.13	-4.48		
hsa-miR-140-3p	7.79	9.97	-4.53		
hsa-miR-497-5p	1.45	3.68	-4.71	*CACNB1*	59.2203
				CLCN3	58.8451
				KCNJ2	79.86623
				SCN2A	50.7198
				SCN3A	53.0799
				SCN8A	96.29279
				TRPC1	62.25408
hsa-miR-224-5p	1.44	3.75	-4.96	*SCN9A*	90.4179
hsa-miR-8084	1.92	4.24	-5.01		
hsa-miR-297	1.21	3.59	-5.21		
hsa-miR-210-3p	5.23	8.15	-7.55		
hsa-miR-126-3p	0.44	3.57	-8.73		

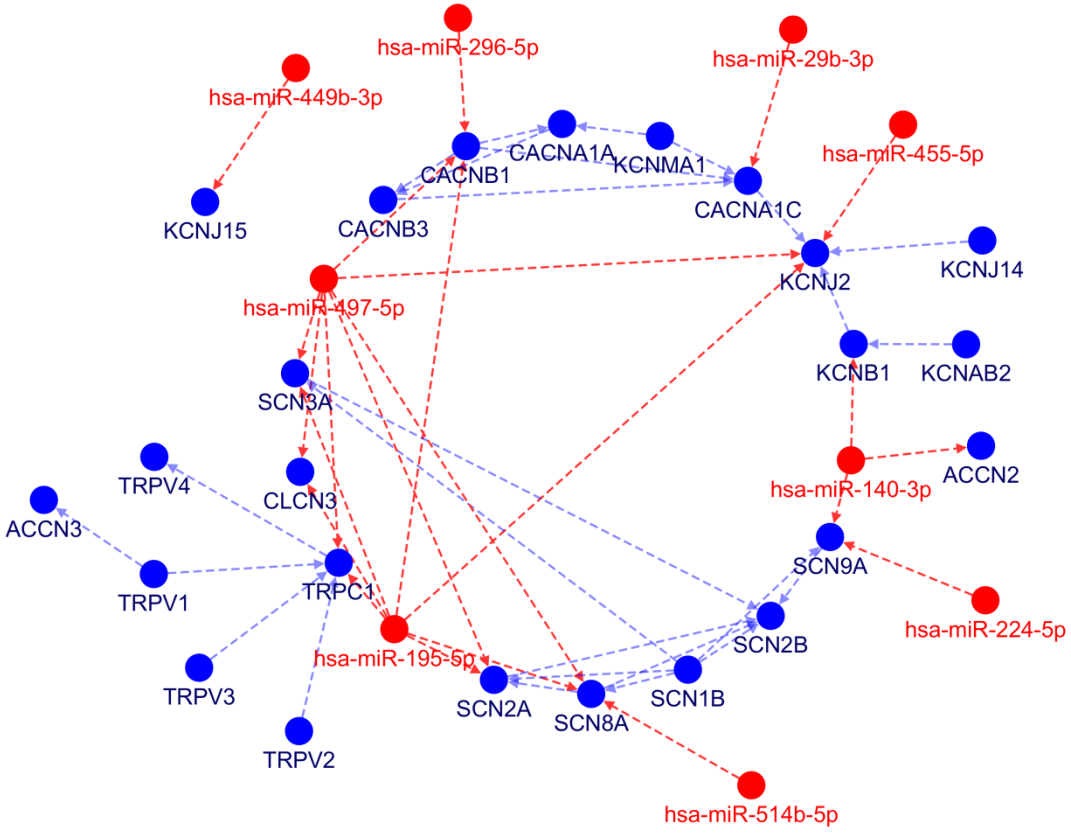

Figure 47. **Network interaction map of miRNAs down-regulated in pectus carinatum.** All miRNAs (red nodes) found to be down-regulated by 3-fold or more are shown as well as their ion channel targets (blue nodes). Interactions between miRNA and ion channel targets are indicated by a dotted red line and arrow. Ion channel interactions with other ion channels are indicated by a dotted blue line and arrow.

Any miRNAs that target our genes of interest (e.g. ACCN1 and KCNN2) will not show changes when analyzed by RT-PCR but only by Western blot or any other protein quantification assay. Although changes to gene expression levels cannot not be directly tied to miRNAs specific to the gene of interest, miRNA regulation of transcription factors and other regulators

may help explain specific gene expression changes. Also, another possible mechanism for the downregulation of ACCN1 and KCNN2 are epigenetic modifications. These modifications may include methylation of the DNA or of the histones resulting in decreased RNA transcription. The epigenetic state of these genes have not been assessed but are an ideal target for future work.

CHAPTER 4

CONCLUSION

The study here aimed to provide insight into the basic biology of costal cartilage in order to better understand the how pectus deformities may occur. We have previously looked into the structural aspects of costal cartilage (Stacey et al., 2013; Stacey et al., 2012), however, more recently, ion channel signalling in cartilage has garnered increased interest in relation to disease pathology. Although ion channels have previously been identified in cartilage, inconsistencies in cartilage species and type could be misleading when trying to study human costal cartilage. Using ion channel arrays for 84 common neuronal ion channels, an expression profile was produced for chondrocytes from normal, fetal, PE-affected, and PC-affected costal cartilage as well as articular chondrocytes (n=3 for each sample type). It is important to note that a limitation in this method is that these generated profiles are only at the transcription level and further confirmation at the protein level is necessary. Costal chondrocytes express many ion channels in common with articular chondrocytes, however there are some that are specific to costal and articular chondrocytes. These differences are likely to be tied to the functional differences between the two cartilage types. Additionally, fetal costal chondrocytes had several other ion channels which are likely to be tied to the differentiation status of the chondrocytes. In chicken mesenchymal stem cells undergoing chondrogenesis, intracellular calcium oscillations were important for progression through chondrogenesis with $Ca_V1.2$ and $Ca_V3.1$ consistently expressed throughout the process (Fodor et al., 2013). We found significant expression of $Ca_V3.1$ in fetal costal chondrocytes, but not in adolescent costal chondrocytes nor in adult articular chondrocytes. Gene expression analysis of normal, PC, and PE chondrocytes found consistent down-regulation of both ACCN1 (ASIC2) and KCNN2 (SK2), though only ASIC2 exhibited

decreased protein levels. As a proton-gated channel, the decreased ASIC2 levels may be causing desensitization of the cells to extracellular acidosis. Analysis of cell stress via mitochondrial metabolic levels (MTT assay) instead revealed that normal cells were less affected by low pH at early time points. Additionally, we analyzed calcium response following acidosis and found that PC cells exhibited a delayed response. It is possible that decreased ASIC2 expression may help explain our observation of delayed calcium transient formation.. More investigation is needed into the mechanism of acidosis and the contribution of ASICs in chondrocyte signalling and homeostasis. Examination of connexins by immunofluorescence found that Cx43 was present in chondrocytes with phosphorylated Cx43 localizing in and around the nucleus. ATP release in chondrocyte-like cells was found to be connexin-mediated; however, external acidosis was not found to induce ATP release. Unlike chondrocytes challenged by mechanical or osmolar stress, external acidosis response does not seem to involve external ATP release. Microarray analysis of microRNAs found multiple microRNAs to be upregulated and several down-regulated in PC2 cells versus Con8, but further studies need to be done to identify a possible microRNA signature for pectus deformities. Currently, the microRNA data is limited by the samples size, and more samples will need to be run in the future. Overall, there is a serious lack of evidence regarding ion channels in costal chondrocytes and the cause of pectus deformities. Our results have produced an expression profile for the costal chondrocyte ion channelome, as well as identified a candidate channel relating to pectus deformities. The contribution of this channel to the pathogenesis of chest wall deformities is unknown and should be further explored.

REFERENCES

Almeida, M.I., A.M. Silva, D.M. Vasconcelos, C.R. Almeida, H. Caires, M.T. Pinto, G.A. Calin, S.G. Santos, and M.A. Barbosa. 2016. miR-195 in human primary mesenchymal stromal/stem cells regulates proliferation, osteogenesis and paracrine effect on angiogenesis. *Oncotarget*. 7:7-22.

Asmar, A., R. Barrett-Jolley, A. Werner, R. Kelly, Jr., and M. Stacey. 2016. Membrane channel gene expression in human costal and articular chondrocytes. *Organogenesis*. 12:94-107.

Baglio, S.R., V. Devescovi, D. Granchi, and N. Baldini. 2013. MicroRNA expression profiling of human bone marrow mesenchymal stem cells during osteogenic differentiation reveals Osterix regulation by miR-31. *Gene*. 527:321-331.

Baron, A., R. Waldmann, and M. Lazdunski. 2002. ASIC-like, proton-activated currents in rat hippocampal neurons. *J Physiol*. 539:485-494.

Barrett-Jolley, R., R. Lewis, R. Fallman, and A. Mobasheri. 2010. The emerging chondrocyte channelome. *Frontiers in physiology*. 1:135.

Bassett, A.R., G. Azzam, L. Wheatley, C. Tibbit, T. Rajakumar, S. McGowan, N. Stanger, P.A. Ewels, S. Taylor, C.P. Ponting, J.L. Liu, T. Sauka-Spengler, and T.A. Fulga. 2014. Understanding functional miRNA-target interactions in vivo by site-specific genome engineering. *Nature communications*. 5:4640.

Batra, N., S. Burra, A.J. Siller-Jackson, S. Gu, X. Xia, G.F. Weber, D. DeSimone, L.F. Bonewald, E.M. Lafer, E. Sprague, M.A. Schwartz, and J.X. Jiang. 2012. Mechanical

stress-activated integrin alpha5beta1 induces opening of connexin 43 hemichannels. *Proc Natl Acad Sci U S A.* 109:3359-3364.

Bean, B.P. 1989. Classes of calcium channels in vertebrate cells. *Annual review of physiology*. 51:367-384.

Beebe, S.J., P.F. Blackmore, J. White, R.P. Joshi, and K.H. Schoenbach. 2004. Nanosecond pulsed electric fields modulate cell function through intracellular signal transduction mechanisms. *Physiological measurement*. 25:1077-1093.

Bergfeld, G.R., and T. Forrester. 1992. Release of ATP from human erythrocytes in response to a brief period of hypoxia and hypercapnia. *Cardiovasc Res*. 26:40-47.

Bernstein, S.A., and G.E. Morley. 2006. Gap junctions and propagation of the cardiac action potential. *Advances in cardiology*. 42:71-85.

Bienertova-Vasku, J., P. Mazanek, R. Hezova, A. Curdova, J. Nekvindova, L. Kren, J. Sterba, and O. Slaby. 2013. Extension of microRNA expression pattern associated with high-risk neuroblastoma. *Tumour biology : the journal of the International Society for Oncodevelopmental Biology and Medicine*. 34:2315-2319.

Boiko, N., V. Kucher, B. Wang, and J.D. Stockand. 2014. Restrictive expression of acid-sensing ion channel 5 (asic5) in unipolar brush cells of the vestibulocerebellum. *PLoS One*. 9:e91326.

Boileau, C., J. Martel-Pelletier, J. Brunet, D. Schrier, C. Flory, M. Boily, and J.P. Pelletier. 2006. PD-0200347, an alpha2delta ligand of the voltage gated calcium channel, inhibits in vivo

activation of the Erk1/2 pathway in osteoarthritic chondrocytes: a PKCalpha dependent effect. *Ann Rheum Dis*. 65:573-580.

Bourinet, E., C. Altier, M.E. Hildebrand, T. Trang, M.W. Salter, and G.W. Zamponi. 2014. Calcium-permeable ion channels in pain signaling. *Physiological reviews*. 94:81-140.

Brackenbury, W.J., and L.L. Isom. 2008. Voltage-gated Na+ channels: potential for beta subunits as therapeutic targets. *Expert opinion on therapeutic targets*. 12:1191-1203.

Brochhausen, C., S. Turial, F.K. Muller, V.H. Schmitt, W. Coerdt, J.M. Wihlm, F. Schier, and C.J. Kirkpatrick. 2012. Pectus excavatum: history, hypotheses and treatment options. *Interact Cardiovasc Thorac Surg*. 14:801-806.

Cai, J., H. Guan, L. Fang, Y. Yang, X. Zhu, J. Yuan, J. Wu, and M. Li. 2013. MicroRNA-374a activates Wnt/beta-catenin signaling to promote breast cancer metastasis. *J Clin Invest*. 123:566-579.

Cannell, I.G., Y.W. Kong, S.J. Johnston, M.L. Chen, H.M. Collins, H.C. Dobbyn, A. Elia, T.R. Kress, M. Dickens, M.J. Clemens, D.M. Heery, M. Gaestel, M. Eilers, A.E. Willis, and M. Bushell. 2010. p38 MAPK/MK2-mediated induction of miR-34c following DNA damage prevents Myc-dependent DNA replication. *Proc Natl Acad Sci U S A*. 107:5375-5380.

Cant, N., N. Pollock, and R.C. Ford. 2014. CFTR structure and cystic fibrosis. *The international journal of biochemistry & cell biology*. 52:15-25.

Chandran, P.L., and F. Horkay. 2012. Aggrecan, an unusual polyelectrolyte: review of solution behavior and physiological implications. *Acta Biomater*. 8:3-12.

Chang, Y.Y., W.H. Kuo, J.H. Hung, C.Y. Lee, Y.H. Lee, Y.C. Chang, W.C. Lin, C.Y. Shen, C.S. Huang, F.J. Hsieh, L.C. Lai, M.H. Tsai, K.J. Chang, and E.Y. Chuang. 2015. Deregulated microRNAs in triple-negative breast cancer revealed by deep sequencing. *Molecular cancer*. 14:36.

Chao, P.H., A.C. West, and C.T. Hung. 2006. Chondrocyte intracellular calcium, cytoskeletal organization, and gene expression responses to dynamic osmotic loading. *Am J Physiol Cell Physiol*. 291:C718-725.

Chen, S., and D.E. Birk. 2013. The regulatory roles of small leucine-rich proteoglycans in extracellular assembly. *FEBS J*.

Chen, T.Y. 2005. Structure and function of clc channels. *Annual review of physiology*. 67:809-839.

Chendrimada, T.P., R.I. Gregory, E. Kumaraswamy, J. Norman, N. Cooch, K. Nishikura, and R. Shiekhattar. 2005. TRBP recruits the Dicer complex to Ago2 for microRNA processing and gene silencing. *Nature*. 436:740-744.

Cheng, J., Y. Chen, H. Xing, H. Jiang, and X. Ye. 2015. Down-regulation of ASICs current and the calcium transients by disrupting PICK1 protects primary cultured mouse cortical neurons from OGD-Rep insults. *International journal of clinical and experimental pathology*. 8:10272-10282.

Chien, L.T., and H.C. Hartzell. 2008. Rescue of volume-regulated anion current by bestrophin mutants with altered charge selectivity. *J Gen Physiol*. 132:537-546.

Choe, S. 2002. Potassium channel structures. *Nature reviews. Neuroscience*. 3:115-121.

Clark, R.B., N. Hatano, C. Kondo, D.D. Belke, B.S. Brown, S. Kumar, B.J. Votta, and W.R. Giles. 2010. Voltage-gated K+ currents in mouse articular chondrocytes regulate membrane potential. *Channels*. 4:179-191.

Clark, R.B., C. Kondo, D.D. Belke, and W.R. Giles. 2011. Two-pore domain K(+) channels regulate membrane potential of isolated human articular chondrocytes. *J Physiol*. 589:5071-5089.

Collins, J.A., R.J. Moots, R. Winstanley, P.D. Clegg, and P.I. Milner. 2013. Oxygen and pH-sensitivity of human osteoarthritic chondrocytes in 3-D alginate bead culture system. *Osteoarthritis Cartilage*. 21:1790-1798.

Coste, B., B. Xiao, J.S. Santos, R. Syeda, J. Grandl, K.S. Spencer, S.E. Kim, M. Schmidt, J. Mathur, A.E. Dubin, M. Montal, and A. Patapoutian. 2012. Piezo proteins are pore-forming subunits of mechanically activated channels. *Nature*. 483:176-181.

Creswick, H.A., M.W. Stacey, R.E. Kelly, Jr., T. Gustin, D. Nuss, H. Harvey, M.J. Goretsky, E. Vasser, J.C. Welch, K. Mitchell, and V.K. Proud. 2006. Family study of the inheritance of pectus excavatum. *J Pediatr Surg*. 41:1699-1703.

Dang, X., B.W. Doble, and E. Kardami. 2003. The carboxy-tail of connexin-43 localizes to the nucleus and inhibits cell growth. *Molecular and cellular biochemistry*. 242:35-38.

Das, R.H., G.J. van Osch, M. Kreukniet, J. Oostra, H. Weinans, and H. Jahr. 2010. Effects of individual control of pH and hypoxia in chondrocyte culture. *Journal of orthopaedic research : official publication of the Orthopaedic Research Society*. 28:537-545.

Dascalu, A., R. Korenstein, Y. Oron, and Z. Nevo. 1996. A hyperosmotic stimulus regulates intracellular pH, calcium, and S-100 protein levels in avian chondrocytes. *Biochem Biophys Res Commun*. 227:368-373.

Delmas, P., and D.A. Brown. 2005. Pathways modulating neural KCNQ/M (Kv7) potassium channels. *Nature reviews. Neuroscience*. 6:850-862.

Djuranovic, S., A. Nahvi, and R. Green. 2012. miRNA-mediated gene silencing by translational repression followed by mRNA deadenylation and decay. *Science*. 336:237-240.

Du, A., S. Zhao, L. Wan, T. Liu, Z. Peng, Z. Zhou, Z. Liao, and H. Fang. 2016. MicroRNA expression profile of human periodontal ligament cells under the influence of Porphyromonas gingivalis LPS. *Journal of cellular and molecular medicine*. 20:1329-1338.

Dudhia, J. 2005. Aggrecan, aging and assembly in articular cartilage. *Cell Mol Life Sci*. 62:2241-2256.

Duncan, L.M., J. Deeds, J. Hunter, J. Shao, L.M. Holmgren, E.A. Woolf, R.I. Tepper, and A.W. Shyjan. 1998. Down-regulation of the novel gene melastatin correlates with potential for melanoma metastasis. *Cancer Res*. 58:1515-1520.

Duval, E., S. Leclercq, J.M. Elissalde, M. Demoor, P. Galera, and K. Boumediene. 2009. Hypoxia-inducible factor 1alpha inhibits the fibroblast-like markers type I and type III collagen during hypoxia-induced chondrocyte redifferentiation: hypoxia not only induces type II collagen and aggrecan, but it also inhibits type I and type III collagen in the hypoxia-inducible factor 1alpha-dependent redifferentiation of chondrocytes. *Arthritis Rheum*. 60:3038-3048.

Edlich, M., C.E. Yellowley, C.R. Jacobs, and H.J. Donahue. 2001. Oscillating fluid flow regulates cytosolic calcium concentration in bovine articular chondrocytes. *J Biomech*. 34:59-65.

Emery, E.C., G.T. Young, and P.A. McNaughton. 2012. HCN2 ion channels: an emerging role as the pacemakers of pain. *Trends in pharmacological sciences*. 33:456-463.

Enyedi, P., and G. Czirjak. 2010. Molecular background of leak K+ currents: two-pore domain potassium channels. *Physiological reviews*. 90:559-605.

Evans, W.H., and P.E. Martin. 2002. Gap junctions: structure and function (Review). *Molecular membrane biology*. 19:121-136.

Eyre, D. 2002. Collagen of articular cartilage. *Arthritis research*. 4:30-35.

Fan, Z., R.E. Kumon, J. Park, and C.X. Deng. 2010. Intracellular delivery and calcium transients generated in sonoporation facilitated by microbubbles. *Journal of controlled release : official journal of the Controlled Release Society*. 142:31-39.

Fodor, J., C. Matta, T. Olah, T. Juhasz, R. Takacs, A. Toth, B. Dienes, L. Csernoch, and R. Zakany. 2013. Store-operated calcium entry and calcium influx via voltage-operated calcium channels regulate intracellular calcium oscillations in chondrogenic cells. *Cell calcium*. 54:1-16.

Forman, J.L., E. del Pozo de Dios, C.A. Dalmases, and R.W. Kent. 2010. The contribution of the perichondrium to the structural mechanical behavior of the costal-cartilage. *J Biomech Eng*. 132:094501.

Funabashi, K., S. Ohya, H. Yamamura, N. Hatano, K. Muraki, W. Giles, and Y. Imaizumi. 2010. Accelerated Ca2+ entry by membrane hyperpolarization due to Ca2+-activated K+ channel activation in response to histamine in chondrocytes. *Am J Physiol Cell Physiol*. 298:C786-797.

Gago-Fuentes, R., P. Carpintero-Fernandez, M.B. Goldring, P.R. Brink, M.D. Mayan, and F.J. Blanco. 2014. Biochemical evidence for gap junctions and Cx43 expression in immortalized human chondrocyte cell line: a potential model in the study of cell communication in human chondrocytes. *Osteoarthritis Cartilage*. 22:586-590.

Garcia, M., and M.M. Knight. 2010. Cyclic loading opens hemichannels to release ATP as part of a chondrocyte mechanotransduction pathway. *Journal of orthopaedic research : official publication of the Orthopaedic Research Society*. 28:510-515.

Gavenis, K., C. Schumacher, U. Schneider, J. Eisfeld, J. Mollenhauer, and B. Schmidt-Rohlfing. 2009. Expression of ion channels of the TRP family in articular chondrocytes from osteoarthritic patients: changes between native and in vitro propagated chondrocytes. *Molecular and cellular biochemistry*. 321:135-143.

Giepmans, B.N. 2004. Gap junctions and connexin-interacting proteins. *Cardiovasc Res*. 62:233-245.

Glaser, T., R.R. Resende, and H. Ulrich. 2013. Implications of purinergic receptor-mediated intracellular calcium transients in neural differentiation. *Cell communication and signaling : CCS*. 11:12.

Gonzalez, C., D. Baez-Nieto, I. Valencia, I. Oyarzun, P. Rojas, D. Naranjo, and R. Latorre. 2012. K(+) channels: function-structural overview. *Comprehensive Physiology*. 2:2087-2149.

Gopalakrishnan, M., C.C. Shieh, and J. Chen. 2006. Potassium Channels: Overview of Molecular, Biophysical and Pharmacological Properties. *In* Voltage-Gated Ion Channels as Drug Targets. Vol. 29. D.J. Triggle, M. Gopalakrishnan, D. Rampe, and W. Zheng, editors. Wiley-VCH Verlag GmbH & Co. KGaA, Weinheim, FRG.

Gray, M.L., A.M. Pizzanelli, A.J. Grodzinsky, and R.C. Lee. 1988. Mechanical and physiochemical determinants of the chondrocyte biosynthetic response. *Journal of orthopaedic research : official publication of the Orthopaedic Research Society*. 6:777-792.

Grynkiewicz, G., M. Poenie, and R.Y. Tsien. 1985. A new generation of Ca2+ indicators with greatly improved fluorescence properties. *J Biol Chem*. 260:3440-3450.

Guan, Y., M. Mizoguchi, K. Yoshimoto, N. Hata, T. Shono, S.O. Suzuki, Y. Araki, D. Kuga, A. Nakamizo, T. Amano, X. Ma, K. Hayashi, and T. Sasaki. 2010. MiRNA-196 is upregulated in glioblastoma but not in anaplastic astrocytoma and has prognostic significance. *Clin Cancer Res*. 16:4289-4297.

Gueguinou, M., A. Chantome, G. Fromont, P. Bougnoux, C. Vandier, and M. Potier-Cartereau. 2014. KCa and Ca(2+) channels: the complex thought. *Biochim Biophys Acta*. 1843:2322-2333.

Hall, A.C., E.R. Horwitz, and R.J. Wilkins. 1996a. The cellular physiology of articular cartilage. *Experimental physiology*. 81:535-545.

Hall, A.C., I. Starks, C.L. Shoults, and S. Rashidbigi. 1996b. Pathways for K+ transport across the bovine articular chondrocyte membrane and their sensitivity to cell volume. *The American journal of physiology*. 270:C1300-1310.

Han, S.K., W. Wouters, A. Clark, and W. Herzog. 2012. Mechanically induced calcium signaling in chondrocytes in situ. *Journal of orthopaedic research : official publication of the Orthopaedic Research Society*. 30:475-481.

Hanukoglu, I., and A. Hanukoglu. 2016. Epithelial sodium channel (ENaC) family: Phylogeny, structure-function, tissue distribution, and associated inherited diseases. *Gene*. 579:95-132.

Harteneck, C. 2005. Function and pharmacology of TRPM cation channels. *Naunyn-Schmiedeberg's archives of pharmacology*. 371:307-314.

Hatakeyama, T., P. Dai, Y. Harada, H. Hino, F. Tsukahara, Y. Maru, E. Otsuji, and T. Takamatsu. 2013. Connexin43 functions as a novel interacting partner of heat shock cognate protein 70. *Scientific reports*. 3:2719.

Hayes, A.J., S. MacPherson, H. Morrison, G. Dowthwaite, and C.W. Archer. 2001. The development of articular cartilage: evidence for an appositional growth mechanism. *Anatomy and embryology*. 203:469-479.

Hibino, H., A. Inanobe, K. Furutani, S. Murakami, I. Findlay, and Y. Kurachi. 2010. Inwardly rectifying potassium channels: their structure, function, and physiological roles. *Physiological reviews*. 90:291-366.

Hino, H., P. Dai, T. Yoshida, T. Hatakeyama, Y. Harada, E. Otsuji, T. Okuda, and T. Takamatsu. 2015. Interaction of Cx43 with Hsc70 regulates G1/S transition through CDK inhibitor p27. *Scientific reports*. 5:15365.

Holakovska, B., L. Grycova, J. Bily, and J. Teisinger. 2011. Characterization of calmodulin binding domains in TRPV2 and TRPV5 C-tails. *Amino acids*. 40:741-748.

Hornstein, E., J.H. Mansfield, S. Yekta, J.K. Hu, B.D. Harfe, M.T. McManus, S. Baskerville, D.P. Bartel, and C.J. Tabin. 2005. The microRNA miR-196 acts upstream of Hoxb8 and Shh in limb development. *Nature*. 438:671-674.

Hu, W., F.H. Chen, F.L. Yuan, T.Y. Zhang, F.R. Wu, C. Rong, S. Jiang, J. Tang, C.C. Zhang, and M.Y. Lin. 2012. Blockade of acid-sensing ion channels protects articular chondrocytes from acid-induced apoptotic injury. *Inflammation research : official journal of the European Histamine Research Society ... [et al.]*. 61:327-335.

Huang, S., S. Wang, C. Bian, Z. Yang, H. Zhou, Y. Zeng, H. Li, Q. Han, and R.C. Zhao. 2012. Upregulation of miR-22 promotes osteogenic differentiation and inhibits adipogenic differentiation of human adipose tissue-derived mesenchymal stem cells by repressing HDAC6 protein expression. *Stem cells and development*. 21:2531-2540.

Iida, H. 2010. Surgical repair of pectus excavatum. *Gen Thorac Cardiovasc Surg*. 58:55-61.

Inanobe, A., Y. Yoshimoto, Y. Horio, K.I. Morishige, H. Hibino, S. Matsumoto, Y. Tokunaga, T. Maeda, Y. Hata, Y. Takai, and Y. Kurachi. 1999. Characterization of G-protein-gated K+ channels composed of Kir3.2 subunits in dopaminergic neurons of the substantia nigra. *J Neurosci*. 19:1006-1017.

Iozzo, R.V. 1999. The biology of the small leucine-rich proteoglycans. Functional network of interactive proteins. *J Biol Chem*. 274:18843-18846.

Isom, L.L. 2001. Sodium channel beta subunits: anything but auxiliary. *The Neuroscientist : a review journal bringing neurobiology, neurology and psychiatry*. 7:42-54.

Jentsch, T.J., I. Neagoe, and O. Scheel. 2005. CLC chloride channels and transporters. *Current opinion in neurobiology*. 15:319-325.

Jentsch, T.J., V. Stein, F. Weinreich, and A.A. Zdebik. 2002. Molecular structure and physiological function of chloride channels. *Physiological reviews*. 82:503-568.

Jordan, K., R. Chodock, A.R. Hand, and D.W. Laird. 2001. The origin of annular junctions: a mechanism of gap junction internalization. *J Cell Sci*. 114:763-773.

June, R.K., and D.P. Fyhrie. 2010. Temperature effects in articular cartilage biomechanics. *J Exp Biol*. 213:3934-3940.

Karginov, F.V., C. Conaco, Z. Xuan, B.H. Schmidt, J.S. Parker, G. Mandel, and G.J. Hannon. 2007. A biochemical approach to identifying microRNA targets. *Proc Natl Acad Sci U S A*. 104:19291-19296.

Kato, R.B., B. Roy, F.S. De Oliveira, E.P. Ferraz, P.T. De Oliveira, A.G. Kemper, M.Q. Hassan, A.L. Rosa, and M.M. Beloti. 2014. Nanotopography directs mesenchymal stem cells to osteoblast lineage through regulation of microRNA-SMAD-BMP-2 circuit. *Journal of cellular physiology*. 229:1690-1696.

Kelly, R.E., Jr., T.F. Cash, R.C. Shamberger, K.K. Mitchell, R.B. Mellins, M.L. Lawson, K. Oldham, R.G. Azizkhan, A.V. Hebra, D. Nuss, M.J. Goretsky, R.J. Sharp, G.W. Holcomb, 3rd, W.K. Shim, S.M. Megison, R.L. Moss, A.H. Fecteau, P.M. Colombani, T. Bagley, A. Quinn, and A.B. Moskowitz. 2008. Surgical repair of pectus excavatum

markedly improves body image and perceived ability for physical activity: multicenter study. *Pediatrics*. 122:1218-1222.

Kluess, H.A., J.B. Buckwalter, J.J. Hamann, and P.S. Clifford. 2005. Acidosis attenuates P2X purinergic vasoconstriction in skeletal muscle arteries. *Am J Physiol Heart Circ Physiol*. 288:H129-132.

Knight, M.M., S.R. McGlashan, M. Garcia, C.G. Jensen, and C.A. Poole. 2009. Articular chondrocytes express connexin 43 hemichannels and P2 receptors - a putative mechanoreceptor complex involving the primary cilium? *J Anat*. 214:275-283.

Kolker, S.J., R.Y. Walder, Y. Usachev, J. Hillman, D.L. Boyle, G.S. Firestein, and K.A. Sluka. 2010. Acid-sensing ion channel 3 expressed in type B synoviocytes and chondrocytes modulates hyaluronan expression and release. *Ann Rheum Dis*. 69:903-909.

Kruger, L.C., and L.L. Isom. 2016. Voltage-Gated Na+ Channels: Not Just for Conduction. *Cold Spring Harbor perspectives in biology*. 8.

Kurita, T., H. Yamamura, Y. Suzuki, W.R. Giles, and Y. Imaizumi. 2015. The ClC-7 Chloride Channel Is Downregulated by Hypoosmotic Stress in Human Chondrocytes. *Mol Pharmacol*. 88:113-120.

Kweon, H.J., and B.C. Suh. 2013. Acid-sensing ion channels (ASICs): therapeutic targets for neurological diseases and their regulation. *BMB reports*. 46:295-304.

Lai, W.M., J.S. Hou, and V.C. Mow. 1991. A triphasic theory for the swelling and deformation behaviors of articular cartilage. *J Biomech Eng*. 113:245-258.

Lam, J.K., M.Y. Chow, Y. Zhang, and S.W. Leung. 2015. siRNA Versus miRNA as Therapeutics for Gene Silencing. *Molecular therapy. Nucleic acids*. 4:e252.

Lambers, T.T., A.F. Weidema, B. Nilius, J.G. Hoenderop, and R.J. Bindels. 2004. Regulation of the mouse epithelial Ca2(+) channel TRPV6 by the Ca(2+)-sensor calmodulin. *J Biol Chem*. 279:28855-28861.

Lanner, J.T., D.K. Georgiou, A.D. Joshi, and S.L. Hamilton. 2010. Ryanodine receptors: structure, expression, molecular details, and function in calcium release. *Cold Spring Harbor perspectives in biology*. 2:a003996.

Lee, W., H.A. Leddy, Y. Chen, S.H. Lee, N.A. Zelenski, A.L. McNulty, J. Wu, K.N. Beicker, J. Coles, S. Zauscher, J. Grandl, F. Sachs, F. Guilak, and W.B. Liedtke. 2014. Synergy between Piezo1 and Piezo2 channels confers high-strain mechanosensitivity to articular cartilage. *Proc Natl Acad Sci U S A*. 111:E5114-5122.

Lewis, R., K.E. Asplin, G. Bruce, C. Dart, A. Mobasheri, and R. Barrett-Jolley. 2011a. The role of the membrane potential in chondrocyte volume regulation. *Journal of cellular physiology*. 226:2979-2986.

Lewis, R., and R. Barrett-Jolley. 2015. Changes in Membrane Receptors and Ion Channels as Potential Biomarkers for Osteoarthritis. *Frontiers in physiology*. 6:357.

Lewis, R., C.H. Feetham, and R. Barrett-Jolley. 2011b. Cell volume regulation in chondrocytes. *Cellular physiology and biochemistry : international journal of experimental cellular physiology, biochemistry, and pharmacology*. 28:1111-1122.

Li, D., Y. Zhao, C. Liu, X. Chen, Y. Qi, Y. Jiang, C. Zou, X. Zhang, S. Liu, X. Wang, D. Zhao, Q. Sun, Z. Zeng, A. Dress, M.C. Lin, H.F. Kung, H. Rui, L.Z. Liu, F. Mao, B.H. Jiang, and L. Lai. 2011. Analysis of MiR-195 and MiR-497 expression, regulation and role in breast cancer. *Clin Cancer Res*. 17:1722-1730.

Li, H., C. Yin, B. Zhang, Y. Sun, L. Shi, N. Liu, S. Liang, S. Lu, Y. Liu, J. Zhang, F. Li, W. Li, F. Liu, L. Sun, and Y. Qi. 2013. PTTG1 promotes migration and invasion of human non-small cell lung cancer cells and is modulated by miR-186. *Carcinogenesis*. 34:2145-2155.

Li, X., F.R. Wu, R.S. Xu, W. Hu, D.L. Jiang, C. Ji, F.H. Chen, and F.L. Yuan. 2014. Acid-sensing ion channel 1a-mediated calcium influx regulates apoptosis of endplate chondrocytes in intervertebral discs. *Expert opinion on therapeutic targets*. 18:1-14.

Liang, H., L. Yang, T. Ma, and Y. Zhao. 2010. Functional expression of cystic fibrosis transmembrane conductance regulator in mouse chondrocytes. *Clinical and experimental pharmacology & physiology*. 37:506-508.

Lopushinsky, S.R., and A.H. Fecteau. 2008. Pectus deformities: a review of open surgery in the modern era. *Semin Pediatr Surg*. 17:201-208.

Macri, V., D. Angoli, and E.A. Accili. 2012. Architecture of the HCN selectivity filter and control of cation permeation. *Scientific reports*. 2:894.

Marionneau, C., B. Couette, J. Liu, H. Li, M.E. Mangoni, J. Nargeot, M. Lei, D. Escande, and S. Demolombe. 2005. Specific pattern of ionic channel gene expression associated with pacemaker activity in the mouse heart. *J Physiol*. 562:223-234.

Martina, M., J.W. Mozrzymas, and F. Vittur. 1997. Membrane stretch activates a potassium channel in pig articular chondrocytes. *Biochim Biophys Acta*. 1329:205-210.

Martinez, A.D., R. Acuna, V. Figueroa, J. Maripillan, and B. Nicholson. 2009. Gap-junction channels dysfunction in deafness and hearing loss. *Antioxidants & redox signaling*. 11:309-322.

Matta, C., J. Fodor, N. Miosge, R. Takacs, T. Juhasz, H. Rybaltovszki, A. Toth, L. Csernoch, and R. Zakany. 2015a. Purinergic signalling is required for calcium oscillations in migratory chondrogenic progenitor cells. *Pflugers Archiv : European journal of physiology*. 467:429-442.

Matta, C., and R. Zakany. 2013. Calcium signalling in chondrogenesis: implications for cartilage repair. *Front Biosci (Schol Ed)*. 5:305-324.

Matta, C., R. Zakany, and A. Mobasheri. 2015b. Voltage-dependent calcium channels in chondrocytes: roles in health and disease. *Current rheumatology reports*. 17:43.

McFadzean, I., and A. Gibson. 2002. The developing relationship between receptor-operated and store-operated calcium channels in smooth muscle. *Br J Pharmacol*. 135:1-13.

Milenkovic, A., C. Brandl, V.M. Milenkovic, T. Jendryke, L. Sirianant, P. Wanitchakool, S. Zimmermann, C.M. Reiff, F. Horling, H. Schrewe, R. Schreiber, K. Kunzelmann, C.H. Wetzel, and B.H. Weber. 2015. Bestrophin 1 is indispensable for volume regulation in human retinal pigment epithelium cells. *Proc Natl Acad Sci U S A*. 112:E2630-2639.

Milner, P.I., T.P. Fairfax, J.A. Browning, R.J. Wilkins, and J.S. Gibson. 2006. The effect of O2 tension on pH homeostasis in equine articular chondrocytes. *Arthritis Rheum*. 54:3523-3532.

Miyata, R., T. Kakuki, K. Nomura, T. Ohkuni, N. Ogasawara, K. Takano, T. Konno, T. Kohno, N. Sawada, T. Himi, and T. Kojima. 2015. Poly(I:C) induced microRNA-146a regulates epithelial barrier and secretion of proinflammatory cytokines in human nasal epithelial cells. *Eur J Pharmacol*. 761:375-382.

Mobasheri, A., T.C. Gent, A.I. Nash, M.D. Womack, C.A. Moskaluk, and R. Barrett-Jolley. 2007. Evidence for functional ATP-sensitive (K(ATP)) potassium channels in human and equine articular chondrocytes. *Osteoarthritis Cartilage*. 15:1-8.

Mobasheri, A., T.C. Gent, M.D. Womack, S.D. Carter, P.D. Clegg, and R. Barrett-Jolley. 2005. Quantitative analysis of voltage-gated potassium currents from primary equine (Equus caballus) and elephant (Loxodonta africana) articular chondrocytes. *Am J Physiol Regul Integr Comp Physiol*. 289:R172-180.

Mobasheri, A., R. Lewis, A. Ferreira-Mendes, A. Rufino, C. Dart, and R. Barrett-Jolley. 2012. Potassium channels in articular chondrocytes. *Channels*. 6:416-425.

Mobasheri, A., R. Lewis, J.E. Maxwell, C. Hill, M. Womack, and R. Barrett-Jolley. 2010. Characterization of a stretch-activated potassium channel in chondrocytes. *Journal of cellular physiology*. 223:511-518.

Montell, C., and G.M. Rubin. 1989. Molecular characterization of the Drosophila trp locus: a putative integral membrane protein required for phototransduction. *Neuron*. 2:1313-1323.

Morris, C.E., and P.F. Juranka. 2007. Nav channel mechanosensitivity: activation and inactivation accelerate reversibly with stretch. *Biophys J*. 93:822-833.

Mudduluru, G., P. Ceppi, R. Kumarswamy, G.V. Scagliotti, M. Papotti, and H. Allgayer. 2011. Regulation of Axl receptor tyrosine kinase expression by miR-34a and miR-199a/b in solid cancer. *Oncogene*. 30:2888-2899.

Nakaoka, T., S. Uemura, T. Yoshida, T. Tanimoto, and H. Miyake. 2010. Overgrowth of costal cartilage is not the etiology of pectus excavatum. *J Pediatr Surg*. 45:2015-2018.

Nuss, D. 2008. Minimally invasive surgical repair of pectus excavatum. *Semin Pediatr Surg*. 17:209-217.

Nuss, D., R.E. Kelly, Jr., D.P. Croitoru, and M.E. Katz. 1998. A 10-year review of a minimally invasive technique for the correction of pectus excavatum. *J Pediatr Surg*. 33:545-552.

O'Conor, C.J., N. Case, and F. Guilak. 2013. Mechanical regulation of chondrogenesis. *Stem cell research & therapy*. 4:61.

O'Conor, C.J., H.A. Leddy, H.C. Benefield, W.B. Liedtke, and F. Guilak. 2014. TRPV4-mediated mechanotransduction regulates the metabolic response of chondrocytes to dynamic loading. *Proc Natl Acad Sci U S A*. 111:1316-1321.

Okumura, N., S. Imai, F. Toyoda, E. Isoya, K. Kumagai, H. Matsuura, and Y. Matsusue. 2009. Regulatory role of tyrosine phosphorylation in the swelling-activated chloride current in isolated rabbit articular chondrocytes. *J Physiol*. 587:3761-3776.

Palumbo, T., F.R. Faucz, M. Azevedo, P. Xekouki, D. Iliopoulos, and C.A. Stratakis. 2013. Functional screen analysis reveals miR-26b and miR-128 as central regulators of pituitary

somatomammotrophic tumor growth through activation of the PTEN-AKT pathway. *Oncogene*. 32:1651-1659.

Parvizi, J., V. Parpura, J.F. Greenleaf, and M.E. Bolander. 2002. Calcium signaling is required for ultrasound-stimulated aggrecan synthesis by rat chondrocytes. *Journal of orthopaedic research : official publication of the Orthopaedic Research Society*. 20:51-57.

Pascual-Font, A., and J.R. Sanudo. 2016. Laryngeal Cartilages. *In* Bergman's Comprehensive Encyclopedia of Human Anatomic Variation. R.A. Bergman, R.S. Tubbs, M.M. Shoja, and M. Loukas, editors. John Wiley & Sons, Inc, Hoboken, NJ, USA. 1209-1211.

Pedersen, S.F., G. Owsianik, and B. Nilius. 2005. TRP channels: an overview. *Cell calcium*. 38:233-252.

Phan, M.N., H.A. Leddy, B.J. Votta, S. Kumar, D.S. Levy, D.B. Lipshutz, S.H. Lee, W. Liedtke, and F. Guilak. 2009. Functional characterization of TRPV4 as an osmotically sensitive ion channel in porcine articular chondrocytes. *Arthritis Rheum*. 60:3028-3037.

Philipson, L.H., A. Kuznetsov, P.T. Toth, J.F. Murphy, G. Szabo, G.H. Ma, and R.J. Miller. 1995. Functional expression of an epitope-tagged G protein-coupled K+ channel (GIRK1). *J Biol Chem*. 270:14604-14610.

Plotkin, L.I., T.L. Speacht, and H.J. Donahue. 2015. Cx43 and mechanotransduction in bone. *Current osteoporosis reports*. 13:67-72.

Prakriya, M., and R.S. Lewis. 2015. Store-Operated Calcium Channels. *Physiological reviews*. 95:1383-1436.

Puchalowicz, K., M. Tarnowski, I. Baranowska-Bosiacka, D. Chlubek, and V. Dziedziejko. 2014. P2X and P2Y receptors-role in the pathophysiology of the nervous system. *International journal of molecular sciences*. 15:23672-23704.

Ravitch, M.M. 1949. The Operative Treatment of Pectus Excavatum. *Annals of surgery*. 129:429-444.

Rong, C., F.H. Chen, S. Jiang, W. Hu, F.R. Wu, T.Y. Chen, and F.L. Yuan. 2012. Inhibition of acid-sensing ion channels by amiloride protects rat articular chondrocytes from acid-induced apoptosis via a mitochondrial-mediated pathway. *Cell biology international*. 36:635-641.

Rook, M.B., M.M. Evers, M.A. Vos, and M.F. Bierhuizen. 2012. Biology of cardiac sodium channel Nav1.5 expression. *Cardiovasc Res*. 93:12-23.

Rosenbaum, T., A. Gordon-Shaag, M. Munari, and S.E. Gordon. 2004. Ca2+/calmodulin modulates TRPV1 activation by capsaicin. *J Gen Physiol*. 123:53-62.

Sabuncu, A.C., A.J. Asmar, M.W. Stacey, and A. Beskok. 2015. Differential dielectric responses of chondrocyte and Jurkat cells in electromanipulation buffers. *Electrophoresis*. 36:1499-1506.

Sah, P., and E.S. Faber. 2002. Channels underlying neuronal calcium-activated potassium currents. *Progress in neurobiology*. 66:345-353.

Sallustio, F., G. Serino, V. Costantino, C. Curci, S.N. Cox, G. De Palma, and F.P. Schena. 2013. miR-1915 and miR-1225-5p regulate the expression of CD133, PAX2 and TLR2 in adult renal progenitor cells. *PLoS One*. 8:e68296.

Sanchez-Jimenez, C., I. Carrascoso, J. Barrero, and J.M. Izquierdo. 2013. Identification of a set of miRNAs differentially expressed in transiently TIA-depleted HeLa cells by genome-wide profiling. *BMC molecular biology*. 14:4.

Sanchez, J.C., T.A. Danks, and R.J. Wilkins. 2003. Mechanisms involved in the increase in intracellular calcium following hypotonic shock in bovine articular chondrocytes. *General physiology and biophysics*. 22:487-500.

Sanchez, J.C., and R.J. Wilkins. 2004. Changes in intracellular calcium concentration in response to hypertonicity in bovine articular chondrocytes. *Comparative biochemistry and physiology. Part A, Molecular & integrative physiology*. 137:173-182.

Schwartz, V., K. Friedrich, G. Polleichtner, and S. Grunder. 2015. Acid-sensing ion channel (ASIC) 4 predominantly localizes to an early endosome-related organelle upon heterologous expression. *Scientific reports*. 5:18242.

Semenov, I., S. Xiao, and A.G. Pakhomov. 2013. Primary pathways of intracellular Ca(2+) mobilization by nanosecond pulsed electric field. *Biochim Biophys Acta*. 1828:981-989.

Shi, Q., S. Gu, X.S. Yu, T.W. White, E.A. Banks, and J.X. Jiang. 2015. Connexin Controls Cell-Cycle Exit and Cell Differentiation by Directly Promoting Cytosolic Localization and Degradation of E3 Ligase Skp2. *Dev Cell*. 35:483-496.

Shukla, G.C., J. Singh, and S. Barik. 2011. MicroRNAs: Processing, Maturation, Target Recognition and Regulatory Functions. *Molecular and cellular pharmacology*. 3:83-92.

Somogyi, C.S., C. Matta, Z. Foldvari, T. Juhasz, E. Katona, A.R. Takacs, T. Hajdu, N. Dobrosi, P. Gergely, and R. Zakany. 2015. Polymodal Transient Receptor Potential Vanilloid

(TRPV) Ion Channels in Chondrogenic Cells. *International journal of molecular sciences*. 16:18412-18438.

Sophia Fox, A.J., A. Bedi, and S.A. Rodeo. 2009. The basic science of articular cartilage: structure, composition, and function. *Sports health*. 1:461-468.

Stacey, M., D. Dutta, W. Cao, A. Asmar, H. Elsayed-Ali, R. Kelly, Jr., and A. Beskok. 2013. Atomic force microscopy characterization of collagen 'nanostraws' in human costal cartilage. *Micron*. 44:483-487.

Stacey, M.W., J. Grubbs, A. Asmar, J. Pryor, H. Elsayed-Ali, W. Cao, A. Beskok, D. Dutta, D.A. Darby, A. Fecteau, A. Werner, and R.E. Kelly, Jr. 2012. Decorin expression, straw-like structure, and differentiation of human costal cartilage. *Connect Tissue Res*. 53:415-421.

Steward, A.J., D.J. Kelly, and D.R. Wagner. 2014. The role of calcium signalling in the chondrogenic response of mesenchymal stem cells to hydrostatic pressure. *Eur Cell Mater*. 28:358-371.

Stewart, A.P., J.C. Gomez-Posada, J. McGeorge, M.J. Rouhani, A. Villarroel, R.D. Murrell-Lagnado, and J.M. Edwardson. 2012. The Kv7.2/Kv7.3 heterotetramer assembles with a random subunit arrangement. *J Biol Chem*. 287:11870-11877.

Striggow, F., and B.E. Ehrlich. 1996. Ligand-gated calcium channels inside and out. *Current opinion in cell biology*. 8:490-495.

Strotmann, R., G. Schultz, and T.D. Plant. 2003. Ca2+-dependent potentiation of the nonselective cation channel TRPV4 is mediated by a C-terminal calmodulin binding site. *J Biol Chem*. 278:26541-26549.

Sugimoto, T., M. Yoshino, M. Nagao, S. Ishii, and H. Yabu. 1996. Voltage-gated ionic channels in cultured rabbit articular chondrocytes. *Comparative biochemistry and physiology. Part C, Pharmacology, toxicology & endocrinology*. 115:223-232.

Sun, H.B., L. Cardoso, and H. Yokota. 2011. Mechanical intervention for maintenance of cartilage and bone. *Clinical medicine insights. Arthritis and musculoskeletal disorders*. 4:65-70.

Szczupak, L. 2016. Functional contributions of electrical synapses in sensory and motor networks. *Current opinion in neurobiology*. 41:99-105.

Thoms, B.L., K.A. Dudek, J.E. Lafont, and C.L. Murphy. 2013. Hypoxia promotes the production and inhibits the destruction of human articular cartilage. *Arthritis Rheum*. 65:1302-1312.

Tian, C., R. Zhu, L. Zhu, T. Qiu, Z. Cao, and T. Kang. 2014. Potassium channels: structures, diseases, and modulators. *Chemical biology & drug design*. 83:1-26.

Tie, J., Y. Pan, L. Zhao, K. Wu, J. Liu, S. Sun, X. Guo, B. Wang, Y. Gang, Y. Zhang, Q. Li, T. Qiao, Q. Zhao, Y. Nie, and D. Fan. 2010. MiR-218 inhibits invasion and metastasis of gastric cancer by targeting the Robo1 receptor. *PLoS Genet*. 6:e1000879.

Tran, C.M., N. Fujita, B.L. Huang, J.R. Ong, K.M. Lyons, I.M. Shapiro, and M.V. Risbud. 2013. Hypoxia-inducible factor (HIF)-1alpha and CCN2 form a regulatory circuit in hypoxic nucleus pulposus cells: CCN2 suppresses HIF-1alpha level and transcriptional activity. *J Biol Chem*. 288:12654-12666.

Tsantoulas, C., L. Zhu, Y. Shaifta, J. Grist, J.P. Ward, R. Raouf, G.J. Michael, and S.B. McMahon. 2012. Sensory neuron downregulation of the Kv9.1 potassium channel subunit mediates neuropathic pain following nerve injury. *J Neurosci*. 32:17502-17513.

Tsuga, K., N. Tohse, M. Yoshino, T. Sugimoto, T. Yamashita, S. Ishii, and H. Yabu. 2002. Chloride conductance determining membrane potential of rabbit articular chondrocytes. *The Journal of membrane biology*. 185:75-81.

Vandenberg, J.I., M.D. Perry, M.J. Perrin, S.A. Mann, Y. Ke, and A.P. Hill. 2012. hERG K(+) channels: structure, function, and clinical significance. *Physiological reviews*. 92:1393-1478.

Varga, Z., T. Juhasz, C. Matta, J. Fodor, E. Katona, A. Bartok, T. Olah, A. Sebe, L. Csernoch, G. Panyi, and R. Zakany. 2011. Switch of voltage-gated K+ channel expression in the plasma membrane of chondrogenic cells affects cytosolic Ca2+-oscillations and cartilage formation. *PLoS One*. 6:e27957.

Vazquez, G., B.J. Wedel, O. Aziz, M. Trebak, and J.W. Putney, Jr. 2004. The mammalian TRPC cation channels. *Biochim Biophys Acta*. 1742:21-36.

Vo, N.V., R.A. Hartman, T. Yurube, L.J. Jacobs, G.A. Sowa, and J.D. Kang. 2013. Expression and regulation of metalloproteinases and their inhibitors in intervertebral disc aging and degeneration. *The spine journal : official journal of the North American Spine Society*. 13:331-341.

Voets, T., G. Droogmans, U. Wissenbach, A. Janssens, V. Flockerzi, and B. Nilius. 2004. The principle of temperature-dependent gating in cold- and heat-sensitive TRP channels. *Nature*. 430:748-754.

Wang, J., M. Li, Y. Deng, and Y. Pan. 2010. Recent advances in clustering methods for protein interaction networks. *BMC Genomics*. 11 Suppl 3:S10.

Wang, M., Y. Huang, Z. Liang, D. Liu, Y. Lu, Y. Dai, G. Feng, and C. Wang. 2016. Plasma miRNAs might be promising biomarkers of chronic obstructive pulmonary disease. *The clinical respiratory journal*. 10:104-111.

Wang, X., and I.M. El Naqa. 2008. Prediction of both conserved and nonconserved microRNA targets in animals. *Bioinformatics*. 24:325-332.

Wang, Z., H. Cai, L. Lin, M. Tang, and H. Cai. 2014. Upregulated expression of microRNA-214 is linked to tumor progression and adverse prognosis in pediatric osteosarcoma. *Pediatr Blood Cancer*. 61:206-210.

Wemmie, J.A., R.J. Taugher, and C.J. Kreple. 2013. Acid-sensing ion channels in pain and disease. *Nature reviews. Neuroscience*. 14:461-471.

Wilczynska, A., and M. Bushell. 2015. The complexity of miRNA-mediated repression. *Cell death and differentiation*. 22:22-33.

Wildman, S.S., B.F. King, and G. Burnstock. 1997. Potentiation of ATP-responses at a recombinant P2x2 receptor by neurotransmitters and related substances. *Br J Pharmacol*. 120:221-224.

Wilkins, R.J., and A.C. Hall. 1992. Measurement of intracellular pH in isolated bovine articular chondrocytes. *Experimental physiology*. 77:521-524.

Wilkins, R.J., and A.C. Hall. 1995. Control of matrix synthesis in isolated bovine chondrocytes by extracellular and intracellular pH. *Journal of cellular physiology*. 164:474-481.

Wong, N., and X. Wang. 2015. miRDB: an online resource for microRNA target prediction and functional annotations. *Nucleic Acids Res*. 43:D146-152.

Wright, M.O., K. Nishida, C. Bavington, J.L. Godolphin, E. Dunne, S. Walmsley, P. Jobanputra, G. Nuki, and D.M. Salter. 1997. Hyperpolarisation of cultured human chondrocytes following cyclical pressure-induced strain: evidence of a role for alpha 5 beta 1 integrin as a chondrocyte mechanoreceptor. *Journal of orthopaedic research : official publication of the Orthopaedic Research Society*. 15:742-747.

Wu, Q.Q., and Q. Chen. 2000. Mechanoregulation of chondrocyte proliferation, maturation, and hypertrophy: ion-channel dependent transduction of matrix deformation signals. *Experimental cell research*. 256:383-391.

Xiao, R., J. Tang, C. Wang, C.K. Colton, J. Tian, and M.X. Zhu. 2008. Calcium plays a central role in the sensitization of TRPV3 channel to repetitive stimulations. *J Biol Chem*. 283:6162-6174.

Xiu, Y., Z. Liu, S. Xia, C. Jin, H. Yin, W. Zhao, and Q. Wu. 2014. MicroRNA-137 upregulation increases bladder cancer cell proliferation and invasion by targeting PAQR3. *PLoS One*. 9:e109734.

Xu, J., W. Wang, C.C. Clark, and C.T. Brighton. 2009. Signal transduction in electrically stimulated articular chondrocytes involves translocation of extracellular calcium through voltage-gated channels. *Osteoarthritis Cartilage*. 17:397-405.

Yamakage, M., and A. Namiki. 2002. Calcium channels--basic aspects of their structure, function and gene encoding; anesthetic action on the channels--a review. *Can J Anaesth*. 49:151-164.

Yang, N.C., W.M. Ho, Y.H. Chen, and M.L. Hu. 2002. A convenient one-step extraction of cellular ATP using boiling water for the luciferin-luciferase assay of ATP. *Analytical biochemistry*. 306:323-327.

Yang, T., Q. Liu, B. Kloss, R. Bruni, R.C. Kalathur, Y. Guo, E. Kloppmann, B. Rost, H.M. Colecraft, and W.A. Hendrickson. 2014. Structure and selectivity in bestrophin ion channels. *Science*. 346:355-359.

Yellowley, C.E., J.C. Hancox, and H.J. Donahue. 2002. Effects of cell swelling on intracellular calcium and membrane currents in bovine articular chondrocytes. *J Cell Biochem*. 86:290-301.

Yokota, H., D.J. Leong, and H.B. Sun. 2011. Mechanical loading: bone remodeling and cartilage maintenance. *Current osteoporosis reports*. 9:237-242.

Yuan, F.L., F.H. Chen, W.G. Lu, X. Li, J.P. Li, C.W. Li, R.S. Xu, F.R. Wu, W. Hu, and T.Y. Zhang. 2010. Inhibition of acid-sensing ion channels in articular chondrocytes by amiloride attenuates articular cartilage destruction in rats with adjuvant arthritis. *Inflammation research : official journal of the European Histamine Research Society ... [et al.]*. 59:939-947.

Yueh, Y.G., D.P. Gardner, and C. Kappen. 1998. Evidence for regulation of cartilage differentiation by the homeobox gene Hoxc-8. *Proc Natl Acad Sci U S A*. 95:9956-9961.

Zhang, L., and M. Spector. 2009. Comparison of three types of chondrocytes in collagen scaffolds for cartilage tissue engineering. *Biomedical materials*. 4:045012.

Zhang, M., J.J. Wang, and Y.J. Chen. 2006. Effects of mechanical pressure on intracellular calcium release channel and cytoskeletal structure in rabbit mandibular condylar chondrocytes. *Life sciences*. 78:2480-2487.

Zhang, X., Y. Wu, Z. Pan, H. Sun, J. Wang, D. Yu, S. Zhu, J. Dai, Y. Chen, N. Tian, B.C. Heng, N.D. Coen, H. Xu, and H. Ouyang. 2016. The effects of lactate and acid on articular chondrocytes function: Implications for polymeric cartilage scaffold design. *Acta Biomater*. 42:329-340.

Zhao, G., J.G. Zhang, Y. Liu, Q. Qin, B. Wang, K. Tian, L. Liu, X. Li, Y. Niu, S.C. Deng, and C.Y. Wang. 2013. miR-148b functions as a tumor suppressor in pancreatic cancer by targeting AMPKalpha1. *Molecular cancer therapeutics*. 12:83-93.

Zheng, J. 2013. Molecular mechanism of TRP channels. *Comprehensive Physiology*. 3:221-242.

Zhou, R., X. Wu, Z. Wang, J. Ge, and F. Chen. 2015. Interleukin-6 enhances acid-induced apoptosis via upregulating acid-sensing ion channel 1a expression and function in rat articular chondrocytes. *International immunopharmacology*. 29:748-760.

Zhou, R.P., X.S. Wu, Z.S. Wang, Y.Y. Xie, J.F. Ge, and F.H. Chen. 2016. Novel Insights into Acid-Sensing Ion Channels: Implications for Degenerative Diseases. *Aging and disease*. 7:491-501.

APPENDIX

Appendix 1. **Expression values of potassium channels for articular chondrocytes**

Gene	Name	Art Cq Avg	Art Cq SD	Art ΔCq Avg	Art ΔCq SD
KCNMA1	$K_{Ca}1.1\alpha$	22.34	0.65	1.88E-01	2.68E-02
KCNMB4	$K_{Ca}1.1\beta$	32.30	1.67	1.51E-04	9.65E-05
KCNN1	$K_{Ca}2.1$	33.22	1.47	6.68E-05	2.73E-05
KCNN2	$K_{Ca}2.2$	28.93	0.77	2.56E-03	9.44E-04
KCNN3	$K_{Ca}2.3$	33.24	1.70	6.81E-05	4.61E-05
KCNJ1	$K_{ir}1.1$	34.66	0.76	3.60E-05	1.15E-05
KCNJ2	$K_{ir}2.1$	25.83	0.96	1.52E-02	4.49E-03
KCNJ12	$K_{ir}2.2$	30.35	2.69	6.91E-04	9.14E-04
KCNJ4	$K_{ir}2.3$	33.13	1.90	5.99E-05	3.20E-05
KCNJ14	$K_{ir}2.4$	29.59	2.22	7.45E-04	5.77E-04
KCNJ3	$K_{ir}3.1$	34.56	0.99	3.60E-05	1.15E-05
KCNJ6	$K_{ir}3.2$	34.64	0.66	5.13E-05	1.76E-05
KCNJ9	$K_{ir}3.3$	31.91	2.68	1.41E-04	1.46E-04
KCNJ5	$K_{ir}3.4$	34.79	0.48	3.60E-05	1.15E-05
KCNJ15	$K_{ir}4.2$	28.56	1.40	3.58E-03	4.41E-03
KCNJ16	$K_{ir}5.1$	34.48	1.17	3.60E-05	1.15E-05
KCNJ11	$K_{ir}6.2$	33.27	1.76	6.59E-05	4.24E-05
KCNJ13	$K_{ir}7.1$	31.87	1.52	1.87E-04	9.84E-05
KCNAB1	$K_V\ \beta1$	32.07	1.29	2.14E-04	2.08E-04
KCNAB2	$K_V\ \beta2$	27.34	0.86	5.53E-03	2.74E-03
KCNAB3	$K_V\ \beta3$	32.37	1.76	9.20E-05	2.54E-05
KCNA1	$K_V1.1$	31.63	2.01	6.19E-04	6.81E-04
KCNA2	$K_V1.2$	30.37	4.11	5.08E-04	7.87E-04

Appendix 1 continued

Gene	Name	Art Cq Avg	Art Cq SD	Art ΔCq Avg	Art ΔCq SD
KCNA5	K_V1.5	33.67	1.74	5.26E-05	1.98E-05
KCNA6	K_V1.6	34.60	0.71	3.83E-05	8.30E-06
KCNH1	K_V10.1	32.00	1.57	1.47E-04	8.58E-05
KCNH2	K_V11.1	32.14	2.83	1.73E-04	2.28E-04
KCNH6	K_V11.2	33.64	1.77	5.53E-05	2.43E-05
KCNH7	K_V11.3	32.54	2.45	1.30E-04	1.53E-04
KCNH3	K_V12.2	34.03	1.05	4.98E-05	1.89E-05
KCNB1	K_V2.1	28.84	2.10	1.98E-03	1.52E-03
KCNB2	K_V2.2	34.50	0.71	3.71E-05	9.93E-06
KCNC1	K_V3.1	33.20	1.98	1.59E-04	2.03E-04
KCNC2	K_V3.2	33.65	1.92	4.32E-05	6.39E-06
KCND3	K_V4.2	29.79	1.46	6.25E-04	4.63E-05
KCNQ1	K_V4.3	30.32	2.57	5.32E-04	6.45E-04
KCNQ2	K_V7.1	33.21	1.39	9.89E-05	7.57E-05
KCNQ3	K_V7.2	34.08	0.99	4.62E-05	9.77E-06
KCNS1	K_V7.3	31.19	0.80	3.88E-04	1.99E-04
KCNK1	K_V9.1	30.99	2.13	3.43E-04	2.64E-04

Appendix 2. **Expression values of potassium channels for costal chondrocytes**

Gene	Name	Con Cq Avg	Con Cq SD	Con ΔCq Avg	Con ΔCq SD	Con ΔΔCq Avg	Con ΔΔCq SD	Con ΔΔCq p-Val
KCNMA1	K_{Ca}1.1α	23.56	0.89	6.84E-02	2.06E-02	1.02	1.32	0.8986
KCNMB4	K_{Ca}1.1β	29.70	1.29	1.04E-03	5.22E-04	-1.35	2.44	0.2595
KCNN1	K_{Ca}2.1	33.73	0.81	7.91E-05	6.46E-05	1.02	1.84	0.5796

Appendix 2 continued

Gene	Name	Con Cq Avg	Con Cq SD	Con ΔCq Avg	Con ΔCq SD	Con ΔΔCq Avg	Con ΔΔCq SD	Con ΔΔCq p-Val
KCNN2	$K_{Ca}2.2$	31.61	3.18	5.27E-04	5.08E-04	64.81	35.94	0.0041
KCNN3	$K_{Ca}2.3$	34.36	0.83	3.78E-05	7.53E-06	3.41	1.87	0.0283
KCNJ1	$K_{ir}1.1$	34.68	0.55	3.01E-05	4.89E-06	-1.26	1.21	0.2663
KCNJ2	$K_{ir}2.1$	29.35	1.66	1.60E-03	1.27E-03	8.93	3.03	0.0004
KCNJ12	$K_{ir}2.2$	31.51	2.42	4.35E-04	5.10E-04	1.66	4.32	0.4145
KCNJ4	$K_{ir}2.3$	34.05	1.65	5.35E-05	3.66E-05	4.27	3.02	0.0509
KCNJ14	$K_{ir}2.4$	29.01	0.67	1.59E-03	6.01E-04	1.27	2.89	0.7450
KCNJ3	$K_{ir}3.1$	32.93	3.59	3.47E-04	5.44E-04	1.13	1.53	0.8974
KCNJ6	$K_{ir}3.2$	34.03	1.68	5.46E-05	3.85E-05	-93.74	87.26	0.0766
KCNJ9	$K_{ir}3.3$	32.36	1.57	1.68E-04	8.60E-05	5.37	5.81	0.1040
KCNJ5	$K_{ir}3.4$	34.70	0.53	2.99E-05	5.23E-06	-1.05	1.47	0.5750
KCNJ15	$K_{ir}4.2$	29.27	0.36	1.50E-03	8.57E-04	-2.84	4.42	0.0167
KCNJ16	$K_{ir}5.1$	35.00	0.00	2.60E-05	1.15E-05	1.45	1.71	0.4424
KCNJ11	$K_{ir}6.2$	35.00	0.00	2.60E-05	1.15E-05	3.46	2.22	0.0527
KCNJ13	$K_{ir}7.1$	29.84	0.99	1.12E-03	9.98E-04	-1.44	2.07	0.1752
KCNAB1	K_V β1	31.20	0.56	3.35E-04	4.65E-05	-1.46	2.21	0.2227
KCNAB2	K_V β2	27.03	0.83	6.27E-03	2.41E-03	1.12	1.28	0.7373
KCNAB3	K_V β3	30.75	1.30	7.22E-04	5.49E-04	1.27	2.32	0.8459
KCNA1	$K_V1.1$	33.32	1.81	9.16E-05	6.31E-05	2.83	5.37	0.4574
KCNA2	$K_V1.2$	30.98	4.34	1.85E-03	2.89E-03	34.97	46.78	0.1428
KCNA5	$K_V1.5$	34.78	0.39	2.86E-05	7.18E-06	2.93	2.57	0.1638
KCNA6	$K_V1.6$	33.30	2.94	3.55E-04	5.74E-04	1.14	1.18	0.9741
KCNH1	$K_V10.1$	31.41	1.55	3.40E-04	2.07E-04	-35.01	40.91	0.0053
KCNH6	$K_V11.1$	31.79	2.79	3.97E-04	3.48E-04	-2.06	9.72	0.1744

Appendix 2 continued

Gene	Name	Con Cq Avg	Con Cq SD	Con ΔCq Avg	Con ΔCq SD	Con ΔΔCq Avg	Con ΔΔCq SD	Con ΔΔCq p-Val
KCNH7	K_V11.2	34.75	0.43	2.90E-05	6.63E-06	3.02	2.66	0.1589
KCNH3	K_V11.3	33.42	2.74	1.40E-04	1.86E-04	8.24	7.96	0.0814
KCNB1	K_V12.2	32.02	0.75	2.24E-04	1.61E-04	1.40	1.27	0.2378
KCNB2	K_V2.1	32.13	3.05	3.66E-04	4.60E-04	-1.44	6.92	0.3276
KCNC1	K_V2.2	35.00	0.00	2.60E-05	1.15E-05	1.33	0.26	0.4932
KCNC2	K_V3.1	33.14	1.61	1.14E-04	9.86E-05	2.44	4.02	0.3080
KCND2	K_V3.2	34.75	0.43	2.90E-05	6.55E-06	3.33	3.76	0.2305
KCND3	K_V4.2	33.83	2.02	7.13E-05	6.74E-05	27.51	22.52	0.0310
KCNQ1	K_V4.3	31.64	4.40	1.47E-03	2.43E-03	5.17	5.39	0.1025
KCNQ2	K_V7.1	33.71	1.76	1.16E-04	1.53E-04	2.78	1.54	0.0414
KCNQ3	K_V7.2	35.00	0.00	2.60E-05	1.15E-05	1.77	0.31	0.0562
KCNS1	K_V7.3	30.10	0.67	8.68E-04	6.81E-04	-5.53	2.38	0.0151
KCNK1	K_V9.1	28.08	2.60	7.85E-03	1.16E-02	9.82	7.29	0.0212

Appendix 3. **Expression values of potassium channels for fetal costal chondrocytes**

Gene	Name	Fetal Cq Avg	Fetal Cq SD	Fetal ΔCq Avg	Fetal ΔCq SD	Fetal ΔΔCq Avg	Fetal ΔΔCq SD	Fetal ΔΔCq p-Val
KCNMA1	K_{Ca}1.1α	21.93	1.44	6.84E-02	2.06E-02	-2.39	0.73	0.0255
KCNMB4	K_{Ca}1.1β	31.54	3.03	1.04E-03	5.22E-04	3.98	1.99	0.0624
KCNN1	K_{Ca}2.1	32.43	2.28	7.91E-05	6.46E-05	-1.20	3.43	0.5417
KCNN2	K_{Ca}2.2	34.73	0.47	5.27E-04	5.08E-04	17.23	17.59	0.0604
KCNN3	K_{Ca}2.3	34.82	0.31	3.78E-05	7.53E-06	1.28	0.26	0.5714
KCNJ1	K_{ir}1.1	33.98	1.35	3.01E-05	4.89E-06	-1.39	0.23	0.2543
KCNJ2	K_{ir}2.1	28.85	1.20	1.60E-03	1.27E-03	-1.06	2.99	0.7558

Appendix 3 continued

Gene	Name	Fetal Cq Avg	Fetal Cq SD	Fetal ΔCq Avg	Fetal ΔCq SD	Fetal ΔΔCq Avg	Fetal ΔΔCq SD	Fetal ΔΔCq p-Val
KCNJ12	$K_{ir}2.2$	30.62	1.16	4.35E-04	5.10E-04	-1.49	3.73	0.3911
KCNJ4	$K_{ir}2.3$	35.00	0.00	5.35E-05	3.66E-05	1.96	1.34	0.2530
KCNJ14	$K_{ir}2.4$	29.14	1.63	1.59E-03	6.01E-04	1.29	1.50	0.5314
KCNJ3	$K_{ir}3.1$	34.62	0.66	3.47E-04	5.44E-04	10.82	17.60	0.2237
KCNJ6	$K_{ir}3.2$	26.95	2.11	5.46E-05	3.85E-05	-64.91	43.90	0.1795
KCNJ9	$K_{ir}3.3$	32.70	0.88	1.68E-04	8.60E-05	2.35	1.21	0.0901
KCNJ5	$K_{ir}3.4$	34.61	0.67	2.99E-05	5.23E-06	-1.08	1.32	0.5527
KCNJ15	$K_{ir}4.2$	26.30	1.61	1.50E-03	8.57E-04	-5.97	7.20	0.0079
KCNJ16	$K_{ir}5.1$	35.00	0.00	2.60E-05	1.15E-05	-1.05	1.89	0.6596
KCNJ11	$K_{ir}6.2$	35.00	0.00	2.60E-05	1.15E-05	-1.11	1.92	0.5500
KCNJ13	$K_{ir}7.1$	29.68	4.61	1.12E-03	9.98E-04	3.08	2.75	0.7147
KCNAB1	K_V β1	30.67	2.55	3.35E-04	4.65E-05	-1.01	1.31	0.5351
KCNAB2	K_V β2	27.32	1.46	6.27E-03	2.41E-03	1.31	1.51	0.3869
KCNAB3	K_V β3	32.37	2.28	7.22E-04	5.49E-04	4.50	4.78	0.0647
KCNA1	$K_V1.1$	32.00	2.57	9.16E-05	6.31E-05	-1.87	1.96	0.4010
KCNA2	$K_V1.2$	33.40	1.50	1.85E-03	2.89E-03	25.92	41.44	0.2047
KCNA5	$K_V1.5$	35.00	0.00	2.86E-05	7.18E-06	1.05	1.44	0.8270
KCNA6	$K_V1.6$	35.00	0.00	3.55E-04	5.74E-04	11.86	20.00	0.2335
KCNH1	$K_V10.1$	26.47	1.64	3.40E-04	2.07E-04	-30.07	33.76	0.0299
KCNH2	$K_V11.1$	29.46	1.77	3.97E-04	3.48E-04	-1.88	11.43	0.3017
KCNH6	$K_V11.2$	35.00	0.00	2.90E-05	6.63E-06	1.06	1.41	0.8528
KCNH7	$K_V11.3$	35.00	0.00	1.40E-04	1.86E-04	5.11	6.80	0.2167
KCNH3	$K_V12.2$	34.27	0.77	2.24E-04	1.61E-04	6.04	4.33	0.0350
KCNB1	$K_V2.1$	26.93	2.99	3.66E-04	4.60E-04	-9.83	52.54	0.2932

Appendix 3 continued

Gene	Name	Fetal Cq Avg	Fetal Cq SD	Fetal ΔCq Avg	Fetal ΔCq SD	Fetal ΔΔCq Avg	Fetal ΔΔCq SD	Fetal ΔΔCq p-Val
KCNB2	K_V2.2	35.00	0.00	2.60E-05	1.15E-05	-1.05	1.89	0.6596
KCNC1	K_V3.1	32.86	1.08	1.14E-04	9.86E-05	1.72	2.65	0.4401
KCNC2	K_V3.2	35.00	0.00	2.90E-05	6.55E-06	1.06	1.40	0.8567
KCND2	K_V4.2	34.00	1.73	7.13E-05	6.74E-05	1.72	2.82	0.5343
KCND3	K_V4.3	32.55	1.06	1.47E-03	2.43E-03	7.05	14.27	0.3046
KCNQ1	K_V7.1	34.39	1.05	1.16E-04	1.53E-04	3.29	5.62	0.2735
KCNQ2	K_V7.2	35.00	0.00	2.60E-05	1.15E-05	-1.05	1.89	0.6596
KCNQ3	K_V7.3	28.30	2.39	8.68E-04	6.81E-04	-2.39	1.98	0.1395
KCNS1	K_V9.1	33.17	1.72	7.85E-03	1.16E-02	133.91	197.22	0.1618
KCNK1	TWIK1	24.71	1.84	3.08E-02	1.33E-02	1.26	1.66	0.6759

Appendix 4. **Expression values of calcium channels for articular chondrocytes**

Gene	Name	Art Cq Avg	Art Cq SD	Art ΔCq Avg	Art ΔCq SD
CACNB1	Ca_V β1	27.75	0.88	3.59E-03	7.00E-04
CACNB2	Ca_V β2	29.76	1.98	6.62E-04	4.83E-04
CACNB3	Ca_V β3	26.92	0.90	6.95E-03	1.78E-03
CACNG2	Ca_V γ2	32.14	2.44	1.47E-04	1.65E-04
CACNG4	Ca_V γ4	33.65	1.87	2.36E-04	3.57E-04
CACNA1C	Ca_V1.2	28.48	2.19	1.15E-03	3.35E-04
CACNA1D	Ca_V1.3	31.88	1.44	2.86E-04	1.49E-04
CACNA1A	Ca_V2.1	28.06	1.45	2.45E-03	1.03E-03
CACNA1B	Ca_V2.2	34.26	1.25	3.60E-05	1.15E-05
CACNA1G	Ca_V3.1	30.97	1.96	2.44E-04	1.49E-04
CACNA1I	Ca_V3.3	32.65	2.18	1.24E-04	1.42E-04

Appendix 4 continued

Gene	Name	Art Cq Avg	Art Cq SD	Art ΔCq Avg	Art ΔCq SD
RYR3	RYR3	30.14	1.31	8.09E-04	5.45E-04

Appendix 5. **Expression values of calcium channels for costal chondrocytes**

Gene	Name	Con Cq Avg	Con Cq SD	Con ΔCq Avg	Con ΔCq SD	Con ΔΔCq Avg	Con ΔΔCq SD	Con ΔΔCq p-Val
CACNB1	Ca_V β1	26.55	0.88	8.74E-03	3.07E-03	-1.47	0.26	0.2104
CACNB2	Ca_V β2	28.89	1.58	1.87E-03	9.69E-04	1.89	2.62	0.9544
CACNB3	Ca_V β3	26.64	0.60	8.12E-03	2.45E-03	1.13	1.36	0.4707
CACNG2	Ca_V γ2	33.84	2.01	7.10E-05	6.68E-05	9.42	7.55	0.0393
CACNG4	Ca_V γ4	33.15	1.70	1.32E-04	1.45E-04	5.98	10.53	0.3085
CACNA1C	Ca_V1.2	29.53	2.12	1.42E-03	1.26E-03	1.24	2.88	0.8524
CACNA1D	Ca_V1.3	30.90	2.05	5.29E-04	3.79E-04	-1.72	1.79	0.0580
CACNA1A	Ca_V2.1	28.36	0.79	2.44E-03	6.28E-04	-1.29	1.94	0.3191
CACNA1B	Ca_V2.2	35.00	0.00	2.60E-05	1.15E-05	1.67	1.49	0.2452
CACNA1G	Ca_V3.1	29.26	2.87	2.30E-03	2.40E-03	-1.22	3.08	0.4429
CACNA1I	Ca_V3.3	34.67	0.57	3.03E-05	4.64E-06	6.66	4.70	0.0311
RYR3	RYR3	29.10	0.39	1.68E-03	1.10E-03	-1.14	2.13	0.4679

Appendix 6. **Expression values of calcium channels for fetal costal chondrocytes**

Gene	Name	Fetal Cq Avg	Fetal Cq SD	Fetal ΔCq Avg	Fetal ΔCq SD	Fetal ΔΔCq Avg	Fetal ΔΔCq SD	Fetal ΔΔCq p-Val
CACNB1	Ca_V β1	26.73	2.26	8.74E-03	3.07E-03	1.54	0.54	0.6310
CACNB2	Ca_V β2	29.12	2.80	1.87E-03	9.69E-04	2.79	1.45	0.5971
CACNB3	Ca_V β3	26.74	0.96	8.12E-03	2.45E-03	1.31	0.40	0.1995
CACNG2	Ca_V γ2	34.77	0.39	7.10E-05	6.68E-05	2.36	3.00	0.2430

Appendix 6 continued

Gene	Name	Fetal Cq Avg	Fetal Cq SD	Fetal ΔCq Avg	Fetal ΔCq SD	Fetal ΔΔCq Avg	Fetal ΔΔCq SD	Fetal ΔΔCq p-Val
CACNG4	Ca_V γ4	35.00	0.00	1.32E-04	1.45E-04	4.81	5.30	0.1540
CACNA1C	$Ca_V1.2$	27.91	2.90	1.42E-03	1.26E-03	-1.97	3.91	0.2707
CACNA1D	$Ca_V1.3$	30.86	1.16	5.29E-04	3.79E-04	1.18	2.81	0.7316
CACNA1A	$Ca_V2.1$	26.76	2.09	2.44E-03	6.28E-04	-1.82	0.49	0.2828
CACNA1B	$Ca_V2.2$	35.00	0.00	2.60E-05	1.15E-05	-1.05	1.89	0.6596
CACNA1G	$Ca_V3.1$	30.34	0.37	2.30E-03	2.40E-03	3.26	4.92	0.2007
CACNA1I	$Ca_V3.3$	35.00	0.00	3.03E-05	4.64E-06	1.11	1.30	0.9569
RYR3	RYR3	29.20	2.02	1.68E-03	1.10E-03	1.72	2.22	0.4957

Appendix 7. **Expression values of chloride channels for articular chondrocytes**

Gene	Name	Art Cq Avg	Art Cq SD	Art ΔCq Avg	Art ΔCq SD
CLCN2	CLC2	30.30	0.86	7.21E-04	2.84E-04
CLCN3	CLC3	24.76	0.88	3.23E-02	1.15E-02
CLCN7	CLC7	25.75	1.14	1.69E-02	1.24E-02

Appendix 8. **Expression values of chloride channels for costal chondrocytes**

Gene	Name	Con Cq Avg	Con Cq SD	Con ΔCq Avg	Con ΔCq SD	Con ΔΔCq Avg	Con ΔΔCq SD	Con ΔΔCq p-Val
CLCN2	CLC2	29.14	0.46	1.65E-03	1.16E-03	-1.49	1.25	0.1966
CLCN3	CLC3	24.12	0.79	4.53E-02	6.05E-03	-1.04	1.42	0.7105
CLCN7	CLC7	25.46	1.03	1.81E-02	3.57E-03	-1.65	1.73	0.1085

Appendix 9. **Expression values of chloride channels for fetal costal chondrocytes**

Gene	Name	Fetal Cq Avg	Fetal Cq SD	Fetal ΔCq Avg	Fetal ΔCq SD	Fetal ΔΔCq Avg	Fetal ΔΔCq SD	Fetal ΔΔCq p-Val
CLCN2	CLC2	28.92	1.84	1.65E-03	1.16E-03	1.64	2.24	0.5791
CLCN3	CLC3	24.24	1.39	4.53E-02	6.05E-03	1.38	0.18	0.1697
CLCN7	CLC7	25.13	0.89	1.81E-02	3.57E-03	-1.58	0.29	0.1851

Appendix 10. **Expression values of sodium channels for articular chondrocytes**

Gene	Name	Art Cq Avg	Art Cq SD	Art ΔCq Avg	Art ΔCq SD
SCN1A	$Na_V1.1\alpha$	32.94	2.09	5.90E-05	3.05E-05
SCN1B	$Na_V\beta1$	26.06	0.86	1.21E-02	3.91E-03
SCN2A	$Na_V1.2$	28.84	1.31	1.38E-03	4.87E-04
SCN2B	$Na_V\beta2$	28.13	1.81	2.06E-03	1.24E-03
SCN3A	$Na_V1.3$	28.96	1.16	2.52E-03	2.47E-03
SCN8A	$Na_V1.6$	27.33	1.09	4.50E-03	1.15E-03
SCN9A	$Na_V1.7$	28.34	1.11	3.08E-03	2.07E-03
SCN10A	$Na_V1.8$	34.15	1.18	3.60E-05	1.15E-05
SCN11A	$Na_V1.9$	34.48	1.16	3.60E-05	1.15E-05

Appendix 11. **Expression values of sodium channels for costal chondrocytes**

Gene	Name	Con Cq Avg	Con Cq SD	Con ΔCq Avg	Con ΔCq SD	Con ΔΔCq Avg	Con ΔΔCq SD	Con ΔΔCq p-Val
SCN1A	$Na_V1.1\alpha$	33.15	2.64	1.56E-04	1.99E-04	5.56	5.56	0.1128
SCN1B	$Na_V\beta1$	26.21	0.93	1.08E-02	2.25E-03	-2.88	1.04	0.0001
SCN2A	$Na_V1.2$	31.51	4.52	1.83E-03	3.06E-03	6.31	4.26	0.0305
SCN2B	$Na_V\beta2$	28.32	2.79	4.76E-03	6.20E-03	1.77	2.29	0.2879
SCN3A	$Na_V1.3$	30.79	1.96	8.50E-04	1.08E-03	20.49	17.50	0.0407

Appendix 11 continued

Gene	Name	Con Cq Avg	Con Cq SD	Con ΔCq Avg	Con ΔCq SD	Con ΔΔCq Avg	Con ΔΔCq SD	Con ΔΔCq p-Val
SCN8A	$Na_V1.6$	27.21	1.02	5.41E-03	1.25E-03	-2.58	1.00	0.0776
SCN9A	$Na_V1.7$	28.28	2.81	4.61E-03	4.52E-03	11.39	5.86	0.0054
SCN10A	$Na_V1.8$	35.00	0.00	2.60E-05	1.15E-05	1.44	1.44	0.4091
SCN11A	$Na_V1.9$	33.46	1.55	1.09E-04	1.26E-04	-2.12	1.07	0.0859

Appendix 12. **Expression values of sodium channels for fetal costal chondrocytes**

Gene	Name	Fetal Cq Avg	Fetal Cq SD	Fetal ΔCq Avg	Fetal ΔCq SD	Fetal ΔΔCq Avg	Fetal ΔΔCq SD	Fetal ΔΔCq p-Val
SCN1A	$Na_V1.1\alpha$	34.93	0.13	1.56E-04	1.99E-04	5.53	7.04	0.1885
SCN1B	$Na_V\beta1$	24.39	0.90	1.08E-02	2.25E-03	-3.49	0.81	0.0004
SCN2A	$Na_V1.2$	30.96	1.81	1.83E-03	3.06E-03	5.51	13.12	0.3135
SCN2B	$Na_V\beta2$	28.55	2.06	4.76E-03	6.20E-03	2.31	4.52	0.3955
SCN3A	$Na_V1.3$	32.23	2.41	8.50E-04	1.08E-03	8.11	10.27	0.1751
SCN8A	$Na_V1.6$	25.19	1.98	5.41E-03	1.25E-03	-2.63	0.68	0.1707
SCN9A	$Na_V1.7$	30.97	2.00	4.61E-03	4.52E-03	18.08	17.70	0.0664
SCN10A	$Na_V1.8$	34.45	0.96	2.60E-05	1.15E-05	-1.32	1.83	0.3060
SCN11A	$Na_V1.9$	33.18	1.59	1.09E-04	1.26E-04	1.31	3.09	0.8824

Appendix 13. **Expression values of non-selective channels for articular chondrocytes**

Gene	Name	Art Cq Avg	Art Cq SD	Art ΔCq Avg	Art ΔCq SD
ACCN2	ASIC1	28.27	1.85	1.54E-03	4.02E-04
ACCN1	ASIC2	28.75	1.40	2.14E-03	1.57E-03
ACCN3	ASIC3	31.07	1.53	3.33E-04	2.06E-04
HCN1	BCNG1	31.99	2.80	2.33E-04	3.32E-04

Appendix 13 continued

Gene	Name	Art Cq Avg	Art Cq SD	Art ΔCq Avg	Art ΔCq SD
HCN2	BCNG2	29.21	1.98	1.42E-03	9.64E-04
BEST1	BEST1	29.91	1.75	9.31E-04	6.57E-04
SLC12A5	SLC12A5	31.69	3.23	1.32E-04	1.56E-04
TRPA1	TRPA1	31.77	3.04	1.78E-04	2.36E-04
TRPC1	TRPC1	25.93	1.13	1.16E-02	3.90E-03
TRPC3	TRPC3	30.73	2.57	5.65E-04	4.90E-04
TRPC6	TRPC6	31.19	2.17	2.84E-04	1.56E-04
TRPM1	TRPM1	35.00	0.00	3.60E-05	1.15E-05
TRPM2	TRPM2	32.84	2.08	8.13E-05	6.89E-05
TRPM6	TRPM6	34.66	0.76	3.60E-05	1.15E-05
TRPM8	TRPM8	30.89	3.23	4.54E-04	6.61E-04
TRPV1	TRPV1	29.50	1.18	1.01E-03	4.18E-04
TRPV2	TRPV2	25.10	0.69	2.61E-02	3.78E-03
TRPV3	TRPV3	29.37	1.47	1.13E-03	5.14E-04
TRPV4	TRPV4	27.46	1.07	4.77E-03	1.54E-03

Appendix 14. **Expression values of non-selective channels for costal chondrocytes**

Gene	Name	Con Cq Avg	Con Cq SD	Con ΔCq Avg	Con ΔCq SD	Con ΔΔCq Avg	Con ΔΔCq SD	Con ΔΔCq p-Val
ACCN2	ASIC1	27.52	0.67	4.58E-03	2.11E-03	1.31	2.38	0.7397
ACCN1	ASIC2	31.16	3.13	8.32E-04	1.17E-03	34.92	18.47	0.0040
ACCN3	ASIC3	29.76	0.32	9.55E-04	3.77E-04	1.58	1.69	0.6915
HCN1	BCNG1	33.06	3.35	2.68E-04	4.08E-04	13.27	10.90	0.0375
HCN2	BCNG2	30.63	1.92	6.15E-04	4.71E-04	1.42	2.63	0.6257
BEST1	BEST1	27.88	0.21	3.67E-03	1.71E-03	-2.59	6.11	0.0482

Appendix 14 continued

Gene	Name	Con Cq Avg	Con Cq SD	Con ΔCq Avg	Con ΔCq SD	Con ΔΔCq Avg	Con ΔΔCq SD	Con ΔΔCq p-Val
SLC12A5	SLC12A5	33.45	1.99	9.09E-05	8.08E-05	22.35	25.25	0.0970
TRPA1	TRPA1	32.67	1.73	1.43E-04	1.03E-04	3.31	5.69	0.4572
TRPC1	TRPC1	25.99	0.86	1.26E-02	2.72E-03	-1.04	1.52	0.6014
TRPC3	TRPC3	31.53	1.98	4.55E-04	5.41E-04	12.43	8.52	0.0105
TRPC6	TRPC6	31.34	1.82	3.85E-04	2.68E-04	1.56	3.08	0.9581
TRPM1	TRPM1	35.00	0.00	2.60E-05	1.15E-05	1.00	1.81	0.7398
TRPM2	TRPM2	34.76	0.42	2.89E-05	6.79E-06	5.57	3.98	0.0385
TRPM6	TRPM6	33.94	0.98	7.01E-05	5.16E-05	1.08	1.44	0.8338
TRPM8	TRPM8	33.22	3.09	2.01E-04	2.91E-04	25.51	23.77	0.0514
TRPV1	TRPV1	28.55	0.18	2.21E-03	7.79E-04	-1.13	1.36	0.3456
TRPV2	TRPV2	25.95	0.50	1.30E-02	3.39E-03	1.24	0.18	0.6576
TRPV3	TRPV3	30.20	1.04	8.96E-04	8.33E-04	1.17	1.60	0.8831
TRPV4	TRPV4	26.90	1.90	1.43E-02	1.96E-02	-1.41	0.46	0.0753

Appendix 15. **Expression values of non-selective channels for fetal costal chondrocytes**

Gene	Name	Fetal Cq Avg	Fetal Cq SD	Fetal ΔCq Avg	Fetal ΔCq SD	Fetal ΔΔCq Avg	Fetal ΔΔCq SD	Fetal ΔΔCq p-Val
ACCN2	ASIC1	28.00	2.11	4.58E-03	2.11E-03	1.70	0.79	0.2619
ACCN1	ASIC2	33.14	0.99	8.32E-04	1.17E-03	13.35	18.76	0.1952
ACCN3	ASIC3	30.77	2.15	9.55E-04	3.77E-04	3.46	1.37	0.0521
HCN1	BCNG1	34.95	0.09	2.68E-04	4.08E-04	9.58	14.58	0.2182
HCN2	BCNG2	29.69	0.79	6.15E-04	4.71E-04	-2.03	2.37	0.1318
BEST1	BEST1	28.16	2.37	3.67E-03	1.71E-03	1.33	1.91	0.8371
SLC12A5	SLC12A5	34.94	0.10	9.09E-05	8.08E-05	3.24	2.88	0.1415

Appendix 15 continued

Gene	Name	Fetal Cq Avg	Fetal Cq SD	Fetal ΔCq Avg	Fetal ΔCq SD	Fetal ΔΔCq Avg	Fetal ΔΔCq SD	Fetal ΔΔCq p-Val
TRPA1	TRPA1	31.43	3.09	1.43E-04	1.03E-04	-1.13	2.18	0.4517
TRPC1	TRPC1	25.31	1.93	1.26E-02	2.72E-03	-1.18	1.38	0.5000
TRPC3	TRPC3	33.48	1.66	4.55E-04	5.41E-04	7.28	8.67	0.1430
TRPC6	TRPC6	31.84	2.88	3.85E-04	2.68E-04	1.06	2.84	0.5019
TRPM1	TRPM1	34.93	0.12	2.60E-05	1.15E-05	-1.08	1.90	0.6159
TRPM2	TRPM2	35.00	0.00	2.89E-05	6.79E-06	1.05	1.42	0.8453
TRPM6	TRPM6	34.89	0.20	7.01E-05	5.16E-05	2.29	3.24	0.2102
TRPM8	TRPM8	34.21	0.32	2.01E-04	2.91E-04	5.29	8.86	0.2541
TRPV1	TRPV1	28.22	2.42	2.21E-03	7.79E-04	1.59	1.71	0.9767
TRPV2	TRPV2	25.51	0.93	1.30E-02	3.39E-03	-1.51	0.38	0.1501
TRPV3	TRPV3	28.70	1.91	8.96E-04	8.33E-04	-1.30	2.79	0.4787
TRPV4	TRPV4	26.69	1.32	1.43E-02	1.96E-02	2.09	4.71	0.4216

Appendix 16. **Expression values of potassium channels for costal chondrocytes**

Gene	Name	Con Cq Avg	Con Cq SD	Con ΔCq Avg	Con ΔCq SD
KCNMA1	$K_{Ca}1.1\alpha$	22.34	0.65	1.88E-01	2.68E-02
KCNMB4	$K_{Ca}1.1\beta$	32.30	1.67	1.51E-04	9.65E-05
KCNN1	$K_{Ca}2.1$	33.22	1.47	6.68E-05	2.73E-05
KCNN2	$K_{Ca}2.2$	28.93	0.77	2.56E-03	9.44E-04
KCNN3	$K_{Ca}2.3$	33.24	1.70	6.81E-05	4.61E-05
KCNJ1	$K_{ir}1.1$	34.66	0.76	3.60E-05	1.15E-05
KCNJ2	$K_{ir}2.1$	25.83	0.96	1.52E-02	4.49E-03
KCNJ12	$K_{ir}2.2$	30.35	2.69	6.91E-04	9.14E-04
KCNJ4	$K_{ir}2.3$	33.13	1.90	5.99E-05	3.20E-05

Appendix 16 continued

Gene	Name	Con Cq Avg	Con Cq SD	Con ΔCq Avg	Con ΔCq SD
KCNJ14	$K_{ir}2.4$	29.59	2.22	7.45E-04	5.77E-04
KCNJ3	$K_{ir}3.1$	34.56	0.99	3.60E-05	1.15E-05
KCNJ6	$K_{ir}3.2$	34.64	0.66	5.13E-05	1.76E-05
KCNJ9	$K_{ir}3.3$	31.91	2.68	1.41E-04	1.46E-04
KCNJ5	$K_{ir}3.4$	34.79	0.48	3.60E-05	1.15E-05
KCNJ15	$K_{ir}4.2$	28.56	1.40	3.58E-03	4.41E-03
KCNJ16	$K_{ir}5.1$	34.48	1.17	3.60E-05	1.15E-05
KCNJ11	$K_{ir}6.2$	33.27	1.76	6.59E-05	4.24E-05
KCNJ13	$K_{ir}7.1$	31.87	1.52	1.87E-04	9.84E-05
KCNAB1	K_V β1	32.07	1.29	2.14E-04	2.08E-04
KCNAB2	K_V β2	27.34	0.86	5.53E-03	2.74E-03
KCNAB3	K_V β3	32.37	1.76	9.20E-05	2.54E-05
KCNA1	$K_V1.1$	31.63	2.01	6.19E-04	6.81E-04
KCNA2	$K_V1.2$	30.37	4.11	5.08E-04	7.87E-04
KCNA5	$K_V1.5$	33.67	1.74	5.26E-05	1.98E-05
KCNA6	$K_V1.6$	34.60	0.71	3.83E-05	8.30E-06
KCNH1	$K_V10.1$	32.00	1.57	1.47E-04	8.58E-05
KCNH2	$K_V11.1$	32.14	2.83	1.73E-04	2.28E-04
KCNH6	$K_V11.2$	33.64	1.77	5.53E-05	2.43E-05
KCNH7	$K_V11.3$	32.54	2.45	1.30E-04	1.53E-04
KCNH3	$K_V12.2$	34.03	1.05	4.98E-05	1.89E-05
KCNB1	$K_V2.1$	28.84	2.10	1.98E-03	1.52E-03
KCNB2	$K_V2.2$	34.50	0.71	3.71E-05	9.93E-06
KCNC1	$K_V3.1$	33.20	1.98	1.59E-04	2.03E-04
KCNC2	$K_V3.2$	33.65	1.92	4.32E-05	6.39E-06

Appendix 16 continued

Gene	Name	Con Cq Avg	Con Cq SD	Con ΔCq Avg	Con ΔCq SD
KCND2	K_V4.2	29.79	1.46	6.25E-04	4.63E-05
KCND3	K_V4.3	30.32	2.57	5.32E-04	6.45E-04
KCNQ1	K_V7.1	33.21	1.39	9.89E-05	7.57E-05
KCNQ2	K_V7.2	34.08	0.99	4.62E-05	9.77E-06
KCNQ3	K_V7.3	31.19	0.80	3.88E-04	1.99E-04
KCNS1	K_V9.1	30.99	2.13	3.43E-04	2.64E-04
KCNK1	TWIK1	24.82	1.30	2.55E-02	9.30E-03

Appendix 17. **Expression values of potassium channels for PE costal chondrocytes**

Gene	Name	PE Cq Avg	PE Cq SD	PE ΔCq Avg	PE ΔCq SD	PE ΔΔCq Avg	PE ΔΔCq SD	PE ΔΔCq p-Val
KCNMA1	K_{Ca}1.1α	23.86	0.61	1.11E-01	5.97E-02	-1.47	1.94	0.1472
KCNMB4	K_{Ca}1.1β	32.66	2.31	3.84E-04	4.08E-04	2.35	4.08	0.3417
KCNN1	K_{Ca}2.1	34.63	0.64	5.87E-05	1.30E-05	-1.48	0.31	0.2189
KCNN2	K_{Ca}2.2	33.21	1.05	1.68E-04	8.95E-05	-10.04	4.78	0.0327
KCNN3	K_{Ca}2.3	35.00	0.00	4.57E-05	1.04E-05	-1.87	0.49	0.1501
KCNJ1	K_{ir}1.1	35.00	0.00	4.57E-05	1.04E-05	1.43	0.33	0.1479
KCNJ2	K_{ir}2.1	27.84	1.44	9.30E-03	9.93E-03	-1.56	3.19	0.2979
KCNJ12	K_{ir}2.2	31.55	0.31	4.96E-04	9.31E-05	-1.28	0.23	0.3067
KCNJ4	K_{ir}2.3	34.88	0.21	4.89E-05	5.37E-06	-1.89	0.21	0.2163
KCNJ14	K_{ir}2.4	29.71	1.51	2.21E-03	1.49E-03	2.06	2.66	0.5858
KCNJ3	K_{ir}3.1	35.00	0.00	4.57E-05	1.04E-05	1.33	1.45	0.3383
KCNJ6	K_{ir}3.2	34.79	0.37	5.58E-05	2.62E-05	1.73	0.81	0.3402
KCNJ9	K_{ir}3.3	33.49	1.33	1.80E-04	1.41E-04	-1.19	3.95	0.4051
KCNJ5	K_{ir}3.4	35.00	0.00	4.57E-05	1.04E-05	1.56	0.36	0.1050
KCNJ15	K_{ir}4.2	30.70	1.82	1.19E-03	8.06E-04	-1.85	4.21	0.3498

Appendix 17 continued

Gene	Name	PE Cq Avg	PE Cq SD	PE ΔCq Avg	PE ΔCq SD	PE ΔΔCq Avg	PE ΔΔCq SD	PE ΔΔCq p-Val
KCNJ16	$K_{ir}5.1$	35.00	0.00	4.57E-05	1.04E-05	1.26	1.43	0.6309
KCNJ11	$K_{ir}6.2$	34.77	0.40	5.70E-05	2.83E-05	-1.47	1.85	0.3237
KCNJ13	$K_{ir}7.1$	31.58	1.12	5.28E-04	2.54E-04	2.39	1.15	0.0811
KCNAB1	K_V β1	33.10	0.47	1.68E-04	1.49E-05	-1.14	0.10	0.4960
KCNAB2	K_V β2	27.24	1.03	1.06E-02	5.48E-03	2.07	1.07	0.0914
KCNAB3	K_V β3	32.75	0.48	2.16E-04	3.98E-05	1.38	0.25	0.9010
KCNA1	$K_V1.1$	30.76	1.15	9.81E-04	5.47E-04	3.77	2.10	0.2446
KCNA2	$K_V1.2$	33.96	1.80	1.84E-04	2.48E-04	-3.39	8.68	0.2831
KCNA5	$K_V1.5$	35.00	0.00	4.57E-05	1.04E-05	-1.39	0.36	0.4445
KCNA6	$K_V1.6$	34.03	1.34	1.24E-04	1.29E-04	3.73	3.87	0.1501
KCNH1	$K_V10.1$	32.29	1.91	4.11E-04	3.05E-04	2.03	3.20	0.6215
KCNH2	$K_V11.1$	33.55	1.26	1.51E-04	1.06E-04	-1.21	2.61	0.4212
KCNH6	$K_V11.2$	35.00	0.00	4.57E-05	1.04E-05	-1.41	0.37	0.4306
KCNH7	$K_V11.3$	34.49	0.88	7.96E-05	6.69E-05	-1.74	2.72	0.3147
KCNH3	$K_V12.2$	34.41	0.51	6.89E-05	1.87E-05	1.39	0.38	0.2633
KCNB1	$K_V2.1$	29.60	1.70	3.22E-03	3.97E-03	1.78	3.62	0.7064
KCNB2	$K_V2.2$	35.00	0.00	4.57E-05	1.04E-05	1.28	1.44	0.1746
KCNC1	$K_V3.1$	33.95	0.93	1.08E-04	7.17E-05	1.23	2.09	0.6341
KCNC2	$K_V3.2$	35.00	0.00	4.57E-05	1.04E-05	-1.41	0.37	0.4869
KCND2	$K_V4.2$	33.59	1.57	1.54E-04	1.27E-04	-6.04	8.33	0.1284
KCND3	$K_V4.3$	32.18	1.85	6.01E-04	7.80E-04	-1.08	4.21	0.4773
KCNQ1	$K_V7.1$	34.71	0.50	5.51E-05	7.15E-06	-1.59	0.21	0.2369
KCNQ2	$K_V7.2$	34.72	0.48	5.47E-05	6.49E-06	1.15	0.14	0.3196
KCNQ3	$K_V7.3$	31.28	1.46	8.57E-04	9.15E-04	2.43	3.37	0.2701

Appendix 17 continued

Gene	Name	PE Cq Avg	PE Cq SD	PE ΔCq Avg	PE ΔCq SD	PE ΔΔCq Avg	PE ΔΔCq SD	PE ΔΔCq p-Val
KCNS1	K_V9.1	31.69	0.70	4.75E-04	2.09E-04	1.17	1.70	0.6980
KCNK1	TWIK1	25.54	1.00	3.41E-02	1.70E-02	1.17	1.76	0.7386

Appendix 18. **Expression values of potassium channels for PC costal chondrocytes**

Gene	Name	PC Cq Avg	PC Cq SD	PC ΔCq Avg	PC ΔCq SD	PC ΔΔCq Avg	PC ΔΔCq SD	PC ΔΔCq p-Val
KCNMA1	K_{Ca}1.1α	23.34	1.19	1.11E-01	5.97E-02	-1.87	0.55	0.0034
KCNMB4	K_{Ca}1.1β	31.84	1.10	3.84E-04	4.08E-04	2.19	2.67	0.1479
KCNN1	K_{Ca}2.1	33.93	0.93	5.87E-05	1.30E-05	-1.79	2.57	0.1258
KCNN2	K_{Ca}2.2	33.51	1.34	1.68E-04	8.95E-05	-13.73	13.21	0.0054
KCNN3	K_{Ca}2.3	35.00	0.00	4.57E-05	1.04E-05	-3.28	1.78	0.0187
KCNJ1	K_{ir}1.1	35.00	0.00	4.57E-05	1.04E-05	-1.22	1.74	0.3500
KCNJ2	K_{ir}2.1	29.16	1.63	9.30E-03	9.93E-03	-1.53	8.71	0.3212
KCNJ12	K_{ir}2.2	32.39	0.58	4.96E-04	9.31E-05	-3.87	1.67	0.0473
KCNJ4	K_{ir}2.3	31.99	2.71	4.89E-05	5.37E-06	4.64	8.36	0.2756
KCNJ14	K_{ir}2.4	29.84	1.11	2.21E-03	1.49E-03	1.55	1.96	0.9153
KCNJ3	K_{ir}3.1	35.00	0.00	4.57E-05	1.04E-05	1.00	2.04	0.8716
KCNJ6	K_{ir}3.2	35.00	0.00	5.58E-05	2.62E-05	-1.24	1.74	0.3347
KCNJ9	K_{ir}3.3	34.50	0.87	1.80E-04	1.41E-04	-2.19	5.95	0.1266
KCNJ5	K_{ir}3.4	34.64	0.62	4.57E-05	1.04E-05	-1.00	1.55	0.8335
KCNJ15	K_{ir}4.2	31.20	0.97	1.19E-03	8.06E-04	-4.19	1.75	0.1049
KCNJ16	K_{ir}5.1	35.00	0.00	4.57E-05	1.04E-05	-1.39	1.80	0.2153
KCNJ11	K_{ir}6.2	35.00	0.00	5.70E-05	2.83E-05	-3.20	1.74	0.0353
KCNJ13	K_{ir}7.1	33.38	1.00	5.28E-04	2.54E-04	-1.53	2.00	0.1452
KCNAB1	K_V β1	32.07	3.26	1.68E-04	1.49E-05	8.65	10.18	0.0936

Appendix 18 continued

Gene	Name	PC Cq Avg	PC Cq SD	PC ΔCq Avg	PC ΔCq SD	PC ΔΔCq Avg	PC ΔΔCq SD	PC ΔΔCq p-Val
KCNAB2	K_V β2	27.50	0.47	1.06E-02	5.48E-03	-1.05	1.56	0.7153
KCNAB3	K_V β3	32.52	1.23	2.16E-04	3.98E-05	1.14	1.81	0.7873
KCNA1	K_V1.1	34.02	1.70	9.81E-04	5.47E-04	-3.05	7.44	0.1334
KCNA2	K_V1.2	32.68	2.02	1.84E-04	2.48E-04	-3.19	6.51	0.1566
KCNA5	K_V1.5	35.00	0.00	4.57E-05	1.04E-05	-2.43	1.32	0.1286
KCNA6	K_V1.6	32.89	3.01	1.24E-04	1.29E-04	12.41	26.71	0.3534
KCNH1	K_V10.1	32.88	3.67	4.11E-04	3.05E-04	3.45	12.15	0.5717
KCNH2	K_V11.1	32.63	2.38	1.51E-04	1.06E-04	1.52	8.15	0.7757
KCNH6	K_V11.2	35.00	0.00	4.57E-05	1.04E-05	-2.48	1.34	0.1259
KCNH7	K_V11.3	35.00	0.00	7.96E-05	6.69E-05	-5.32	2.89	0.0753
KCNH3	K_V12.2	34.58	0.46	6.89E-05	1.87E-05	-1.45	1.87	0.2396
KCNB1	K_V2.1	29.49	0.77	3.22E-03	3.97E-03	1.44	2.67	0.9268
KCNB2	K_V2.2	35.00	0.00	4.57E-05	1.04E-05	-1.37	1.79	0.1481
KCNC1	K_V3.1	34.64	0.62	1.08E-04	7.17E-05	-2.27	2.28	0.1588
KCNC2	K_V3.2	34.43	0.98	4.57E-05	1.04E-05	-1.99	1.12	0.2406
KCND2	K_V4.2	33.71	1.44	1.54E-04	1.27E-04	-1.60	10.14	0.3303
KCND3	K_V4.3	32.01	2.26	6.01E-04	7.80E-04	-1.74	14.49	0.1523
KCNQ1	K_V7.1	34.14	1.49	5.51E-05	7.15E-06	-1.30	3.59	0.5675
KCNQ2	K_V7.2	35.00	0.00	5.47E-05	6.49E-06	-1.83	0.99	0.0104
KCNQ3	K_V7.3	31.01	2.51	8.57E-04	9.15E-04	2.19	8.10	0.4818
KCNS1	K_V9.1	31.49	3.84	4.75E-04	2.09E-04	4.42	17.29	0.4648
KCNK1	TWIK1	25.75	0.96	3.41E-02	1.70E-02	-1.57	0.24	0.0299

Appendix 19. **Expression values of calcium channels for costal chondrocytes**

Gene	Name	Con Cq Avg	Con Cq SD	Con ΔCq Avg	Con ΔCq SD
CACNB1	Ca_V β1	27.75	0.88	3.59E-03	7.00E-04
CACNB2	Ca_V β2	29.76	1.98	6.62E-04	4.83E-04
CACNB3	Ca_V β3	26.92	0.90	6.95E-03	1.78E-03
CACNG2	Ca_V γ2	32.14	2.44	1.47E-04	1.65E-04
CACNG4	Ca_V γ4	33.65	1.87	2.36E-04	3.57E-04
CACNA1C	Ca_V1.2	28.48	2.19	1.15E-03	3.35E-04
CACNA1D	Ca_V1.3	31.88	1.44	2.86E-04	1.49E-04
CACNA1A	Ca_V2.1	28.06	1.45	2.45E-03	1.03E-03
CACNA1B	Ca_V2.2	34.26	1.25	3.60E-05	1.15E-05
CACNA1G	Ca_V3.1	30.97	1.96	2.44E-04	1.49E-04
CACNA1I	Ca_V3.3	32.65	2.18	1.24E-04	1.42E-04
RYR3	RYR3	30.14	1.31	8.09E-04	5.45E-04

Appendix 20. **Expression values of calcium channels for PE costal chondrocytes**

Gene	Name	PE Cq Avg	PE Cq SD	PE ΔCq Avg	PE ΔCq SD	PE ΔΔCq Avg	PE ΔΔCq SD	PE ΔΔCq p-Val
CACNB1	Ca_V β1	28.27	0.61	5.02E-03	2.10E-03	1.31	1.53	0.2786
CACNB2	Ca_V β2	30.32	1.06	1.25E-03	5.57E-04	1.31	1.81	0.9743
CACNB3	Ca_V β3	27.86	0.49	6.40E-03	1.08E-03	-1.07	1.31	0.6028
CACNG2	Ca_V γ2	35.00	0.00	4.57E-05	1.04E-05	-4.01	1.05	0.1301
CACNG4	Ca_V γ4	33.71	1.22	1.44E-04	1.30E-04	2.25	2.94	0.9143
CACNA1C	Ca_V1.2	28.92	1.04	3.39E-03	1.85E-03	1.47	1.95	0.9701
CACNA1D	Ca_V1.3	31.92	0.97	4.16E-04	2.05E-04	1.90	2.02	0.2462
CACNA1A	Ca_V2.1	28.50	0.55	4.12E-03	8.54E-04	1.33	0.28	0.5140
CACNA1B	Ca_V2.2	35.00	0.00	4.57E-05	1.04E-05	1.08	1.42	0.9943

Appendix 20 continued

Gene	Name	PE Cq Avg	PE Cq SD	PE ΔCq Avg	PE ΔCq SD	PE ΔΔCq Avg	PE ΔΔCq SD	PE ΔΔCq p-Val
CACNA1G	$Ca_V3.1$	30.95	0.89	8.01E-04	3.35E-04	1.95	0.81	0.5187
CACNA1I	$Ca_V3.3$	35.00	0.00	4.57E-05	1.04E-05	-2.82	0.74	0.1260
RYR3	RYR3	32.24	1.43	4.01E-04	3.56E-04	-1.82	3.42	0.2055

Appendix 21. **Expression values of calcium channels for PC costal chondrocytes**

Gene	Name	PC Cq Avg	PC Cq SD	PC ΔCq Avg	PC ΔCq SD	PC ΔΔCq Avg	PC ΔΔCq SD	PC ΔΔCq p-Val
CACNB1	Ca_V β1	27.68	0.41	5.02E-03	2.10E-03	-1.02	1.65	0.9022
CACNB2	Ca_V β2	31.59	0.66	1.25E-03	5.57E-04	-3.25	1.65	0.0562
CACNB3	Ca_V β3	27.30	1.52	6.40E-03	1.08E-03	1.05	1.76	0.9093
CACNG2	Ca_V γ2	35.00	0.00	4.57E-05	1.04E-05	-7.02	3.81	0.0353
CACNG4	Ca_V γ4	31.69	2.02	1.44E-04	1.30E-04	7.59	8.30	0.2322
CACNA1C	$Ca_V1.2$	30.08	1.76	3.39E-03	1.85E-03	1.25	4.02	0.7615
CACNA1D	$Ca_V1.3$	32.09	1.35	4.16E-04	2.05E-04	-1.02	7.19	0.7642
CACNA1A	$Ca_V2.1$	28.23	1.21	4.12E-03	8.54E-04	1.16	1.20	0.8668
CACNA1B	$Ca_V2.2$	35.00	0.00	4.57E-05	1.04E-05	-1.62	0.88	0.1165
CACNA1G	$Ca_V3.1$	34.20	0.32	8.01E-04	3.35E-04	-6.20	3.80	0.0452
CACNA1I	$Ca_V3.3$	35.00	0.00	4.57E-05	1.04E-05	-4.94	2.68	0.0271
RYR3	RYR3	31.13	1.85	4.01E-04	3.56E-04	-1.20	2.37	0.3483

Appendix 22. **Expression values of chloride channels for costal chondrocytes**

Gene	Name	Con Cq Avg	Con Cq SD	Con ΔCq Avg	Con ΔCq SD
CLCN2	CLC2	30.30	0.86	7.21E-04	2.84E-04
CLCN3	CLC3	24.76	0.88	3.23E-02	1.15E-02
CLCN7	CLC7	25.75	1.14	1.69E-02	1.24E-02

Appendix 23. **Expression values of chloride channels for PE costal chondrocytes**

Gene	Name	PE Cq Avg	PE Cq SD	PE ΔCq Avg	PE ΔCq SD	PE ΔΔCq Avg	PE ΔΔCq SD	PE ΔΔCq p-Val
CLCN2	CLC2	30.42	0.60	1.15E-03	5.48E-04	1.76	0.84	0.1195
CLCN3	CLC3	25.11	1.11	4.66E-02	2.33E-02	1.52	1.86	0.2383
CLCN7	CLC7	25.86	1.32	2.91E-02	1.62E-02	1.89	2.23	0.2286

Appendix 24. **Expression values of chloride channels for PC costal chondrocytes**

Gene	Name	PC Cq Avg	PC Cq SD	PC ΔCq Avg	PC ΔCq SD	PC ΔΔCq Avg	PC ΔΔCq SD	PC ΔΔCq p-Val
CLCN2	CLC2	30.64	0.82	1.15E-03	5.48E-04	-1.06	1.38	0.6537
CLCN3	CLC3	24.99	1.05	4.66E-02	2.33E-02	-1.04	1.27	0.6565
CLCN7	CLC7	25.52	0.52	2.91E-02	1.62E-02	1.29	1.08	0.5789

Appendix 25. **Expression values of sodium channels for costal chondrocytes**

Gene	Name	Con Cq Avg	Con Cq SD	Con ΔCq Avg	Con ΔCq SD
SCN1A	$Na_V1.1\alpha$	32.94	2.09	5.90E-05	3.05E-05
SCN1B	$Na_V\beta1$	26.06	0.86	1.21E-02	3.91E-03
SCN2A	$Na_V1.2$	28.84	1.31	1.38E-03	4.87E-04
SCN2B	$Na_V\beta2$	28.13	1.81	2.06E-03	1.24E-03
SCN3A	$Na_V1.3$	28.96	1.16	2.52E-03	2.47E-03
SCN8A	$Na_V1.6$	27.33	1.09	4.50E-03	1.15E-03
SCN9A	$Na_V1.7$	28.34	1.11	3.08E-03	2.07E-03
SCN10A	$Na_V1.8$	34.15	1.18	3.60E-05	1.15E-05
SCN11A	$Na_V1.9$	34.48	1.16	3.60E-05	1.15E-05

Appendix 26. **Expression values of sodium channels for PE costal chondrocytes**

Gene	Name	PE Cq Avg	PE Cq SD	PE ΔCq Avg	PE ΔCq SD	PE ΔΔCq Avg	PE ΔΔCq SD	PE ΔΔCq p-Val
SCN1A	$Na_V1.1\alpha$	33.82	2.05	2.18E-04	3.01E-04	2.08	4.59	0.7118
SCN1B	$Na_V\beta1$	25.64	0.45	3.04E-02	9.68E-03	2.45	0.78	0.0139
SCN2A	$Na_V1.2$	31.33	0.98	7.10E-04	5.03E-04	-2.54	3.52	0.1619
SCN2B	$Na_V\beta2$	29.27	1.36	3.44E-03	3.61E-03	1.17	2.86	0.9253
SCN3A	$Na_V1.3$	31.22	1.41	9.02E-04	8.38E-04	-1.84	5.16	0.3198
SCN8A	$Na_V1.6$	28.74	0.37	3.66E-03	1.44E-03	-1.40	0.80	0.2980
SCN9A	$Na_V1.7$	30.62	1.81	1.28E-03	9.69E-04	-2.00	4.68	0.1483
SCN10A	$Na_V1.8$	35.00	0.00	4.57E-05	1.04E-05	1.00	1.42	0.7908
SCN11A	$Na_V1.9$	35.00	0.00	4.57E-05	1.04E-05	1.26	1.43	0.6151

Appendix 27. **Expression values of sodium channels for PC costal chondrocytes**

Gene	Name	PC Cq Avg	PC Cq SD	PC ΔCq Avg	PC ΔCq SD	PC ΔΔCq Avg	PC ΔΔCq SD	PC ΔΔCq p-Val
SCN1A	$Na_V1.1\alpha$	34.46	0.94	2.18E-04	3.01E-04	-1.41	3.57	0.3008
SCN1B	$Na_V\beta1$	25.48	0.39	3.04E-02	9.68E-03	1.53	2.21	0.3762
SCN2A	$Na_V1.2$	29.42	2.03	7.10E-04	5.03E-04	1.26	2.29	0.8633
SCN2B	$Na_V\beta2$	28.20	0.27	3.44E-03	3.61E-03	1.03	1.56	0.6273
SCN3A	$Na_V1.3$	27.49	2.02	9.02E-04	8.38E-04	5.20	3.46	0.0156
SCN8A	$Na_V1.6$	27.71	1.64	3.66E-03	1.44E-03	1.23	1.85	0.6645
SCN9A	$Na_V1.7$	26.74	2.21	1.28E-03	9.69E-04	5.76	3.77	0.0086
SCN10A	$Na_V1.8$	35.00	0.00	4.57E-05	1.04E-05	-1.75	0.95	0.0737
SCN11A	$Na_V1.9$	35.00	0.00	4.57E-05	1.04E-05	-1.39	1.80	0.2156

Appendix 28. **Expression values of non-selective channels for costal chondrocytes**

Gene	Name	Con Cq Avg	Con Cq SD	Con ΔCq Avg	Con ΔCq SD
ACCN2	ASIC1	28.27	1.85	1.54E-03	4.02E-04
ACCN1	ASIC2	28.75	1.40	2.14E-03	1.57E-03
ACCN3	ASIC3	31.07	1.53	3.33E-04	2.06E-04
HCN1	BCNG1	31.99	2.80	2.33E-04	3.32E-04
HCN2	BCNG2	29.21	1.98	1.42E-03	9.64E-04
BEST1	BEST1	29.91	1.75	9.31E-04	6.57E-04
SLC12A5	SLC12A5	31.69	3.23	1.32E-04	1.56E-04
TRPA1	TRPA1	31.77	3.04	1.78E-04	2.36E-04
TRPC1	TRPC1	25.93	1.13	1.16E-02	3.90E-03
TRPC3	TRPC3	30.73	2.57	5.65E-04	4.90E-04
TRPC6	TRPC6	31.19	2.17	2.84E-04	1.56E-04
TRPM1	TRPM1	35.00	0.00	3.60E-05	1.15E-05
TRPM2	TRPM2	32.84	2.08	8.13E-05	6.89E-05
TRPM6	TRPM6	34.66	0.76	3.60E-05	1.15E-05
TRPM8	TRPM8	30.89	3.23	4.54E-04	6.61E-04
TRPV1	TRPV1	29.50	1.18	1.01E-03	4.18E-04
TRPV2	TRPV2	25.10	0.69	2.61E-02	3.78E-03
TRPV3	TRPV3	29.37	1.47	1.13E-03	5.14E-04
TRPV4	TRPV4	27.46	1.07	4.77E-03	1.54E-03

Appendix 29. **Expression values of non-selective channels for PE costal chondrocytes**

Gene	Name	PE Cq Avg	PE Cq SD	PE ΔCq Avg	PE ΔCq SD	PE ΔΔCq Avg	PE ΔΔCq SD	PE ΔΔCq p-Val
ACCN2	ASIC1	28.74	0.78	3.65E-03	1.57E-03	1.36	1.67	0.9511
ACCN1	ASIC2	33.71	1.87	2.09E-04	2.70E-04	-9.17	26.33	0.0301

Appendix 29 continued

Gene	Name	PE Cq Avg	PE Cq SD	PE ΔCq Avg	PE ΔCq SD	PE ΔΔCq Avg	PE ΔΔCq SD	PE ΔΔCq p-Val
ACCN3	ASIC3	29.75	1.39	2.06E-03	1.62E-03	5.35	4.19	0.0572
HCN1	BCNG1	35.00	0.00	4.57E-05	1.04E-05	-4.45	1.17	0.1237
HCN2	BCNG2	30.19	1.70	1.71E-03	1.60E-03	1.22	2.73	0.9506
BEST1	BEST1	30.43	1.34	1.24E-03	8.06E-04	1.44	2.10	0.7088
SLC12A5	SLC12A5	35.00	0.00	4.57E-05	1.04E-05	-5.46	1.43	0.2180
TRPA1	TRPA1	34.47	0.47	7.12E-05	3.48E-05	-3.32	2.47	0.2446
TRPC1	TRPC1	26.21	0.56	2.03E-02	5.39E-03	1.49	0.40	0.1465
TRPC3	TRPC3	34.42	1.00	7.21E-05	3.60E-05	-6.74	3.06	0.0475
TRPC6	TRPC6	35.00	0.00	4.57E-05	1.04E-05	-7.73	2.02	0.2594
TRPM1	TRPM1	35.00	0.00	4.57E-05	1.04E-05	1.81	0.41	0.1132
TRPM2	TRPM2	34.15	0.77	8.57E-05	3.36E-05	-1.32	1.70	0.3545
TRPM6	TRPM6	34.70	0.51	5.54E-05	7.61E-06	1.74	0.24	0.0178
TRPM8	TRPM8	33.95	1.82	1.89E-04	2.56E-04	-2.31	7.19	0.2054
TRPV1	TRPV1	29.37	0.61	2.28E-03	6.25E-04	2.00	0.55	0.0289
TRPV2	TRPV2	27.21	1.58	1.33E-02	9.87E-03	-1.81	3.86	0.0567
TRPV3	TRPV3	30.77	0.53	9.02E-04	4.21E-04	-1.38	1.77	0.2748
TRPV4	TRPV4	27.83	1.03	7.05E-03	3.69E-03	1.50	1.78	0.2384

Appendix 30. **Expression values of non-selective channels for PC costal chondrocytes**

Gene	Name	PC Cq Avg	PC Cq SD	PC ΔCq Avg	PC ΔCq SD	PC ΔΔCq Avg	PC ΔΔCq SD	PC ΔΔCq p-Val
ACCN2	ASIC1	28.11	0.29	3.65E-03	1.57E-03	1.38	1.50	0.9171
ACCN1	ASIC2	31.99	2.20	2.09E-04	2.70E-04	-6.41	12.01	0.0069
ACCN3	ASIC3	31.40	0.77	2.06E-03	1.62E-03	1.02	1.72	0.7472

Appendix 30 continued

Gene	Name	PC Cq Avg	PC Cq SD	PC ΔCq Avg	PC ΔCq SD	PC ΔΔCq Avg	PC ΔΔCq SD	PC ΔΔCq p-Val
HCN1	BCNG1	34.05	1.22	4.57E-05	1.04E-05	2.23	5.10	0.7850
HCN2	BCNG2	31.44	1.10	1.71E-03	1.60E-03	-3.36	6.36	0.0273
BEST1	BEST1	29.90	0.76	1.24E-03	8.06E-04	1.39	1.69	0.7035
SLC12A5	SLC12A5	34.68	0.56	4.57E-05	1.04E-05	-7.50	4.17	0.0979
TRPA1	TRPA1	34.05	1.65	7.12E-05	3.48E-05	-1.21	3.90	0.2624
TRPC1	TRPC1	25.98	0.52	2.03E-02	5.39E-03	1.08	1.07	0.8603
TRPC3	TRPC3	31.61	0.80	7.21E-05	3.60E-05	-1.78	1.43	0.0525
TRPC6	TRPC6	33.37	1.42	4.57E-05	1.04E-05	-1.01	7.52	0.6064
TRPM1	TRPM1	35.00	0.00	4.57E-05	1.04E-05	1.03	1.69	0.8039
TRPM2	TRPM2	35.00	0.00	8.57E-05	3.36E-05	-4.33	2.35	0.0327
TRPM6	TRPM6	34.78	0.20	5.54E-05	7.61E-06	-1.11	1.70	0.5682
TRPM8	TRPM8	34.10	1.56	1.89E-04	2.56E-04	-5.50	3.88	0.0590
TRPV1	TRPV1	29.53	0.69	2.28E-03	6.25E-04	1.07	1.30	0.9816
TRPV2	TRPV2	26.31	1.27	1.33E-02	9.87E-03	-2.09	0.87	0.0007
TRPV3	TRPV3	31.35	1.76	9.02E-04	4.21E-04	-2.34	3.91	0.0198
TRPV4	TRPV4	27.21	1.50	7.05E-03	3.69E-03	1.73	3.94	0.5754

VITA

Anthony J. Asmar
Department of Biological Sciences
Frank Reidy Research Center for Bioelectrics
Old Dominion University, Norfolk, VA 23508

Education

Bachelor of Science, Biology; May 2010
Virginia Polytechnic Institute and State University, Blacksburg, VA
Master of Science, Biology; May 2013
Old Dominion University, Norfolk, VA
Doctor of Philosophy, Biomedical Sciences; August 2017
Old Dominion University, Norfolk, VA

Publications

Semenov I, **Asmar A**, Kelly Jr R, Stacey M. (2017). Aberrant Calcium Signaling in Costal Cartilage from Patients with Chest Wall Deformities. In preparation.

Asmar A, Barrett-Jolley R, Kelly Jr R, Stacey M. (2017). Membrane Channel Gene Expression in Costal Cartilage from Patients with Chest Wall Deformities. In preparation.

Dutta D, Palmer X-L, **Asmar A**, Stacey M, Qian Z. (2017). Nanosecond Pulsed Electric Field Induced Changes in Cell Surface Charge Density. *Micron*. In press.

Coluzzi E, Buonsante R, Leone S, **Asmar A**, Miller K, Cimini D, Sgura A. (2016). Transient ALT activation protects human primary cells from chromosome instability induced by low chronic oxidative stress. *Scientific Reports.* **7**:43309.

Asmar A, Barrett-Jolley R, Werner A, Kelly Jr R, Stacey M. (2016). Membrane channel gene expression in human costal and articular chondrocytes. *Organogenesis*. 12:94–107.

Sabuncu AC, **Asmar AJ**, Stacey MW, Beskok A. (2015). Differential Dielectric Responses of Chondrocyte and Jurkat cells in Electromanipulation Buffers. *Electrophoresis*. 36:1499-1506.

Dutta D*, **Asmar A***, Stacey M. (2015). Effects of Nanosecond Pulse Electric Fields on Cellular Elasticity. *Micron*. 17:15-20.

Basu G, Downey H, Guo S, Israel A, **Asmar A**, Hargrave B and Heller R. (2014). Prevention of Distal Flap Necrosis in a Rat Random Skin Flap Model by Gene Electrotransfer Delivering $VEGF_{165}$ Plasmid. *J Gene Med.* 16:55-65.

Stacey M, Dutta D, Cao W, **Asmar A**, El-Sayed Ali H, Kelly Jr R and Beskok A. (2013). Atomic Force Microscopy Characterization of Collagen 'Nanostraws' in Human Costal Cartilage. *Micron.* 44:483-7.

Stacey MW, Grubb J, **Asmar A**, Pryor J, El-Sayed Ali H, Cao W, Beskok A, Dutta D, Darby DA, Fecteau A, Werner A and Kelly RE Jr. (2012). Decorin Expression, Straw-like Structure, and Differentiation of Human Costal Cartilage. *Connective Tissue Research*. 53(5):415-21.